THE ROLE OF NCB5OR IN FATTY ACID METABOLISM AND REDOX HOMEOSTASIS

BY

Ming Xu

Submitted to the graduate degree program in Rehabilitation Science and the Graduate Faculty of the University of Kansas in partial fulfillment of the requirements for the degree of Doctor of Philosophy.

_____
WenFang Wang, Ph.D. (co-chair)

_____
Lisa Stehno-Bittel, Ph.D. (co-chair)

_____
Hao Zhu, Ph.D.

_____
Hartmut Jaeschke, Ph.D.

_____
Russell H. Swerdlow, M.D.

Date Defended: 8/26/2011

The Dissertation Committee for Ming Xu

certifies that this is the approved version of the following dissertation:

THE ROLE OF NCB5OR IN FATTY ACID METABOLISM AND REDOX HOMEOSTASIS

_____

WenFang Wang, Ph.D. (co-chair)

_____

Lisa Stehno-Bittel, Ph.D. (co-chair)

Date approved:

Abstract

The endoplasmic reticulum (ER)-associated NADH cytochrome b5 oxidoreductase (Ncb5or) is widely distributed in animal tissues. It contains two redox domains that are homologous to microsomal cytochrome b5 (Cyb5A) at the N terminus and its cognate reductase (Cyb5R3) at the C terminus. Ncb5or null mice develop diabetes at age 7 weeks and have increased susceptibility to the diabetogenic agent streptozotocin. Ncb5or deficiency also results in lipoatrophy and increased hepatocyte sensitivity to cytotoxic effects of saturated fatty acids. Here we investigate the mechanisms of these phenomena in prediabetic Ncb5or$^{-/-}$ mice. We find that, despite increased rates of fatty acid uptake and synthesis and higher stearoyl-CoA desaturase (SCD) expression, Ncb5or $^{-/-}$ liver accumulates less triacylglycerol (TAG) than wild-type (WT). Ncb5or$^{-/-}$ hepatocytes readily incorporate exogenous fatty acids into TAG but accumulate more free fatty acids (FFA). A high-fat diet rich in palmitate and oleate stimulates both lipogenesis and fatty acid catabolism in Ncb5or $^{-/-}$ liver, resulting in TAG levels similar to WT but increased intracellular FFA accumulation. Hepatic SCD specific activity is 2-fold lower in Ncb5or$^{-/-}$ than in WT mice when up to 8 fold increases in Scd1 mRNA and protein levels are considered. Accumulation of saturated fatty acids in Ncb5or$^{-/-}$ hepatocytes increases mitochondrial content, peroxisome proliferator-activated receptor-γ coactivator 1α (PGC-1α) expression, fatty acid oxidation rates, oxidative stress response gene expression, oxidized glutathione content and cell death. These phenotypes could be alleviated by co-incubation with oleic acid via TAG channeling. Taken together, these findings suggest that increased FFA accumulation and catabolism and oxidative stress are major consequences of Ncb5or deficiency in liver. Our study has provided new insight into fatty acid metabolism and revealed a novel role of Ncb5or in preventing saturated fatty acid induced oxidative stress.

Acknowledgement

First, I would like to thank my mentors: Dr. Hao Zhu and Dr. WenFang Wang for the great mentorship and generous support over the past 5 years. I really appreciate their scientific training which leaded me to become a good researcher. I benefited a lot from their excellent leadership, positive attitude and depth of knowledge. They also helped me to get used to the life in United States and treated me like their family members. I am so proud to have working and learning experience in their lab.

Second, I am very grateful to Dr. Stehno-Bittel, Dr. Swerdlow and Dr. Jaeschke for their time and effort to serve as the members of my thesis committee. I would like to thank them and the members in their labs for invaluable and generous support on several key experiments.

Third, I would like to thank Jennifer Frontera for help with mouse breeding and improving my English skill. I appreciate the general help and support from Janette Williams and Dr. Lesya Novikova. In addition, I would like to thank all my friends and colleagues at KUMC who have shared my joy and frustration during my graduate studies.

Forth, I sincerely thank the Physical Therapy and Rehabilitation Science Department for giving me such a chance. I am grateful to all the faculty and Ph.D. students in this department for the encouragement and help. Especially, I thank Dr. Smirnova, Floyd Huang, Lisa Vanhoose and Kevin Farmer for their help. I thank School of Allied Health for the scholarships and Student Union Council for the travel grants. All these funds were very helpful to me.

Last but not least, I would like to thank my parents for their love and guidance throughout my life. I want to thank my uncle and aunt who supported me a lot. Finally, I am very grateful to my wife, Chun Guo, for her love, understanding and support.

Table of contents

List of Abbreviations

ACC: Acetyl-CoA carboxylase
ACSL: Long-chain fatty acid-CoA ligases
ACOX: Acyl CoA oxidase
AGPAT: Acylglycerol-3-phosphate acyltransferase
AMPK: 5' AMP-activated protein kinase
ARE: Antioxidant response element
ATF4: Activating transcription factor 4
ATF6: Activating transcription factor 6
Bax: Bcl2-2-associated X protein
BCN: Cytochrome b5 complete null
BiP: Binding immunoglobulin protein
C16:0: Palmitic acid
C18:1: Oleic acid
CD36: Cluster of Differentiation 36
CHOP: CCAAT/enhancer binding protein
CPT: Carnitine palmitoyltransferase
Cyb5A: Microsomal cytochrome b5
Cyb5R3: Microsomal cytochrome b5 reductase
Cybrd1: Duodenal cytochrome b-like ferrireductase or DcytB
DAG: Diacylglycerol
DCF: 2',7'-dichlorofluorescein
DGAT: Diacylglycerol acyltransferase
DMT1: Divalent metal transporter 1
eIF2α: eukaryotic Initiation Factor 2, α-subunit
ER: Endoplasmic reticulum
ERAD: ER-associated degradation
Ero1: ER oxidoreductin 1
ETC: Electron transport chain
FAD: Flavin-adenine dinucleotide
FAS: Fatty acid synthase
FATP: Fatty acid transporters
FBS: Fetal bovine serum
FCCP: Carbonylcyanide-p-trifluoromethoxyphenylhydrazone
FECH: Ferrochelatase
FeS: iron-sulfur clusters
FFA: Free fatty acids
FPN: Ferroportin
GCLC: Glutamate-cysteine ligase, catalytic subunit
GPAT: Glycerol-3-phosphate acyltransferase
GPX: GSH peroxidase
GSH: Thiol-reduced form of glutathione
GSSG: Disulfide-oxidized form of glutathione

GST: GSH S-transferase (GST)
HBN: Hepatic microsomal b5 null
HFE: Hereditary hemochromatosis protein
HMOX1: Heme oxygenase 1
IRE: Iron regulatory elements
IRE1α: Inositol requiring protein 1α
IRP1: Iron regulatory protein 1
IRP2: Iron regulatory protein 2
JNK: C-jun N-terminal kinase
Keap1: Kelch like-ECH-associated protein 1
LKB1: Serine/threonine kinase 11
LIP: Labile iron pool
LIPIN: Phosphatidic acid phosphohydrolase
LPA: Lysophosphatidic acid
LPL: Lipoprotein lipases
Mfrn: Mitoferrin
MT: Metallothionein
MUFA: Monounsaturated fatty acid
Ncb5or: NADH cytochrome b5 oxidoreductase
NEFA: Nonesterified fatty acids
NOX: NAPDH oxidase
NRAMP1: Natural resistance-associated macrophages protein 1
NRF: Nuclear respiratory factor
Nrf2: Nuclear factor E2-related factor 2
OCR: Oxygen consumption rate
PA: Phosphatidic acid
PCBP1: Poly(rC)-binding protein 1
PERK: Protein kinase-like Endoplasmic Reticulum Kinase
PGC1α: Peroxisome proliferator-activated receptor gamma coactivator-1 α
PPARα: Peroxisome proliferator-activated receptor α
PPARγ: Peroxisome proliferator-activated receptor γ
PPARδ/β: Peroxisome proliferator-activated receptor δ/β
PPRE: Peroxisome proliferator response elements
PUFA: Polyunsaturated fatty acids
RER: Respiratory exchange rate
RXR: Retinoid X receptor
ROS: Reactive oxygen species
SCD: Stearoyl-CoA desaturase
SFA: Saturated fatty acid
SIRT1: Sirtuin
SOD: Superoxide dismutase
STEAP: Six-transmembrane epithelial antigen of prostate
TAG: Triacylglycerol
TF: Transferrin
TFR1: Transferrin receptor-1
UPR: Unfolded protein response

UTR: Untranslated regions
VLDL: Very low-density lipoprotein
XBP1: X-box binding protein 1
ZIP14: ZRT/IRT-like protein 14

Chapter 1

Introduction

1.1 Ncb5or and its biology

1.1.1 Ncb5or

NADH cytochrome b5 oxidoreductase (Ncb5or) is a highly conserved enzyme in the animal kingdom and is widely expressed in most tissues [1]. It was identified from bioinformatics search of novel proteins that contain NAD(P)H and flavin binding sites in the expressed sequence tag (EST) database [1]. After the cDNA was cloned from human cell lines, Ncb5or was found to contain two redox domains that are homologous to microsomal cytochrome b5 (b5, encoded by Cyb5A) at the N terminus and cytochrome b5 reductase (b5R, encoded by Cyb5R3) at the C terminus. These two domains are connected by a hinge domain, which contains a well conserved CHORD and SGT1 (CS) motif [2]. Similar to other b5 and b5R proteins, the b5 domain of Ncb5or contains heme, and the b5R domain has flavin-adenine dinucleotide (FAD) and NAD(P)H binding domains [3; 4]. Unlike their single-domain homologs, however, Ncb5or has no known membrane anchor. A recent study from our laboratory provides the x-ray crystal structure of the b5 domain of Ncb5or, revealing a unique heme environment compared to that in other members of the b5 superfamily [5].

Ncb5or in animals is a unique protein family because it is the first example of a natural fusion protein of b5, CS and b5R domains found in animals. It is a soluble protein associated with ER [6] and able to reduce cytochrome c, methemoglobin, ferricyanide and molecular oxygen *in vitro*. Its low redox potential, -0.108 V at the heme center [6] makes it a more potent electron donor than Cyb5A, whose redox potential is around 0 V [7; 8].

There is one functional Ncb5or gene in each animal, although a pseudogene has been found in mouse and rat genomes. All Ncb5or genes have 16 exons with conserved splicing sites. Interestingly, rat and mouse also generate a splice variant of Ncb5or, which is highly expressed in testis, brain and skeletal muscle [9]. This splice variant is considered to be a dominant negative form because it lacks the entire exon 12, which encodes the FAD binding site [9]. Promoter batching studies showed that the 5' UTR regions at 216-157 bp and 60-30 bp upstream of the transcription start site are the two most important regions for the promoter activity [10]. In addition, a consensus ARE (antioxidant-response element) was found in the Ncb5or promoter region, suggesting a potential role of Ncb5or in antioxidant response [11].

1.1.2 Cytochrome b5 and its cognate reductase

Cytochrome b5 is a ubiquitous heme protein involved in numerous cellular processes. It has two isoforms in mammals, microsomal cytochrome b5 (Cyb5A) and outer mitochondrial cytochrome b5 (Cyb5B) [12]. Cyb5A can form a complex with its cognate reductase, Cyb5R3, in the ER membranes, which has been shown to function as an electron donor of Δ^9 stearoyl-CoA desaturase (SCD) *in vitro* to reconstitute fatty acid desaturation [13-15]. Genetic studies of human patients with methemoglobinemia show that soluble forms of Cyb5A and Cyb5R3 proteins are responsible to reduce methemoglobin to hemoglobin [16; 17].

Cyb5A can also modulate cytochrome P450 activity, which is involved in a number of processes including cholesterol, steroid hormone, exogenous xenobiotics and drug metabolism *in vitro* [18- 22] and *in vivo* [23]. In the latter case, hepatic b5 null

(HBN) mice , in which Cyb5A is disrupted specifically in hepatocytes, showed a major P450-dependent defect in drug and chemical metabolism [23]. However, no fatty acid desaturation defect was observed due to the similarity between these mice and wild-type (WT) littermates in hepatic lipid profiles [23] and SCD activity (H. Zhu, unpublished data). Subsequently, a global Cyb5A null mouse model (BCN) was also generated, and their liver phenotype further supported the role of Cyb5A in drug metabolism *in vivo* [24]. BCN mice also showed 10-fold higher levels of methemoglobin in red blood cells and a minor SCD defect in total hepatic lipids compared to WT [25]. Cyb5B is located in outer-mitochondrial membrane. It was found to play a role in androgen synthesis in Leydig cells [26]. However, its biological function is still not fully understood.

Cytochrome b5 reductase (Cyb5R3) is a member of ferredoxin: $NADP^+$ reductase superfamily and contains well conserved FAD and NAD(P)H binding sites [4]. Cyb5R3 has been found to localize in ER and mitochondria to reduce both Cyb5A and Cyb5B [27]. More than thirty missense mutations in Cyb5R3 gene have been identified in methemoglobinemia patients [28], but none in other diseases.

1.1.3 Ncb5or$^{-/-}$ mouse model

The biological function of Ncb5or was revealed in 2004 by the phenotypes of Ncb5or$^{-/-}$ mouse. A majority of these mice started to develop diabetes around 7 weeks of age [29], and they were more sensitive to diabetogenic agent streptozotocin (STZ) [30]. Notably, the insulin sensitivity in these Ncb5or$^{-/-}$ mice was not altered [29]. Due to the normal insulin sensitivity and lack of lymphocyte infiltration, the diabetes mellitus in Ncb5or$^{-/-}$ mice does not belong to either type 2 or autoimmune mediated type 1diabetes.

Instead, it is similar to maturity onset diabetes in the young (MODY) in the sense that these subtypes of diabetes are caused by mutations in a single gene to alter the beta-cell function [31; 32]. Screening of human patients with non-inflammatory diabetes, such as MODY and Type 2 diabetes, failed to identify mutations in Ncb5or gene [33].

Our most recent work shows that beta cell dysfunction and loss in Ncb5or$^{-/-}$ mice is associated with fatty acid overload, oxidative and ER stress [34]. The onset of diabetes is delayed by two weeks in mice that lack both Ncb5or and Chop, a key gene involved in ER stress-induced cell death [35], or accelerated by two weeks on an alloxan-sensitive (ALS) genetic background [34]. A high-fat (HF) diet accelerates the onset of diabetes by 2-3 weeks in Ncb5or$^{-/-}$ mice through exacerbating ER stress in beta cells of these mice (W.F.Wang, unpublished data).

The other major phenotype of Ncb5or$^{-/-}$ (knockout, KO) mice is lipoatrophy. These mice had significantly lower body weight and smaller white adipose tissues (WAT) than WT [36]. Since diabetes is known to increase fatty acid catabolism due to deficiency in glucose metabolism, lipoatrophy could be caused by diabetes directly or by a diabetes-independent source. To dissect these two possibilities, Ncb5or$^{-/-}$ mice were transplanted with WT islets to prevent the development of diabetes. These transplanted KO (TKO) mice had similar fasting blood glucose levels and glucose tolerance as WT, but still developed lipoatrophy. This evidence strongly suggests that lipoatrophy is independent of diabetes [36].

Besides the loss of WAT, TKO mice also had lower lipid content and impaired Δ^9 fatty acid desaturation in liver than WT [36], indicating the role of Ncb5or in Δ^9

desaturation *in vivo*. Our recent studies show that Ncb5or$^{-/-}$ hepatocytes are more susceptible than WT to SFA, not MUFA, with increased ER and cell death [35; 36]. Moreover, cytotoxicity of saturated fatty acid (SFA) and ER stress are attenuated by co-treatment with monounsaturated fatty acid (MUFA) [35; 36]. Both *in vivo* and *in vitro* evidence leads us to hypothesize that Ncb5or plays an important role in fatty acid desaturation (Figure 1.1).

1.1.4 Fatty acid Δ^9desaturation

Δ^9 fatty acid desaturation is important for triacylglycerol (TAG) synthesis [37], skin permeability and early liver and skin development [38]. This SCD pathway converts palmitic acid (C16:0) and stearic acid (C18:0) to palmitoleic acid (C16:1) and oleic acid (C18:1), respectively (Figure 1.1). So far, four SCD isoforms (SCD1-SCD4) have been identified in rodents [39]. SCD1 colocalizes with diacylglycerol acyltransferase 2 (DGAT2, discussed below), which is a rate-limiting enzyme in TAG synthesis [40].

Global SCD1 null mice are lean and protected from high-fat induced obesity [41]. Surprisingly, hepatic SCD1 null mice are protected from high-carbohydrate diet rather than high-fat diet induced obesity [42], indicating that hepatic SCD1 is mainly responsible for carbohydrate induced lipid synthesis. Although hepatic SCD1 is more involved in carbohydrate induced *de novo* lipogenesis, primary hepatocytes treated with SCD1 inhibitor were found to have increased apoptosis and cell death in response to palmitate [43], which suggests that SCD1 is also important for exogenous SFA metabolism for hepatocytes *per se*. In comparison, SCD2 has been shown to be crucial

for Δ^9desaturation in early development [38]. Since SCD2 null mice die shortly after birth due to skin permeability, the role of SCD2 in the adult stage still remains unknown.

SCDs have no intrinsic Cyb5A-like domain. This is different from Δ^5, Δ^6 desaturases (FADS), which function in inflammatory and immune response [44] and have a Cyb5A-like domain fused to a desaturase domain [45; 46]. This suggests that SCD relies on separate electron donors. Cyb5A and Cyb5R3 have long been considered as electron donors of SCD [15] with electrons flowing from NADH to FAD (in Cyb5R3) to heme (in Cyb5A) and then to the iron center in SCDs for desaturation of fatty acids (Figure 1.1). However, BCN and HBN mice display mild or no defect in fatty acid desaturation [23; 25] suggesting that Cyb5A, along with its cognate reductase, is not an exclusive electron donor for SCDs. Prediabetic Ncb5or KO mice display a more severe defect in fatty acid desaturation than the Cyb5A KO mice, we thus hypothesize that Ncb5or functions as an alternative electron donor for SCDs *in vivo*.

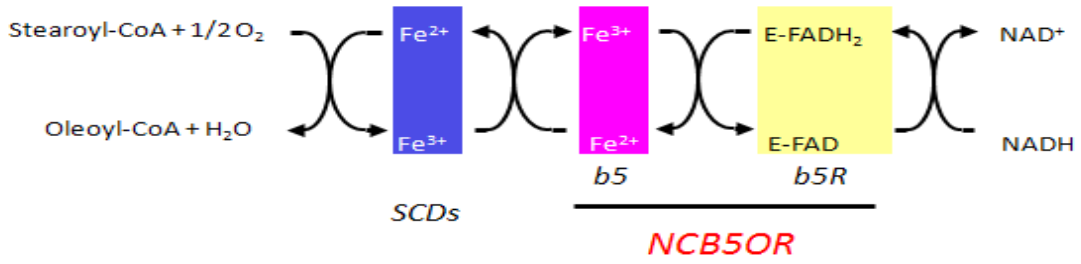

Figure 1.1 Overview of Δ^9 fatty acid desaturation. Ncb5or contains two redox domains that are homologous to microsomal Cyb5A (b5) and Cyb5R3 (b5R). We hypothesize that Cyb5A/Cyb5R3 and Ncb5or can serve as electron donors for stearoyl-CoA desaturase (SCD). SFA can be converted to MUFA by SCD, and electrons flow from NADH to FAD in b5R, to heme in b5 and then to iron in SCDs.

1.2 Fatty acid metabolism

Obesity affects more than 20% of the population in the Unites States [47] and has become a major health issue in the past 20 years. Obesity increases the risk of coronary heart disease, type 2 diabetes, cancers, hypertension, stroke, and fatty liver [48]. One major cause for these diseases is the significant increase in caloric intake and saturated fat content of an average Western diet, especially fast food. Based on these facts, a better understanding of fatty acid metabolism becomes increasingly important and can provide insight for potential intervention.

1.2.1 Fatty acid metabolism pathways

Fatty acids are categorized into three groups based on the number of double bonds in the hydrocarbon chain: saturated fatty acid (SFA), monounsaturated fatty acid (MUFA) and polyunsaturated fatty acid (PUFA) [49]. They can also be grouped on the basis of chain length to short-chain (fewer than 8 carbons), medium-chain (8-12 carbons), long-chain (14-22 carbons), and very-long-chain (24 carbons or longer) fatty acids. SFA and MUFA come from both diets and *de novo* synthesis, whereas PUFAs only from diets.

Dietary lipids contain mainly TAG with some free fatty acids (FFA) and cholesterol. These lipids are hydrolyzed by pancreatic lipases to monoacylglycerols and long-chain free fatty acids in the intestinal lumen. These fatty acids then enter enterocytes in the intestine and are resynthesized into diacylglycerol (DAG), TAG and cholesterol esters. They are packaged with apolipoprotein B to form lipoprotein particles, mainly as chylomicrons and very low-density lipoprotein (VLDL) particles, to enter the circulation via the lymph system. At tissue sites, such as liver and WAT, they are hydrolyzed to

release fatty acids by lipoprotein lipases (LPL). Upon entering cells through fatty acid transporters (FATPs), fatty acids are either bound by fatty acid-binding proteins (FABPs) and remain as free fatty acids (FFA), or be activated to CoA esters by long-chain fatty acid-CoA ligases (ACSLs) for re-esterification or fatty acid oxidation (Figure 1.2).

In lipogenic cells, such as hepatocytes and adipocytes, activated fatty acids can be re-esterified into phospholipids and TAG. Phospholipids (PL) are major constituents of membranes and signal transduction whereas TAG is a major lipid form for energy reserve, especially in adipose tissues. In the latter, some SFAs need to be converted into MUFAs by stearoyl-CoA desaturase (SCD) for further processing. During the TAG or PL synthesis (Figure 1.3), glycerol-3-phosphate is first acylated to form lysophosphatidic acid (LPA) by glycerol-3-phosphate acyltransferase (GPAT) [50]. Then phosphatidic acid (PA) is formed by acylation of LPA by acylglycerol-3-phosphate acyltransferase (AGPAT). PA is then converted by phosphatidic acid phosphohydrolase (LIPIN) into DAG [51], which can form TAG by diacylglycerol acyltransferase (DGAT) [52].

The major form of fatty acid oxidation is β-oxidation, which mainly occurs in mitochondria of skeletal and cardiac muscle. Acyl-CoA in cytosol is conjugated to carnitine by carnitine palmitoyltransferase (CPT), and then shuttled into mitochondria for β-oxidation. Acetyl-CoA, a major product of β-oxidation, can enter the tricarboxylic acid (TCA) cycle to generate NADH and $FADH_2$, which then enter the electron transport chain (ETC) and oxidative phosphorylation to generate ATP.

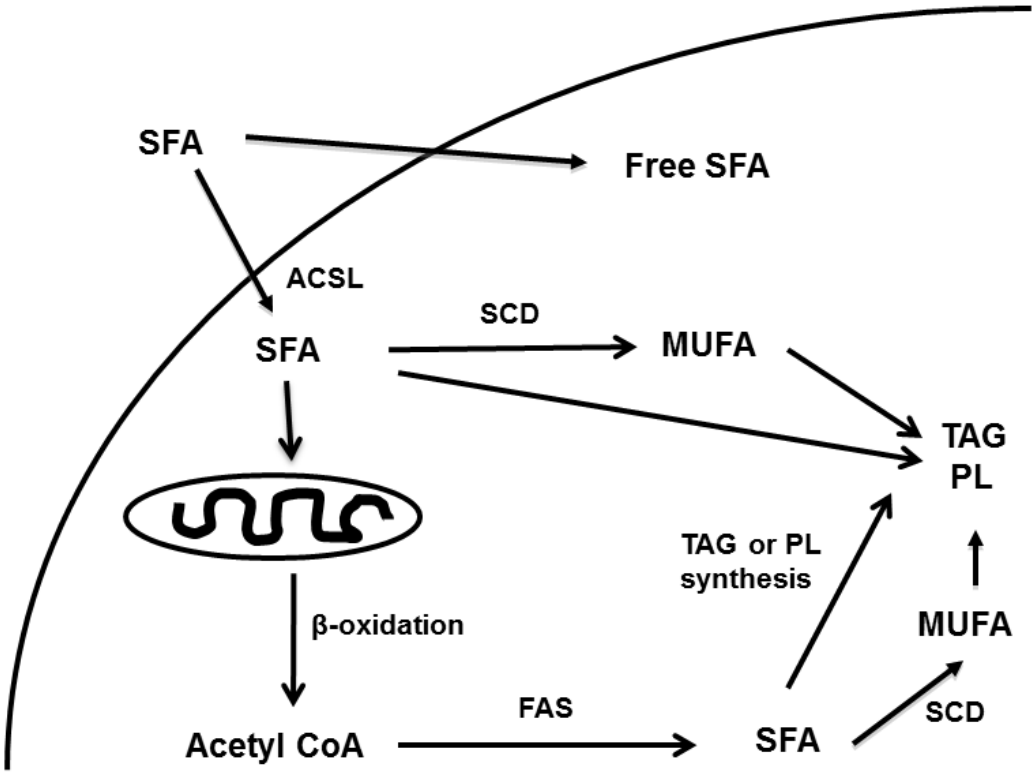

Figure 1.2 Schematic diagram of cellular metabolism of saturated fatty acids (SFA). After SFA enters the cell, it can either stay as free SFA or be activated to its CoA esters by long-chain fatty acid-CoA ligases (ACSLs). The SFA-CoA can be oxidized to acetyl-CoA through β-oxidation for energy or be re-esterified into phospholipids and TAG. Moreover, acetyl-CoAs can be utilized as substrate for *de novo* fatty acids synthesis by fatty acid synthase (FAS) to generate SFA. Both dietary and *de novo* synthesized SFA can be further converted to MUFA through SCD before entering TAG or PL pool.

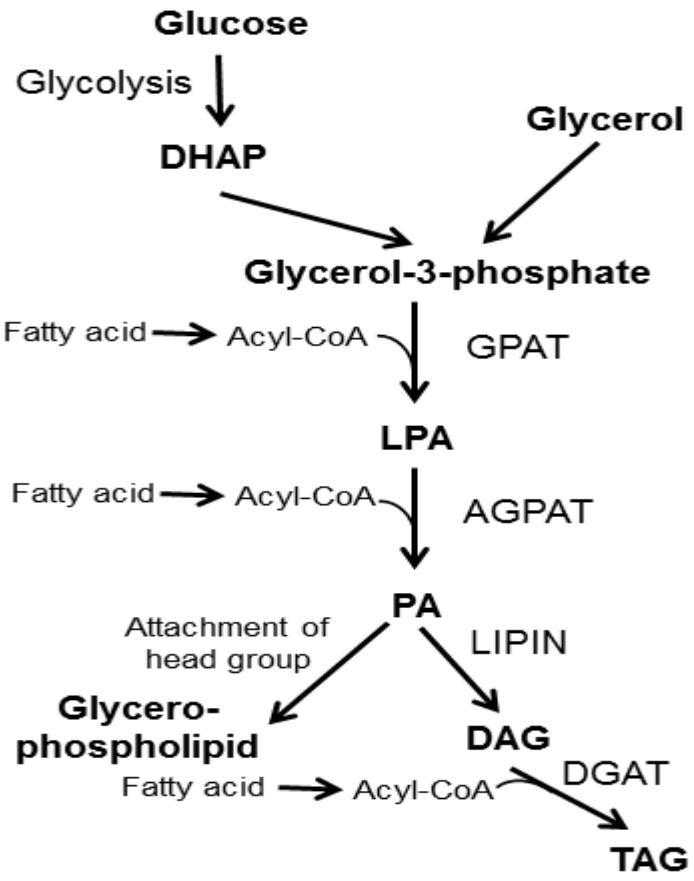

Figures 1.3 Overview of lipid synthesis. Glycerol-3-phosphate from either dihyodroxyacetone phosphate (DHAP) or glycerol is acylated to form lysophosphatidic acid (LPA) by glycerol-3-phosphate acyltransferase (GPAT). Then acylglycerol-3-phosphate acyltransferase (AGPAT) acylates LPA to phosphatidic acid (PA), which can be either further converted to glycerophospholipid by adding head groups or to diacylglycerol (DAG) by phosphatidic acid phosphohydrolase (LIPIN). Finally, TAG can be synthesized by diacylglycerol acyltransferase (DGAT) through acylating DAG. LPA, PA, glycerophospholipid and DAG can serve as signaling molecules. TAG is mainly used for energy reserves.

Fatty acids can come from *de novo* synthesis in the cytosol. The building block is acetyl-CoAs, which is generated from carbohydrates, fatty acid and other nutrients. Acetyl-CoAs are first carboxylated to malonyl-CoA by acetyl-CoA carboxylase (ACC). Then malonyl-CoA and acetyl-CoA can synthesize palmitate (C16:0), one species of SFA, by fatty acid synthase (FAS). Notably, malonyl-CoA is also an inhibitor for CPT by allosteric effect to decrease the β-oxidation rate to prevent futile cycling between β-oxidation and fatty acid synthesis. Both dietary and *de novo* palmitate can be further converted to MUFA through Δ^9 desaturation pathways by the SCD or elongated to SFAs of longer lengths for different metabolic fates.

MUFAs are preferred substrates of TAG synthesis, although both SFAs and MUFAs can be used. This is suggested by the fact that TAGs contain more MUFAs than SFAs [41] and that TAG synthesis is highly dependent on the expression of SCD [37]. Similarly, both SFAs and MUFAs can be used in β-oxidation to generate acetyl CoAs. SFAs have been shown to cause lipotoxicity [53], which can be alleviated by MUFA through channeling intracellular SFA into the TAG pool, a much less toxic fatty acid form [54]. These observations indicate that SFA and MUFA are metabolized differently by cells and that the regulation of these metabolic fates is critically important.

1.2.2 Regulation of fatty acid metabolism

Lipid homeostasis is well controlled in the body. Under a fed state, the liver helps to synthesis TAGs and package them into lipoprotein particles for delivery to adipose TAG pool, in parallel to similar action in adipose tissues. Under fasting or after exercise, TAG in the adipose tissues is hydrolyzed by lipases including hormone-sensitive lipase

(HSL) and adipose triglyceride lipase (ATGL). The products, free fatty acids and glycerol, then enter circulation to other tissues as sources of energy.

Fatty acid oxidation is stimulated by fasting. One regulator of this process is 5' AMP-activated protein kinase (AMPK), which plays a key role in cellular energy homeostasis. When the AMP:ATP ratio within the cell increases (indicating a need for ATP or energy), AMP will bind to AMPK γ subunit to change the conformation of AMPK. This results in exposing the active site (Thr-172) of the α subunit for phosphorylation by upstream kinase, Serine/threonine kinase 11 (LKB1) [55-57]. Upon activation, phosphorylated AMPK inactivates ACC [58], which in turn decreases levels of malonyl-CoA and its inhibition on CPT. As a result, more fatty acids are transported by CPT into the mitochondria, which increases the rate of β-oxidation.

PGC1α is a transcriptional coactivator that is involved in mitochondrial biogenesis, utilization of energy substrates like fatty acids and cellular respiration induction. For example, nuclear respiratory factor 1 and 2 (NRF1 and NRF2, respectively) are two downstream targets of PGC1α [59], which are essential for mitochondrial DNA replication, maintenance and transcription [60; 61]. They also play important roles in regulating expression of genes that are involved in mitochondrial ETC and maintaining proper mitochondrial function [62; 63]. Recently, NRF1 is found to bind antioxidant response element (ARE) to induce antioxidant enzymes [64].

PGC1α exerts its function by interacting and coactivating a variety of genes including peroxisome proliferator-activated receptor α (PPARα), γ (PPARγ) and δ or β (PPARδ/β). PPARs are a group of nuclear receptors that function as transcription factors

to regulate the expression of downstream targets involved in lipid or carbohydrate metabolism, cellular differentiation and development [65]. Upon activation, they heterodimerize with retinoid X receptor (RXR) and then bind to specific peroxisome proliferator response elements (PPREs) in promoter region of target genes [66]. PPARα is mainly expressed in the liver, heart and skeletal muscle. It can be activated by a wide range of SFA and MUFAs [67] and induce pathways of β-oxidation [67; 68]. Recently, it was found to be a dominant regulator for dietary fatty acid induced hepatic gene expression [69]. PPARγ is primarily expressed in adipose tissue to regulate adipocyte differentiation and lipogenesis [70] and PUFAs are preferred natural ligands of PPARγ [71]. PPARδ/β is ubiquitously expressed in most tissues including livers, and similar to PPARα, is induced by fatty acids to regulate fatty acid oxidation [71]. Recent data suggest that PPARδ/β, rather than PPARα, is responsible for sensing plasma FFA in liver [72] and that fatty acid activation enzyme, ACSL3, is a downstream molecular target [73].

Sirtuin (SIRT1) is another key regulator of PGC1α. SIRT1 is a nuclear NAD^+-dependent protein deacetylase. It senses NAD^+/NADH ratio, and is activated by increased intracellular level of NAD^+ [74]. Upon activation, it deacetylates PGC1α [75]. AMPK is also involved in inducing SIRT1 activity by increasing cellular NAD^+ levels through activating fatty acid oxidation [76]. Moreover, AMPK-dependent phosphorylation of PGC1α is required for deacetylation by SIRT1 [76], further supporting the role of AMPK in energy homeostasis. PGC1α can be induced by other stimuli including reactive oxygen species (ROS) [77] and p38 mitogen-activated protein kinases (p38 MAPK), a stress sensor [78]. In conclusion, AMPK, PPARs and PGC1α play essential roles in the maintenance of energy balance, especially lipid metabolism.

1.3 Lipotoxicity

Fatty acid metabolism is well balanced and regulated under physiological states. However, when the intake of fatty acids is much greater than the usage, excess lipids accumulate in both adipose and non-adipose tissues, including liver, heart, pancreas and muscle, resulting in obesity. A balanced fatty acid metabolism is critical for energy homeostasis, membrane structure and intracellular signaling. Over-accumulation of free fatty acids will impair cell function and even cause cell death [79], a phenomenon called "lipotoxicity".

Among all fatty acids, free SFA is considered the most toxic one. SFA can induce C-jun N-terminal kinase (JNK) dependent apoptosis in the cells by activating proapoptotic proteins Bcl-2-associated X protein (Bax), leading to mitochondrial membrane permeabilization, cytochrome *c* release, and caspase 3 and 7 activation [80]. This evidence suggests that apoptosis is one of the major ways for SFA-induced cell death, although the mechanism is still not fully understood.

There are several models of SFA-induced cytotoxicity. The first one is ceramide-mediated pathway. Ceramide is a lipid second messenger known to induce apoptosis. Palmitate is the major substrate for ceramide synthesis and accumulation of palmitate is found to increase *de novo* ceramide synthesis, resulting in apoptosis [81].

The second model is phospholipid remodeling. Under physiological conditions, phospholipids in the membrane have a well-balanced ratio of MUFA vs. SFA. However, accumulation of SFA has been found to lead to phospholipid remodeling, causing a

significantly decrease in the MUFA:SFA ratio [82]. As a consequence, membrane fluidity and function is disrupted, which leads to dysfunction of mitochondria [82].

The third one is oxidative stress. SFA has been shown to induce oxidative stress, which can impair membrane integrity, oxidize DNA and proteins and destroy organelles in the cells [83; 84]. Several possible causes of oxidative stress by SFA are 1) electron leakage from mitochondrial ETC as a result of increased β-oxidation rate; 2) mitochondrial dysfunction caused by membrane phospholipid remodeling, cytochrome c release and disruption of mitochondrial respiratory chain complex III; 3) increased NAPDH oxidase (NOX), which can generate superoxide upon induction by increased diacylglycerol (DAG) level generated from excess SFA [85].

The fourth model is ER stress. SFA can induce ER stress in various cell types [35; 86; 87], potentially due to remodeling of ER membrane lipids or ***via*** oxidative stress. In short, over-accumulation of lipids, especially SFA, is toxic to many cell types and leads to diseases such as diabetes and fatty liver.

1.4 Oxidative stress

1.4.1 Reactive oxygen species

Oxidative stress occurs when there is more generation of reactive oxygen species (ROS) than the removal by anti-oxidant defense. Superoxide (O_2^-), hydrogen peroxide (H_2O_2) and hydroxyl radicals ($HO^\cdot$) are three forms of ROS. O_2^- forms when oxygen is attacked by electrons and becomes partially reduced. Superoxide dismutase (SOD), such

as CuZn-SOD (SOD1) in the cytosol and Mn-SOD (SOD2) in mitochondria, dismutates superoxide to H_2O_2. At high concentrations, H_2O_2 is converted into H_2O by catalase, or at low concentrations, by glutathione peroxidase. When interacted by transition metals, such as Fe^{2+}, H_2O_2 will form hydroxyl free radicals ($HO^{\cdot}$), which is the most potent ROS. This process is called Fenton reaction [49].

ROS can be produced under diverse stimuli including pro-inflammatory cytokines [88], ultraviolet irradiation, nutrient metabolism, ER stress and microsomal cytochrome P450 reactions [89]. At physiological level, ROS can serve as signaling molecule involved in a variety of biological reaction including hormone and growth factor action [90], cell adhesion [91] and immune response [92]. However, high levels of ROS can oxidize DNA and lipids, generate irreversible oxidative modifications of proteins and persistently activate stress-sensing signaling pathways including mitogen-activated protein (MAP) kinase, c-Jun N-terminal kinase (JNK) and p38 MAP kinase [93], leading to apoptosis. In addition, high ROS can also impair mitochondrial membrane permeability, resulting in release of cytochrome *c* and apoptosis [94].

1.4.2 Cellular sources for ROS production

There are three main cellular sources of ROS production. The first one is NADPH oxidase (NOX). NOX is an enzyme that transfers electrons from NADPH to O_2 to generate O_2^- [95]. The reaction by NOX2, which is also called "respiratory burst enzyme", is most active in the plasma membrane of phagocytic cells to kill invading pathogens. A recent study suggests that most cells are able to generate intracellular ROS through NOX2 and other NOX isoforms [95]. For example, ROS can be generated by

NOX2 in skeletal [96] and cardiac muscle [97], NOX3 in hepatocytes [98] and NOX4 in adipocytes [99] in response to various hormones and fatty acids.

The second source of ROS is mitochondria. Mitochondria generate ATP by consuming NADH or $FADH_2$ through electron transport chain (ETC) and oxidative phosphorylation. In this pathway, electrons are transferred from NADH or $FADH_2$ to oxygen through complex I to IV to produce a proton gradient, which drives ATP synthesis or heat production through uncoupling. Even under normal physiological conditions, ROS can be generated through electron leakage from ETC by incomplete transfer in mitochondria [100]. Main sites of mitochondrial ROS production are complex I and III [89]. When metabolic load is high, active fatty acid β-oxidation and glucose flux will generate more NADH and $FADH_2$, resulting in greater ETC flux and proton gradient. If proton gradient cannot be dissipated by more ATP synthesis or heat production, electron leakage will increase significantly to generate more ROS. In addition, mitochondrial membrane dysfunction also increases the chance of electron leakage.

The third source is ER. Enzymatic formation of disulfide bonds during protein folding in ER is estimated to account up to 25% of total ROS generation [101]. More details about this will be described in section 1.4.

Besides these three main sources, peroxisome is also a potential source for ROS [102]. Fatty acid β-oxidation can also occur in peroxisomes especially for very long chain fatty acids. Because no ATP synthesis is coupled here, electrons are transferred to O_2, yielding H_2O_2 instead of generating the proton gradient [49]. H_2O_2 is then converted by catalase into O_2 and H_2O. If generation of H_2O_2 exceeds the capacity of catalase, ROS

level will increase. Acyl CoA oxidase (ACOX) is the peroxisome specific enzyme to catalyze the first oxidation step, which can be used as the marker for peroxisomal β-oxidation.

1.4.3 Antioxidant response

Antioxidant defense also plays an important role in redox homeostasis. Nuclear factor E2-related factor 2 (Nrf2) is a master transcription factor that regulates the antioxidant response. Under normal conditions, Nrf2 is rapidly degraded through Keap1-mediated ubiquitin-dependent proteasomal pathway as well. If oxidative stress increases, several critical cysteine residues in Keap1will be disrupted, inactivating ubiquitination of Nrf2 [103]. In addition, Nrf2 is inactive due to cytoplasmic retention by kelch like-ECH-associated protein 1 (Keap1). As a result, Nrf2 proteins accumulate in the nuclei and exert function. After translocating to the nuclei, Nrf2 can bind to antioxidant response element (ARE) in the promoter regions of downstream anti-oxidant genes, including NAD(P)H quinone oxidoreductase 1 (Nqo1), glutamate-cysteine ligase-catalytic subunit (Gclc), glutamate-cysteine ligase modifier subunit (GCLM), heme oxygenase 1 (HMOX1) and glutathione S-transferase (GST) [100], resulting in elevated expression of these genes and a more active antioxidant system.

There are three major natural antioxidants inside the cells [100]: 1) exogenous small molecule antioxidants, such as lipoic acid, vitamin C and E, which act as reducing agents; 2) endogenous low-molecular-weight antioxidants, namely, glutathione (described more below); and 3) small protein antioxidants, namely, thioredoxin and

glutaredoxin that help reduction of other proteins by forming disulfide bonds and are then reduced by thioredoxin reductase and glutathione, respectively.

Glutathione, a ubiquitous intracellular tripeptide (γ-L-glutamyl-L-cysteinyl-glycine), is one of the major antioxidants. Glutathione exists in two forms: thiol-reduced form (GSH) and disulfide-oxidized form (GSSG). GSH can convert H_2O_2 to H_2O by being oxidized to GSSG. This reaction is catalyzed by glutathione peroxidase (GPX) in a selenium-dependent fashion. Also, GSH can reduce organic peroxides by GPX and GST. The resulting GSSG in turn can be reduced back to GSH by glutathione reductase (GR) using NADPH as cofactor to complete a redox cycle. GSH is particularly important in the mitochondria to reduce H_2O_2 because no catalase exists inside mitochondria [104]. The cellular ability to reduce GSSG to GSH can be overwhelmed under oxidative stress. In this case, accumulation of GSSG happens, leading to high GSSG/GSH ratios. The excess GSSG can form a mixed disulfide (PSSG) by reacting with a protein sulfhydryl group (PSH) or be actively exported out of the cell to keep the intracellular redox equilibrium. As a result, cellular GSH will be eventually depleted under severe oxidative stress [105].

Besides small antioxidant compounds, cells also use enzymatic reactions to defend against oxidative stress. They include SOD, catalase, glutathione reductase, and glutathione peroxidase, as mentioned above, as well as the following three enzymes. 1) GCLC is one of the two subunits of glutamate-cysteine ligase (GLC), which is the first rate limiting enzyme of glutathione synthesis. GCLC has been reported to be induced by oxidative stress [106]. 2) Heme oxygenase 1 (HMOX1) is an essential enzyme to degrade heme into biliverdin, which is rapidly reduced to bilirubin by biliverdin reductase. Bilirubin can be oxidized back to biliverdin again to form a redox cycle, suggesting that

bilirubin is a strong antioxidant [107]. HMOX1 has been shown to be important in preventing oxidative stress due to the fact that heme is required for the synthesis of redox-active heme proteins, many of which can generate ROS, such as P450 and those in mitochondrial complex I-IV [108; 109]. 3) Metallothionein (MT) can bind both physiological and xenobiotic heavy metals through the thiol group of cysteine residues, thus preventing these metals from being used in the Fenton reactions that generate hydroxyl radical [110]. In my studies, expression levels of most of these genes were determined to evaluate cellular oxidative stress.

1.5 ER stress

Endoplasmic reticulum (ER) is a subcellular organelle and its major functions include lipid or protein synthesis, protein folding and trafficking, and Ca^{2+} storage. It has been reported that ER supported approximately one third of protein synthesis and modification for normal functions in a cell [111]. Also, ER provides a unique oxidizing environment for protein folding and modification. Only properly folded proteins are transported to the Golgi organelle. When unfolded or misfolded proteins accumulate in the lumen of the ER, the unfolded protein response (UPR), which is a major form of ER stress, will be activated.

UPR induces ER-associated degradation (ERAD) of misfolded protein, protein folding, mRNA degradation, inhibition of mRNA translation and ER expansion to preserve the function of ER. BiP (binding immunoglobulin protein, also named as GRP78) is an ER chaperone protein for protein folding which also plays a key role in sensing and

regulating the UPR [112]. Under normal conditions, BiP binds to three UPR sensors: protein kinase-like endoplasmic reticulum kinase (PERK), inositol requiring protein 1α (IRE1α) and activating transcription factor 6 (ATF6). If ER stress is induced, some or all three of these sensors will be released from BiP and become activated. Once activated, IRE1α can splice the X-box binding protein 1 (XBP1) transcript to a spliced form, which encodes active XBP1a protein [113]. IRE1α/XBP1 signaling can activate a group of UPR genes, including chaperones, catalysts of folding, and ERAD genes to reduce ER stress. IRE1α also has RNase activity and degrades mRNAs to reduce the load of the ER [114]. Activated ATF6 can increase the induction of several UPR genes to catalyze the protein folding and degradation [115]. PERK, once activated, can phosphorylate its major substrate, eukaryotic initiation factor 2 α-subunit (eIF2α), to inhibit eIF2β activity and decrease the rate of most of mRNA translations [116; 117].

Besides inhibiting the global translation to reduce the ER load, phosphorylation of eIF2α can increase the rate of translation of activating transcription factor 4 (ATF4). ATF4 is a transcription factor to induce expression of genes involved in ERAD, anti-oxidative stress response, amino acid metabolism, ER oxidoreductin 1 (Ero1), NF-κB, growth arrest and DNA damage 34 (GADD34), and CCAAT/enhancer binding protein (CHOP) [112; 118; 119]. CHOP is important for ER stress induced cell death [120; 121; 122]. Furthermore, Nrf2 is a downstream target for PERK [123], suggesting that ER stress and antioxidant capacity are functionally associated.

All these UPR pathways can attenuate ER stress by decreasing the ER work load. However, when these pathways are overwhelmed, cell death will be induced, possibly via apoptosis [124]. Four possible apoptosis pathways are mediated by CHOP, JNK signaling,

Bax, and NF-κB [125-127], and all are activated by excess or prolonged ER stress and trigger apoptosis.

Oxidative formation of disulfide bonds is part of protein folding process and occurs in ER. It requires an oxidizing environment in the ER lumen in contrast to the reducing environment in cytosol [128]. When two cysteines form a disulfide bond, two electrons will be freed. They are first transferred to protein disulfide isomerase (PDI) , then to Ero1, and lastly to O_2 to generate ROS [129]. A high demand for the processing of nascent proteins, especially those rich in disulfide bonds, such as insulin, increases ROS production in ER. It can be further exacerbated when GSH is consumed by protein disulfide isomerase mediated-refolding. Furthermore, Ca^{2+} can be released from ER, its major storage site, when ER is disrupted by ROS or ER stress. Since Ca^{2+} can enhance TCA cycle and stimulate the release of cytochrome c from mitochondria, ER stress can cause greater ROS production in mitochondria through a more active ETC flux and the perturbation of ETC [130; 131]. On the other hand, oxidative stress may cause protein misfolding, which leads to ER stress. All these findings support the fact that ER stress and oxidative stress are tightly connected.

1.6 Significance

Our study of Ncb5or$^{-/-}$ mouse model suggests that Ncb5or plays an important role in the utilization and metabolism of exogenous SFA and that Ncb5or protects cells from SFA-induced oxidative stress and cellular damage. Our study will provide a better understanding of the cellular mechanism of exogenous fatty acids, which will be applied

to the prevention and the treatment of lipotoxicity, diabetes, oxidative stress, and related diseases.

1.7 Research questions

My main research goal is to fill the knowledge gap in our understanding of the role of Ncb5or in fatty acid metabolism and redox homeostasis.

Ncb5or$^{-/-}$ mice receiving WT islet transplants display impaired fatty acid Δ^9 desaturation in the livers at age 12 weeks, but the mechanism is unclear [36]. I will incorporate both prediabetic mouse model and primary hepatocytes to examine the role of Ncb5or in fatty acid metabolism. The functional relationship between Ncb5or and Cyb5A will be investigated in pilot experiments.

Ncb5or null hepatocytes have increased cell death under SFA treatment, possibly from increased ER stress, and the SFA cytotoxicity could be attenuated by co-treatment with MUFA [35; 36]. I will further investigate the underlying mechanism of how SFA causes Ncb5or$^{-/-}$ hepatocyte death and how MUFA rescues the cells from cytotoxicity.

My overall goal is to reveal the physiological function of Ncb5or and provide new knowledge for finding therapeutic targets or effective treatments to obesity and oxidative stress related diseases, including diabetes, atherosclerosis and neurodegenerative diseases.

Chapter 2

The role of Ncb5or in fatty acid metabolism

2.1 Abstract

The endoplasmic reticulum (ER)-associated NADH cytochrome b5 oxidoreductase (Ncb5or) is widely distributed in animal tissues. Ncb5or null mice develop diabetes at age 7 weeks and have increased susceptibility to the diabetogenic agent streptozotocin. Ncb5or deficiency also results in lipoatrophy and increased sensitivity of hepatocytes to cytotoxic effects of saturated fatty acids. Here we investigate the mechanisms of these phenomena in prediabetic Ncb5or$^{-/-}$ mice and find that, despite increased rates of fatty acid uptake and synthesis and elevated levels of expression of stearoyl-CoA desaturase (SCD), Ncb5or $^{-/-}$ liver accumulates less triacylglycerol (TAG) than wild-type (WT). Ncb5or$^{-/-}$ hepatocytes readily incorporate exogenous fatty acids into TAG but accumulate more free fatty acids (FFA). A high-fat diet rich in palmitate and oleate stimulates both lipogenesis and fatty acid catabolism in Ncb5or $^{-/-}$ liver, resulting in similar intracellular TAG levels but greater FFA accumulation compared to WT. In consideration of the 8-fold increase in Scd1 mRNA and protein levels, hepatic SCD specific activity is lower in Ncb5or$^{-/-}$ mice than WT. Together, these findings suggest that increased FFA accumulation and catabolism are major consequences of Ncb5or deficiency in liver.

2.2 Introduction

NADH-cytochrome b5 oxidoreductase (Ncb5or) is an endoplasmic reticulum (ER)-associated protein that has been implicated in lipid metabolism and diabetes. The Ncb5or null (KO) mouse model has two major phenotypes. These mice develop diabetes around 7 weeks of age with similar insulin sensitivity as WT [29].

Ncb5or KO mice also display lipoatrophy with significantly lower body weight and smaller white adipose tissues (WAT) than WT despite similar food intake [36]. The lipoatrophy was later found to be independent of diabetes and accompanied by impaired Δ^9 fatty acid desaturation in Ncb5or$^{-/-}$ livers [36], indicating the role of Ncb5or in desaturation *in vivo*. The lipoatrophy phenotype is similar to the one in the SCD1 null mouse model that is lean and protected from obesity induced by a high-fat diet [41]. In addition, Ncb5or null hepatocytes were found to be more sensitive to SFA cytotoxicity, but not MUFA, by increased ER stress, apoptosis and cell death [35; 36]. Moreover, the SFA cytotoxicity and ER stress in these cells was attenuated by co-treatment with MUFA [35; 36]. Both *in vivo* and *in vitro* evidence led to the hypothesis that Ncb5or plays an important role in fatty acid desaturation pathway.

Microsomal Cyb5A and Cyb5R3 serve as electron donors to Δ^9 stearoyl-CoA desaturase (SCD) to facilitate the fatty acid desaturation *in vitro* [13-15]. However, mouse models with global or hepatic microsomal cytochrome b5 deficiency exhibit only mild or no Δ^9 desaturation defect in the total lipids [25; 132], based on the evidence of similar SCD activity (unpublished data) and lipid profiles in the livers [132]. These findings strongly suggest that Cyb5A and Cyb5R3 are not exclusive electron donors for SCDs. Due to genetic similarity, functional property and more severe fatty acid desaturation defects in Ncb5or KO mice, we considered Ncb5or as an alternative electron donor for SCDs *in vivo*.

To clarify the role of Ncb5or in fatty acid metabolism, we determined early molecular events in liver of prediabetic Ncb5or$^{-/-}$ mice and employed primary hepatocytes to examine the metabolism of exogenous SFA in Ncb5or null cells. We also

used mouse models that lack Ncb5or or Cyb5A or both genes to dissect the different roles of Ncb5or and Cyb5A as electron donors for SCD *in vivo*. We find that, starting early in neonatal development, livers from Ncb5or null mice express higher levels of transcripts than WT for genes in fatty acid uptake, synthesis, activation and desaturation, as well as mitochondrial biogenesis, suggesting futile fatty acid cycling. Ncb5or$^{-/-}$ hepatocytes accumulate more SFA in both TAG and FFA pools under SFA treatment, suggesting an important role of Ncb5or in fatty acid metabolism and Δ^9desaturation pathway.

2.3 Methods

2.3.1 Mouse models

Ncb5or null mouse in BALB/cAnN strain was generated by deleting exon 4 of Ncb5or gene, which results in a non-functional truncated Ncb5or [29]. Ncb5or null mouse in C57BL/6 strain, obtained from Jackson laboratory, was generated using a strategy of outcross and then backcross to C57BL/6 for more than 10 generations. Ncb5or null and WT mice were generated from heterozygous crosses and maintained in a pathogen-free facility at 24°C under a standard 12 hour light and 12 hour dark cycle with free access to food and water.

Hepatic b5 (Cyb5A) null mice (HBN) were generated by crossing albumin (ALB) Cre driver with Cyb5A floxed line, which was obtained from Dr. Roland Wolf [132]. We also generated a double knock-out (DKO) mouse model, which is deficient in Ncb5or (global) and Cyb5A (hepatic specific), through the following scheme. Ncb5or heterozygous (Ncb5or $^{+/-}$, b5 $^{+/+}$) mice were first crossed with HBN mice (Ncb5or $^{+/+}$, b5

$^{lox/lox}$, Cre^{ALB}) to generate first stage mice ($Ncb5or^{+/-}$, $b5^{+/lox}$, Cre^{ALB}). Then by crossing within these first stage mice, male breeding mice ($Ncb5or^{+/-}$, $b5^{lox/lox}$, Cre^{ALB}) were generated and bred with female mice ($Ncb5or^{+/-}$, $b5^{lox/lox}$) to generate DKO mice ($Ncb5or^{-/-}$, $b5^{lox/lox}$, Cre^{ALB}). Genotyping of WT and mutant alleles of Ncb5or and Cyb5A was performed by PCR with allele-specific primers (Figure 2.1).

All the mice in my experiments were pre-diabetic male mice in C57BL/6 strain of age 4-5 weeks. Blood glucose levels were measured to make sure that mice were non-diabetic before use, unless otherwise indicated. The experimental protocol was approved by the Institutional Animal Care and Use Committee at the University of Kansas Medical Center. Standard rodent chow (Purina 5015 from LabDiet, St. Paul, MN or TD 8604 from Harlan Teklad, Madison, WI) was used in all studies, except the 10-day high-fat diet feeding protocol in which the high-fat diet (F5194 from BioServ, Frenchtown, NJ) was initiated immediately after weaning and continued for ten days. The 5015 chow diet contains 3.8 kcal/g, 11% fat content (by weight), and a composition of 33% SFA, 35% MUFA and 32% PUFA, all of which are in the form of TAG. The high-fat diet contained 5.1 kcal/g, 35% fat by weight, anda composition of 40% SFA, 50% MUFA and 10% PUFA. Mice were sacrificed after 4-6 hours fasting, and plasma and tissues were collected, flash frozen in liquid nitrogen, and stored at -80^{o}C until use. Glucose levels were measured using OneTouch Ultra glucometer (LifeScan, Milpitas, CA).

2.3.2 Hepatocytes isolation and fatty acid treatment.

Four week-old $Ncb5or^{-/-}$ and WT mice were used for hepatocyte isolation after a 3-4 hour fasting to minimize dietary effect. These mice were anesthetized using Avertin

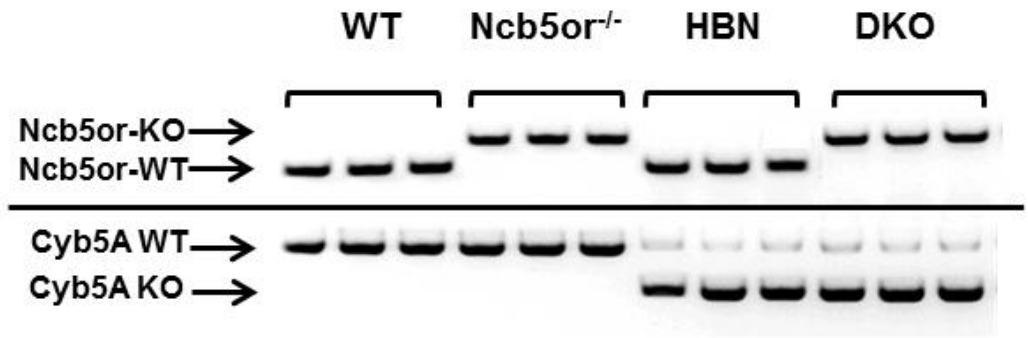

Figure 2.1 Genotyping for livers of WT, HBN, Ncb5or$^{-/-}$ and DKO mice by PCR. Genomic DNA was extracted from liver samples and PCR was performed to detect Ncb5or KO allele and cre-excised Cyb5A loxP allele. The products of KO and WT alleles in Ncb5or gene are 300-bp and 450-bp, respectively, as indicated by arrows. Primers for Cyb5A excised and non-excised loxP/loxP alleles generated around 800-bp and 500-bp products, respectively. The weak Cyb5A WT bands in the liver samples from HBN and DKO mice indicated the existence of small percentage of non-hepatocytes cells in these liver samples. The liver-specific excision of floxed exons 2-5 in Cyb5A is achieved through the use of a Cre transgenic line, whose expression is under the control of an albumin promoter.

by IP injection (0.02ml/g). Then, the viscera of the mouse were exposed by making a ventral incision. A catheter (24g x 1" IV type, Fisher) was inserted into vena cava before perfusion. The portal vein was severed immediately after the perfusion, and the thoracic vena cava was clamped. The perfusion speed was approximately 6 ml/minute. Mouse hepatocytes were isolated by a two-step perfusion procedure using Perfusion Solution I (0.5 mM EGTA, and 5.5mM glucose in HBSS) and Perfusion Solution II (1.5 mM $CaCl_2$, 5.5 mM glucose, with 0.0375% collagenase in HBSS), respectively.

After isolation, hepatocytes were incubated at 37^o C in a humidified atmosphere (5% CO2, 95% air) in nutrient rich Williams' medium E (Invitrogen,) containing penicillin /streptomycin, glutamine and 10% fetal bovine serum (FBS). Hepatocytes were plated into 6 well plates (Corning 3506) with 0.3 million cells per well, or into 96 well plates (Corning 3610) with 12,000 cells per well, or other plates with cell numbers mentioned below.

Fatty acids (in acid form) were complexed with bovine serum albumin (BSA) to avoid non-physiological toxic effects of free fatty acids during treatment. Palmitic acid (C16:0) and oleic acid (C18:1) were dissolved in 1M Tris-HCl (pH 8.0) with 2.1 mM FFA-free BSA [133]. The stock solution was first sonicated and then stirred in 37°C water bath overnight under nitrogen atmosphere to prevent oxidation. The final molar ratio of fatty acid to BSA was lower than 4. The fatty acid solution was adjusted to pH 8.0 with NaOH, and filtered through a 0.2 μm filter. The final concentration of fatty acid was measured using a non-esterified fatty acid C kit (Wako Chemicals, Richmond, VA). All reagents were purchased from Sigma unless otherwise indicated.

2.3.3 RNA extraction and quantitative PCR

RNA was extracted using Trizol (Invitrogen). Liver tissues were homogenized in Trizol for 5 seconds. For hepatocytes, Trizol were added into the wells immediately after I aspirated off the medium and then collected them into tubes. After brief vortexing and incubation at room temperature for 5-10 minutes, 0.2ml chloroform per ml Trizol was added into the tubes and were inverted 20 times to mix thoroughly. These tubes were sit at room temperature for 15-30 minutes for a good phase separation and then spun at 12000g for 10 minutes at 4°C. To improve RNA quality, another run of chloroform extraction could be performed. After the phase separation, the clear supernatant was transferred into a new sterile tube and 0.5ml isopropanol per 1 ml Trizol was added to precipitate the RNA. After inverting tubes 20 times and incubating them at room temperature for 15 minutes, these tubes were spun at 12000g for 10 minutes at 4°C to collect RNA pellet. The pellet was washed with 70% ethanol once by a brief spin at 9000g for 5 minutes at room temperature. After air-drying for 5 minutes at room temperature, RNA was resuspended with DEPC-water and ready for further analysis. The concentration of RNA was assessed by determining absorbance of UV light at 260 and 280 nm wavelengths, with A_{260} for quantity (1 O.D. = 40 ng/μl) and A_{260}/A_{280} ratio for quality (optimal ratio = 1.8).

Two μg of RNA was reverse transcribed to cDNA using M-MLV (Moloney Murine Leukemia Virus) Reverse Transcriptase kit (Invitrogen). Total volume of each reaction was 50μl, containing 400 μM dNTP, 100 ng Random Primer, 4 mM DTT, 25 U RNASE OUT and 125 U M-MLV. The reaction was incubated at 42°C for 15 minutes and then heated at 95°C for 5 minutes in the PCR thermal cycler to deactivate the enzyme.

After reverse transcription, cDNAs were diluted 10 times and prepared for further analysis.

Quantitative PCR (q-PCR) was performed using Power SYBR Green PCR Master Mix (Applied Biosystems) in a 384 well plate. Each reaction had 10 µl in volume and contained 5µl master mix, 0.6 µM each primer, and 2 µl diluted cDNA. All reactions were performed in duplicate for 40 cycles with a two-step protocol (92°C for 15 seconds and 60°C for 1 minute) on a Prism 7900 Sequence Detection System (Applied Biosystems).

The sequences of primers were either adopted from literature or designed by Primer Express 2.0 or primer-BLAST from NCBI. In the latter, parameters for primer designing are: melting temperature is between 58-60°C; one primer from each set has to span two neighboring exons to avoid recognizing genomic DNA, and the length of product is between 100-200 bp for optimal amplification efficiency. The level of each target mRNA was calculated by using comparative CT method, which determines the amount of target after normalization to an endogenous reference, 18S ribosomal RNA (18S) in our cases. The reasons for choosing 18S are: 1) 18S is a house-keeping transcript and does not vary too much between different treatments; 2) 18S expresses in nearly all tissues and cells; 3) 18S produced a good linear standard curve (R^2=0.9978) using different dilutions of cDNA. Potential complications of high expression levels of 18S could be solved by adjusting the baseline setting to reach a linear response range.

2.3.4 Immunoblot Analysis

Small pieces (around 50 mg) of mouse livers were homogenized in lysis buffer (25 mM HEPES, 50 mM KCl, 6% glycerol, 5 mM EDTA, 5 mM EGTA, 0.5% Triton-X100, 50 mM NaF, 40 mM glycerol phosphate, and 25 mM sodium pyrophosphate) with inhibitors of phosphatases (PhosSTOP from Roche, Indianapolis, IN) and proteases (SigmaFAST from Sigma, St. Louis, MO). The lysate was then cleared by centrifugation (16,000g, 10 min, 4°C). Total protein content was determined with Commassie Plus reagents (Pierce, Rockford, IL). Proteins (around 50 µg) were loaded into each lane on a 4-15% gradient SDS-PAGE gel. Signals were developed with horseradish peroxidase (HRP)-conjugated secondary antibodies and SuperSignal West Pico Chemiluminescent Substrate (Pierce). The Adobe Photoshop software was used to quantify intensity of signals.

2.3.5 Lipid profiling and total content assay

Lipids from hepatocytes and frozen liver tissues were extracted using the Folch method. For cultured hepatocytes, cells were washed with room temperature PBS three times and scraped them off from the plates into 500 µl ice-old lysis buffer containing 18 mM Tris-HCl, 300 mM Mannitol, 50 mM EGTA, pH 7.6, with 5 mM phenylmethanesulfonyl fluoride (PMSF). Two 6-wells of the cells (~0.5 million) were combined and used for each assay. The cell suspensions were sonicated for 10 one-second pulses with a micro-tip to lyse the cells. For frozen liver tissues, 50-100 mg of liver was homogenized in 1 ml lysis buffer for each assay. Twenty to 30 µl cell lysate were taken out for measurement of protein concentration, and the rest were added into 2ml methanol with butylated hydroxytoluene (BHT, 0.05% v/v, to prevent the oxidation of the fatty acid during the extraction) and 4 ml chloroform in the glass tubes (4 ml methanol with BHT and 8 ml chloroform were used for liver tissues).

To minimize random errors during sample processing and to serve as internal standards for quantification, heptadecanoic acids in TAG and FFA forms (C17:0, non detectable in animal fat) were added into samples as internal controls before lipid extraction. For hepatocytes, 1 nmole C17:0 TAG, 5 nmole C17:0 PL and 3 nmoles C17:0 FFA were added to each sample. For liver tissues, 50 nmole C17:0 TAG, 50 nmole C17:0 PL and 100 nmole C17:0 FFA were added to each sample. All lipid work was performed with clean glass tubes with Teflon-lined caps. These tubes were vortexed for 10 seconds and rotated for 4 hours to overnight. After the rotation, 0.8 ml 0.15M KCl (1.6 ml for liver tissues) was added into each tube, which was then vortexed for 10 seconds. For liver tissues, before the addition of KCl, the mixture was filtered through a funnel lined with filter paper (Whatman #1) into a new clean glass tube to get rid of precipitates. These tubes were then centrifuged at 500 r.p.m for 5 minutes for phase separation. After the centrifuge, the bottom phase (organic) was carefully transferred with a glass Pasteur pipette to a new glass tube and evaporated under a nitrogen stream in a 35°C water bath to result in lipid pellets.

For the assay of total content of TAG, nonesterified fatty acid, free cholesterol, cholesterol ester and total lipids from livers or plasma, lipid pellets were resuspended with 10% Triton X-100 in isopropyl alcohol and directly measured by colorimetric kits from Sigma or Wako Chemicals.

For further separation of lipid species through thin layer chromatography (TLC), each lipid pellet was dissolved in 50-100 µl dichloromethane (200 µl or more for liver tissues). The mixture was spotted onto silica gel plates, which were pre-dried in 100°C oven for 1 hour. Standards, such as ~10 nmole C17:0 in FFA, TAG and PL forms, were

spotted to serve as markers for each band. The plate was placed in a sealed glass chamber containing 80:20:1 mixture of hexane: ether: acetic acid lined with a piece of Whatman #1 filter paper. After the solvent ran to the top of the plate, the plate was taken out and sprayed with a fluorescent whitening agent (0.1g/L 2,5-Bis (5-tert- butyl-benzoxazolyl)-thiophene (BBOT, in chloroform/methanol (1:1; v/v)). Under a UV-light, each separated lipid group was visualized according to the position of markers. The silica gel containing the lipid of interest was excised with a single edge razor blade and then transferred into a new glass tube.

Transmethylation was performed to prepare fatty acid methyl esters (FAMEs) that are non-reactive and more volatile derivatives of fatty acids. For TAG, a mixture of 0.5 mL BF_3, 0.4 mL Benzene and 1.1mL methanol was added to each sample, and the tubes were filled with nitrogen to prevent oxidation during the transmethylation. These tubes were then placed in a dry heat block at 100°C for 30 minutes. Every two minutes or so, the caps were tightened to prevent leakage. At the end of this treatment, these tubes were immediately placed into ice. After they were cooled down, 2 mL H_2O and 4 mL pentane were added to each tube, and the mixture was vortexed for 1-2 minutes to extract FAMEs. After centrifuging for 5 minutes at 500 r.p.m, the upper pentane phase was transferred with a Pasteur pipette to a Varian 2 mL glass vial with a Teflon-lined cap and was concentrated under a stream of nitrogen. After the lipids were dry, 20µl dichloromethane (100µl for liver tissues) were added to dissolve these lipids. After vortexing, these lipids were ready for analysis as below.

GC-MS (Gas chromatography-mass spectrometry) was used for lipid analysis . The system contained a GC450 with MS220 from Varian (Palo Alto, CA), which used a

100m x 0.25mm Varian FAME Select CP 7420 (df 0.39μm) column. The setting of temperature gradient was: 140°C hold for the initial 5 minutes, then increased to 240°C at a speed of 4°C per minute, and then 240°Chold for 11 minutes. The total time for each run was 41 minutes. The temperature settings for MS were 220°C for trap, 80°C for manifold and 250°C for transferline. The injector temperature was set at 260°C. Supelco 37 component FAME mix standards (Sigma: St. Louis, MO) was used to confirm all FAMEs that were identified in our studies. In addition to elution time, mass spectrum of each FAME peak was also used for identification.

Total ion current (TIC) was used to calculate the absolute amount of each FAME, which was normalized against the C17:0 internal control at a later time. Most of FAMEs in cell or tissue lipids contain a lot of noise when being calculated by the TIC. Therefore, ten most specific and abundant ions of each FAME species were counted to improve the specificity and accuracy. The sum of these ten ions was then divided by a response factor to generate the total ion current for each FAME species. Response factors were calculated by dividing the sum of ten specific ion currents by the sum of total ion currents from the Supelco 37 standards. The total fatty acid amount for each lipid sample was calculated by the sum of absolute amount of all identified FAME species.

2.3.6 Stearoyl-CoA Desaturase (SCD) activity assay

SCD activity was determined by using [^{14}C] stearoyl-CoA substrate (American Radiolabeled Chemicals, St. Louis, MO) as described [134]. Briefly, microsomes were isolated from mouse livers and purified on a continuous density gradient [6]. Fifty μg microsomal proteins were mixed with 2 nmol [^{14}C] stearoyl-CoA and 1 μmol NADH in 0.1

mM Tris-HCl (pH 7.0) and incubated at 37°C for 5 min. Total lipids were extracted and transmethylated as above to yield FAME. Radiolabeled substrates (C18:0) and products (C18:1) were separated by TLC on silica gel plates containing 10% $AgNO_3$ (Analtech, Newark, DE). Each plate was air dried and exposed to a phosphor imager. Signals were stored and quantitated with a Molecular Imager Pro Plus with Quantity One software (Bio-Rad, Hercules, CA). Counts were used to calculate the yield [(C18:1)/(C18:0+C18:1)], which was then converted to SCD activity (nmol/min./mg). All reactions followed linear (first order) kinetics under the above conditions.

2.3.7 Data analysis

One-way analysis of variance (ANOVA) was used to detect the significant difference within and between groups. A value of $p<0.05$ was considered statistically significant. Data are presented as the mean ± standard error of the mean (S.E.).

2.4 Results

2.4.1 Altered lipid metabolism in livers of Ncb5or $^{-/-}$ mice

Microarray analyses of RNA samples from mouse liver suggested that 5-week-old Ncb5or $^{-/-}$ mice had elevated expression levels of lipid metabolism genes compared to WT. This result was further confirmed by quantitative RT-PCR (Table 2.1). These genes included (1) SCD1 and SCD2 (fatty acid desaturation); (2) FAS (fatty acid synthesis); (3) PGC1α (mitochondrial biogenesis); (4) CD36 and LPL (fatty acid uptake) and (5) one isoform of ACSL, ACSL3 (fatty acid activation).

To further examine the temporal progression of expression of these genes in the livers, quantitative RT-PCR was used to measure the transcript levels of these genes in the livers of WT and Ncb5or $^{-/-}$ mice in newborn and at age 2, 3 weeks (Table 2.1). We observed significantly higher levels of SCD1, SCD2, FAS and ACSL3 transcripts in Ncb5or $^{-/-}$ liver than WT at all ages except 3 weeks. The expression of SCD2 is at the highest level in newborn stage whereas SCD1 starts at age 3 weeks as reported previously [38]. Both hepatic SCD1 and SCD2 were up-regulated by at least 2 fold in Ncb5or $^{-/-}$ mice at all ages except for 3 weeks, at which time a transition from SCD2 to SCD1 occurs in the liver. The increased hepatic SCD1 and SCD2 expression might be due to the compensation for the deficiency of fatty acid desaturation, which was further examined below. ACSL3 is more involved in catabolism than anabolism [73]. Other ACSL isoforms displayed no difference between the two genotypes (data not shown).The hepatic expression level of CD36, LPL and PGC1α were higher in Ncb5or $^{-/-}$ mice than WT only at age 3 and 5 weeks, suggesting that the different response may be related to exposure to diet, since mice start to ingest diet at this age.

We did not detect any difference for hepatic expression level of GPAT1, GPAT4, LIPIN and DGAT2 at 5 weeks between WT and Ncb5or $^{-/-}$ mice (data not shown). This suggests that the phospholipid and TAG synthesis in Ncb5or $^{-/-}$ mice is not impaired and that defect in fatty acid metabolism is limited to fatty acid desaturation and synthesis. Likewise, hepatic PPARα, PPARγ, PPARδ/β remained the same in WT and Ncb5or $^{-/-}$ mice (data not shown), indicating that the deficiency is not sufficient to induce the transcription of these nuclear receptor genes.

In summary, we observed increased gene expression levels in all of the following pathways: *de novo* lipogenesis (SCD1, SCD2, FAS), fatty acid uptake (LPL and CD36), fatty acid activation/catabolism (ACSL3), and mitochondrial biogenesis (PGC1α). This suggests that liver of Ncb5or$^{-/-}$ mice has increased fatty acid synthesis in parallel to elevated catabolism, suggesting futile fatty acid cycling, similar to that described in thiazolidinediones (TZDs) treated adipocytes [135].

2.4.2 Reduced hepatic TAG content and impaired fatty acid desaturation in Ncb5or $^{-/-}$ mice

To determine whether altered gene expression pattern resulted in lipid abnormality, we examined the lipid profile of hepatic TAG from WT and Ncb5or $^{-/-}$ mice at different ages.

We found that the three most abundant fatty acid substituents in hepatic TAG are palmitate (C16:0), oleate (C18:1n9c) and linoleate (C18:2n6c) at age 3 weeks (Figure 2.2). Compared to WT, Ncb5or $^{-/-}$ mice had significantly less C16:0, C18:1n9c, palmitoleate (C16:1n7c) and C18:1n7c (the elongated product from C16:1n7c) in hepatic TAG pool whereas most of the other SFA and PUFA content remained the same. C16:0 is the principal product of FAS in *de novo* lipogenesis and can be elongated to C18:0. These SFA can be converted to their corresponding MUFA, C16:1n7c and C18:1n9c, respectively, through Δ^9 desaturation pathway by SCD. This piece of data suggested that liver of Ncb5or $^{-/-}$ mice had impaired Δ^9 desaturation, but not Δ^5, Δ^6 that are required for PUFAs.

Table 2.1 Transcript levels of genes involved in lipid metabolism and mitochondrial biogenesis in newborn, 2-, 3-, 5-week-old Ncb5or$^{-/-}$ and WT mouse livers.

Quantitative PCR was used to detect the relative mRNA levels of genes in lipid metabolism in WT and Ncb5or$^{-/-}$ RNA samples. The level of averaged WT sample was arbitrarily defined as 1 to allow comparison for each target gene. All values are mean ± S.E. (n=6) and relative to 18S ($\times 10^6$). $^a p<0.05$, $^b p<0.01$, $^c p<0.005$. The transcript levels in bold form indicate the significant difference.

SCD: Stearoyl-CoA desaturase; FAS: Fatty acid synthase; PGC1α: Peroxisome proliferator-activated receptor gamma coactivator-1 α; CD36: Cluster of Differentiation 36; LPL: Lipoprotein lipases; ACSL: Long-chain fatty acid-CoA ligases

	Newborn		2-week		3-week		5-week		
	WT	Ncb5or$^{-/-}$	WT	Ncb5or$^{-/-}$	WT	Ncb5or$^{-/-}$	WT	Ncb5or$^{-/-}$	Fold ↑ Ncb5or$^{-/-}$
SCD1	**59.0±7.7**	**134±22^c**	**8.64±1.38**	**19.2±2.9^c**	394±51	222±74	**725 ±58**	**1410±140^c**	1.9
SCD2	**41.1±5.1**	**131±23^c**	4.06±0.43	5.74±0.95	4.09±0.55	5.25±0.55	**1.57±0.35**	**3.79±0.58^a**	2.4
FAS	**5.90±1.11**	**12.5±2.9^c**	**3.10±0.51**	**5.10±0.72^a**	30.9±2.9	20.4±6.3	**16.8±2.5**	**27.9±3.9^a**	1.7
ACSL3	**0.94±0.13**	**1.92±0.32^a**	**0.93±0.10**	**2.31±0.39^c**	2.04±0.21	1.76±0.39	**1.88±0.34**	**3.73±0.58^a**	2.0
PGC1α	28.5±3.9	34.6±1.9	15.7±2.7	21.0±4.2	**11.6±2.6**	**32.0±5.5^b**	**6.24±1.17**	**11.3±0.8^a**	1.8
CD36	22.8±3.9	15.5±1.5	5.28±0.62	6.64±0.98	**5.78±0.95**	**10.6±0.7^b**	**4.76±1.03**	**9.20±1.52^b**	1.9
LPL	105±9	114±23	170±22	138±11	**66.8±11.0**	**209±22^c**	**15.4±2.9**	**37.3±8.8^a**	2.5

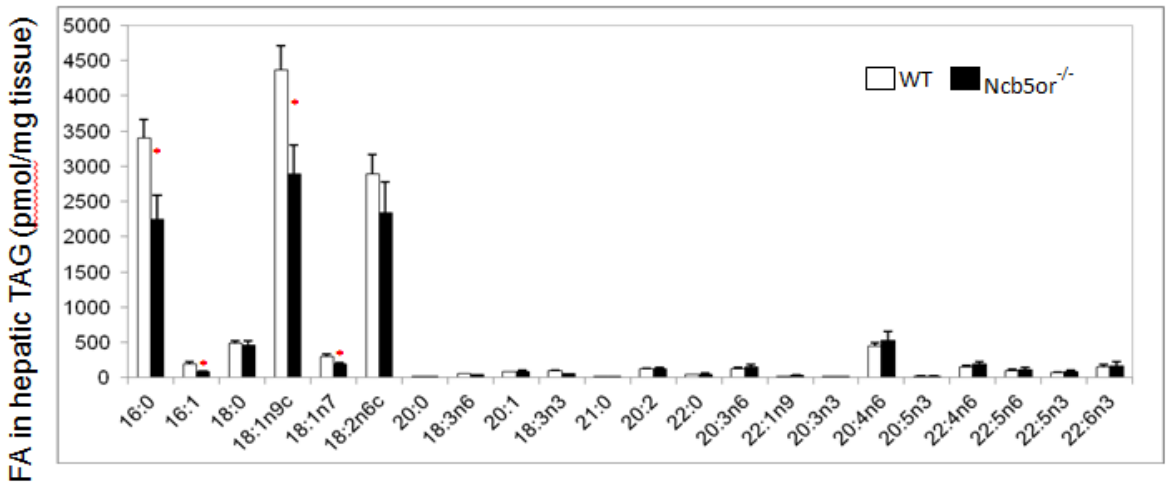

Figure 2.2 Fatty acid composition of hepatic TAG from 3-week-old chow-fed Ncb5or$^{-/-}$ and WT mice. Fatty acid composition of hepatic TAG was determined by GC analysis. Results were obtained from 6-8 animals (n=6-8) in each experimental group and expressed as mean ± S.E. *, p<0.05. White-bar: WT; Black-bar: Ncb5or$^{-/-}$. Dr. WenFang Wang fully contributed to this figure.

To better represent the activity of Δ^9 desaturation pathway in the liver, we calculated the ratio of C16:1n7c to C16:0 as the desaturation index for 16 carbons (DI, C16), and the ratio of C18:1n9c to C18:0 as the desaturation index for 18 carbons (DI, C18), for the profiles of hepatic TAG in 3, 5 and 12 weeks old mice (Figure 2.3 B, 2.3 C). In addition, we calculated the total hepatic TAG content by the sum of all fatty acid substituents (Figure 2.3A).

We found that hepatic TAG content in Ncb5or $^{-/-}$ mice was lower than WT at all ages we examined. The difference of TAG content is at the biggest at age 12 weeks, which is caused by the combination of lipoatrophy and the onset of diabetes. All of the desaturation indices (DI) were significantly lower in hepatic TAG of Ncb5or $^{-/-}$ mice than those in WT with only one exception, i.e., DI of C16 at age 5 weeks. It is likely contributed by the higher expression levels of SCD1 and SCD2 in Ncb5or $^{-/-}$ liver than WT at this age (Figure 2.1), although DI of C18 remained lower in Ncb5or $^{-/-}$ liver. The decreased desaturation indices in prediabetic Ncb5or $^{-/-}$ mice are consistent with our previous findings in TKO mouse [36], suggesting that Ncb5or $^{-/-}$ mice are impaired in Δ^9 fatty acid desaturation.

There are three potential causes for the diminished hepatic TAG contents in Ncb5or $^{-/-}$ mice. The first one is that more hepatic TAGs are secreted into circulation and then taken up by other tissues. To examine this possibility, we measured the total content of TAG, nonesterified (free) fatty acid, free cholesterol and cholesterol ester in the sera of WT and Ncb5or $^{-/-}$ mice. Similar level of these lipids in the circulation (Table 2.2) excludes the increased excretion as the cause.

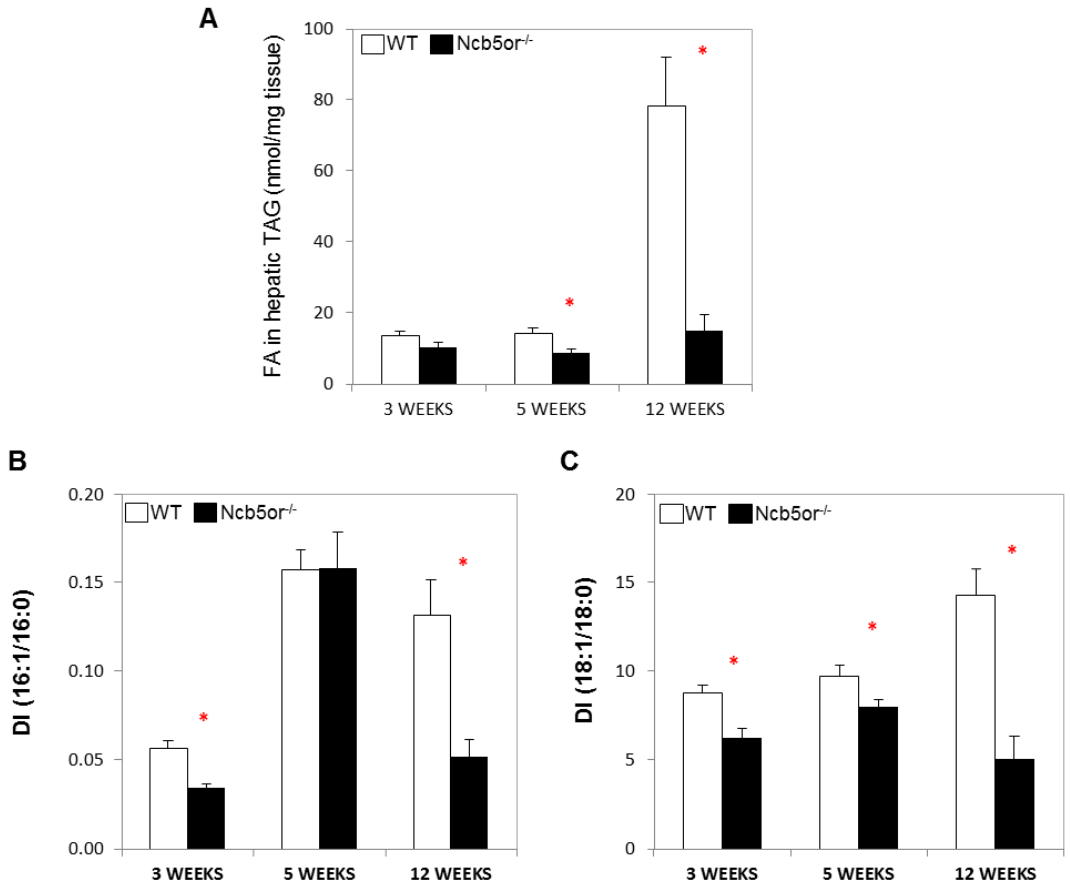

Figure 2.3 Hepatic TAG content of chow-fed Ncb5or$^{-/-}$ and WT mice. Fatty acid compositions of hepatic TAG from 3-, 5- and 12-week-old mice were determined by GC analysis. Values were used to calculate hepatic TAG level (A) and desaturation index (DI) of 16:1/16:0 (B) and 18:1/18:0 (C) at all three ages. Results were obtained from 6-14 animals (n=6-14) in each experimental group and expressed as mean ± S.E. *, p<0.05. White-bar: WT; Black-bar: Ncb5or$^{-/-}$. Dr. WenFang Wang performed analyses of all samples except those at age 5 weeks. More samples were included in the 5-week-old mouse group, resulting in a more accurate result in this figure than that recently reported in [136].

Table 2.2 Body weight and plasma lipid parameters of chow-fed 2-, 3-, and 5-week-old Ncb5or$^{-/-}$ and WT mice. Total content of TAG, free fatty acid (FFA), free cholesterol, and cholesterol ester were directly measured by colorimetric kits. Results were obtained from more than 7 animals (n>7) in each experimental group and expressed as mean ± S.E. $^{a}p<0.01$, $^{b}p<0.05$. $n \geq 7$ in all cases.

Dr. WenFang Wang fully contributed to this table.

Genotype	Age (week)	Body Weight (g)	TAG (mg/dL)	FFA (mM)	Free Cholesterol (mg/dL)	Cholesterol ester (mg/dL)
WT	2	6.96±0.15	47.0±9.4	1.29±0.07	106.0±4.4	33.9±4.6
Ncb5or$^{-/-}$	2	6.07±0.24[a]	93.3±17.8	1.72±0.09	123.6±10.2	47.2±11.1
WT	3	9.17±0.31	79.4±11.8	1.60±0.09	70.4±3.5	44.5±4.5
Ncb5or$^{-/-}$	3	7.55±0.16[a]	57.3±8.9	1.48±0.26	91.5±6.5	54.8±5.8
WT	5	20.27±0.53	75.7±7.0	1.50±0.09	92.6±3.4	22.2±3.8
Ncb5or$^{-/-}$	5	17.67±0.83[b]	101.2±12.9	1.40±0.03	91.9±6.5	25.2±7.2

The second one is that hepatic TAG synthesis is deficient in Ncb5or $^{-/-}$ mice. However, no difference was observed in hepatic transcript levels of DGAT2, GPAT1 and GPAT4 in these mice (data not shown). In addition, isolated WT and Ncb5or $^{-/-}$ hepatocytes incorporated exogenous fatty acid into the TAG pool at a similar rate as WT (data shown below), suggesting that hepatic TAG synthesis remained intact in Ncb5or $^{-/-}$ mice.

The third one is that, due to the deficiency in SCD desaturation, more saturated fatty acids are accumulated and catabolized through β-oxidation than those being converted into MUFA and incorporated into TAG. Increased fatty acid activation/catabolism (ACSL3) and mitochondrial biogenesis (PGC1α) in the livers from Ncb5or $^{-/-}$ mice (Table 2.1), indicating that this is likely the cause. Functional studies supporting this possibility are described in the next chapter.

2.4.3 Increased accumulation of palmitate in the intracellular TAG and FFA pools of Ncb5or $^{-/-}$ hepatocytes upon short term incubation of palmitate

We next studied the metabolism of exogenous SFA in isolated primary hepatocytes from pre-diabetic Ncb5or $^{-/-}$ mice at age 4-5 weeks. The use of cell system allows us to avoid effects (cross-talks) from other tissues, as well as diets and factors related to animal physiology.

We treated WT and Ncb5or $^{-/-}$ hepatocytes with BSA (vehicle control) or palmitate (C16:0) or oleate (C18:1) or both for 8 hours. We chose palmitate and oleate because they are the most abundant form of SFA and MUFA in animal tissues, respectively. Under our experimental conditions, more than 85% of Ncb5or $^{-/-}$

hepatocytes survived after SFA treatment (see Chapter 3), and more than 0.05 mM fatty acids remained in the media after 8 hours of treatment (data not shown), indicating no starvation of nutrient in these cells.

Under C16:0 or C18:1 treatment, a rise of total TAG content occurred in Ncb5or$^{-/-}$ and WT hepatocytes compared to the BSA-treated cells, and no difference was observed between the two genotypes under either condition (Figure 2.4A). This finding is consistent with the fact that transcript levels of genes in TAG synthesis did not differ between the two genotypes (Figure 2.5), suggesting that Ncb5or$^{-/-}$ hepatocytes have intact TAG synthesis.

After 8 hours of C16:0 treatment, Ncb5or$^{-/-}$ hepatocytes exhibited ~1.6 fold lower C16:1/C16:0 ratio of the TAG pool than that in WT cells (Figure 2.4 A). Because transcript levels of SCD1 and SCD2 in Ncb5or$^{-/-}$ cells were similar to those in WT (Figure 2.5), over-abundance of C16:0 and the resulted TAG remodeling in Ncb5or$^{-/-}$ hepatocytes reflects their deficiency in converting exogenous SFA to MUFA , rather than altered TAG synthesis. Under the treatment with C18:1, WT and Ncb5or$^{-/-}$ hepatocytes had similar DI (C18:1/C18:0) values of intracellular TAG (Figure 2.4 A), suggesting that metabolism of MUFA remained intact in Ncb5or$^{-/-}$ hepatocytes. This conclusion is further supported by co-incubation with both C16:0 and C18:1, which abolished the difference of DI (C16) between genotypes and led to an even higher TAG content in Ncb5or$^{-/-}$ hepatocytes than WT (Figure 2.4 A).

In addition to changes in intracellular TAG, Ncb5or$^{-/-}$ hepatocytes displayed significantly higher levels of intracellular FFA, especially SFA, under basal (untreated)

and C16:0 treatment compared to WT cells (Figure 2.4 B, Figure 2.6 B). One explanation is that these SFAs were not converted into MUFAs that were preferred substrates for TAG synthesis and remained as intracellular FFA in Ncb5or$^{-/-}$ hepatocytes, instead of being esterified into the TAG pool. Incubation with C18:1alone seemed to abolish the difference, whereas co-incubation with C16:0 and C18:1 totally abolished the difference in intracellular FFA levels between genotypes (Figure 2.4 B).

The metabolic fate of palmitate in in Ncb5or$^{-/-}$ hepatocytes under these treatments is illustrated in Figure 2.6. These cells accumulate more C16:0 in the FFA pool at basal level compared to WT cells and the amount of C16:0 further increased after C16:0 treatment. Co-incubation with both C16:0 and C18:1 significantly decreased the level of free C16:0 in Ncb5or$^{-/-}$ hepatocytes compared to C16:0 treatment alone (Figure 2.6 B), indicating an active metabolism of C16:0 in these cells. In TAG pool, we observed that C16:0 treatment alone increased more C16:0 amount in Ncb5or$^{-/-}$ hepatocytes than that in the WT cells and co-incubation with both C16:0 and C18:1 further increased the C16:0 amount (Figure 2.6A). The fact that co-incubation increased C16:0 amount in TAG but decreased C16:0 amount in FFA suggests that C18:1 helped to channeled C16:0 to TAG synthesis from the intracellular FFA pool as previously reported [54].

Unlike the TAG pool (Figure 2.4A), intracellular FFA (Figure 2.4B) and phospholipid pools (Figure 3.5) displayed no significant difference in DI of C16 and C18 between Ncb5or$^{-/-}$ and WT hepatocytes under all treatments.

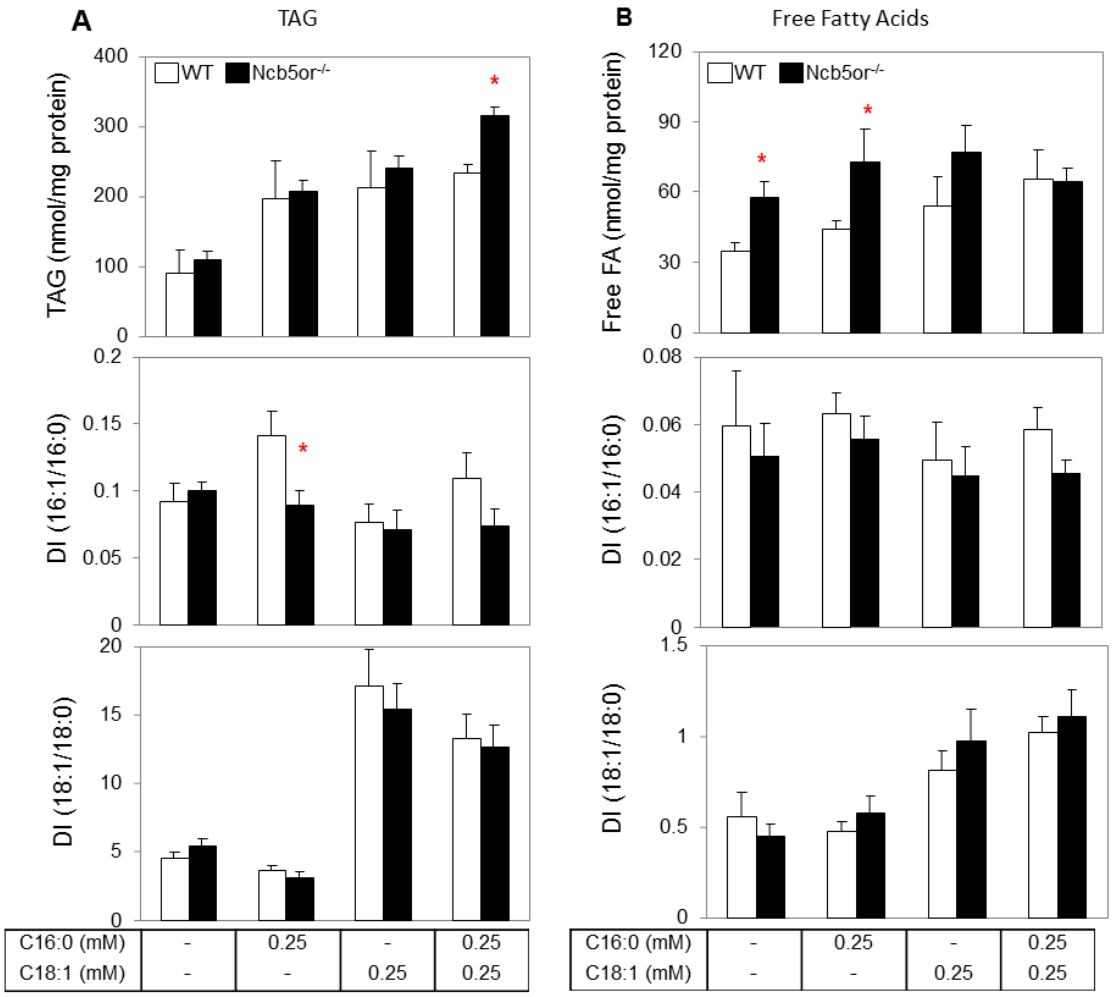

Figure 2.4 Increased accumulation of palmitate in the intracellular TAG and FFA pools in Ncb5or$^{-/-}$ hepatocyte upon short term incubation of palmitate. Hepatocytes were isolated and treated with palmitate or oleate or BSA carrier alone. Intracellular FFA and TAG were prepared and analyzed for determination of lipid profiles by GC/MS. The total content, desaturation index of C16:1/C16:0 and C18:1/C18:0 were determined for TAG (A) and FFA (B). Results were obtained from 4-6 animal-pairs (n=4-6) for TAG and FFA profiling and expressed as mean ± S.E. *, p<0.05. White-bar: WT; Black-bar: Ncb5or$^{-/-}$.

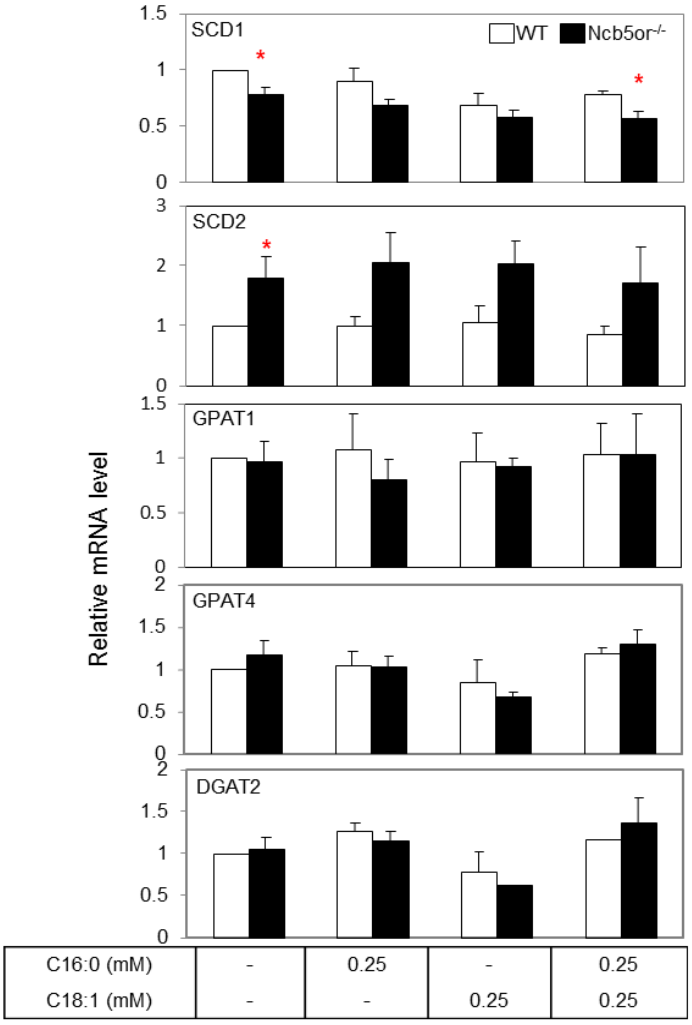

Figure 2.5 Effects of fatty acid incubation on the expression of genes in fatty acid desaturation and TAG synthesis in Ncb5or$^{-/-}$ and WT hepatocytes. Hepatocytes were isolated and treated with palmitate or oleate or BSA alone (vehicle control). Total RNAs were collected and used for quantitative RT-PCR. Results were obtained from 3-5 animal-pairs (n=3-5) and expressed as mean ± S.E. *, p<0.05. White-bar: WT; Black-bar: Ncb5or$^{-/-}$.

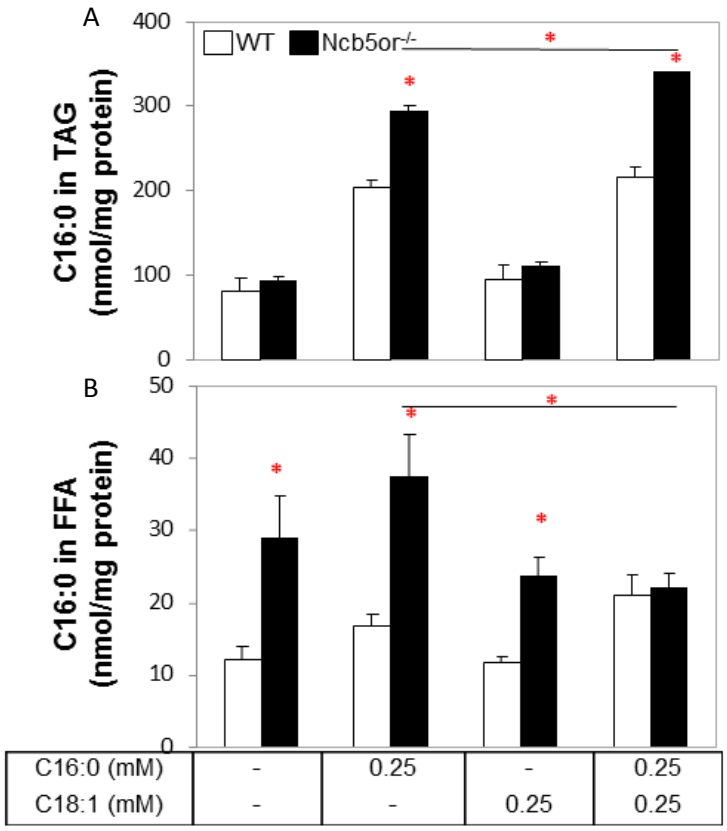

Figure 2.6 Fate of palmitate under incubation and co-incubation with palmitate and oleate in Ncb5or$^{-/-}$ hepatocytes. Hepatocytes were isolated and treated with palmitate or oleate or BSA carrier alone. Intracellular FFA and TAG were prepared and analyzed for determination of lipid profiles by GC/MS. Palmitate (C16:0) levels were determined in TAG (A) and FFA pool (B). Results were obtained from 4-6 animal-pairs (n=4-6) for TAG and FFA profiling and expressed as mean ± S.E. *, $p<0.05$. White-bar: WT; Black-bar: Ncb5or$^{-/-}$.

2.4.4 High fat diet stimulated lipogenesis and fatty acid catabolism in Ncb5or$^{-/-}$ livers

We observed that co-incubation with C16:0 and C18:1 resulted in a higher TAG content in Ncb5or$^{-/-}$ hepatocytes than WT. We next investigated whether the rescue can take place in whole animals. We fed WT and Ncb5or$^{-/-}$ mice a high fat (HF) diet rich in SFAs and MUFAs. BecauseNcb5or$^{-/-}$ mice develops diabetes around 7 weeks [29], we decided to start HF feeding at age 3 weeks, right after weaning. After 10 days on HF, Ncb5or$^{-/-}$ mice maintained lower body weight compared to WT (data not shown), similar to chow-fed counterparts (Table 2.2). However, we found that HF intervention fully restored the hepatic TAG content in Ncb5or$^{-/-}$ mice (Figure 2.7B), consistent with our findings in hepatocytes. Compared to WT, Ncb5or$^{-/-}$ mice displayed significantly higher levels of intracellular free fatty acids (1.2-fold, Figure 2.7 A), higher DI values for C16 (2.0-fold, Figure 2.7 C) and C18 (1.3-fold, Figure 2.7 D) fatty acid substituents of hepatic TAG. These changes in DI, however, were not observed in Ncb5or$^{-/-}$ hepatocytes under co-incubation of C16:0 and C18:1.

To understand the mechanism of increased hepatic TAG synthesis in Ncb5or$^{-/-}$ mice, we measured transcript levels of key enzymes in hepatic lipid metabolism. We found a much bigger fold increase in the expression level of these enzymes in Ncb5or$^{-/-}$ mice (Table 2.3). The higher transcript levels of SCD1 (9.2-fold) and Cyb5A (1.2-fold) correlated to the higher DI values in Ncb5or$^{-/-}$ livers. Higher transcript levels of genes in phospholipid/TAG synthesis, such as GPAT1 (2.3-fold), GPAT4 (2.9-fold), LIPIN (9.0-fold) and DGAT2 (2.3-fold), suggested that elevated levels of key enzymes and over-abundance of fatty acid substrates are responsible for restored hepatic TAG levels in Ncb5or$^{-/-}$ mice. In addition, Ncb5or$^{-/-}$ liver displayed 7-fold higher levels of fatty acid

synthase (FAS) transcripts, which correlated to their higher levels of intracellular FFA than WT.

Primary hepatocytes of Ncb5or$^{-/-}$ mice under the co-incubation of SFA and MUFA displayed no change in expression of fatty acid desaturation and synthesis enzymes (Figure 2.6). This is differed from livers of whole animals fed with HF, suggesting that these changes in hepatocytes may be stimulated by cross-talk with other tissues. Besides these genes, we observed higher transcript levels of enzymes involved in Δ^6 fatty acid desaturation (FADS2, 5.5-fold), fatty acid uptake (LPL, 4.5-fold, and CD36, 2.3-fold), mitochondrial biogenesis (PGC1α, 2.9-fold), fatty acid activation (ACSL1, ACSL4 and ACSL5, 1.3-2.7 fold) and their upstream nuclear receptor regulator (PPARα, 2.5–fold and PPARβ/δ, 3.3-fold). All these changes suggested a more active lipogenesis and fatty acid catabolism in Ncb5or$^{-/-}$ liver in response to HF diet than that with chow.

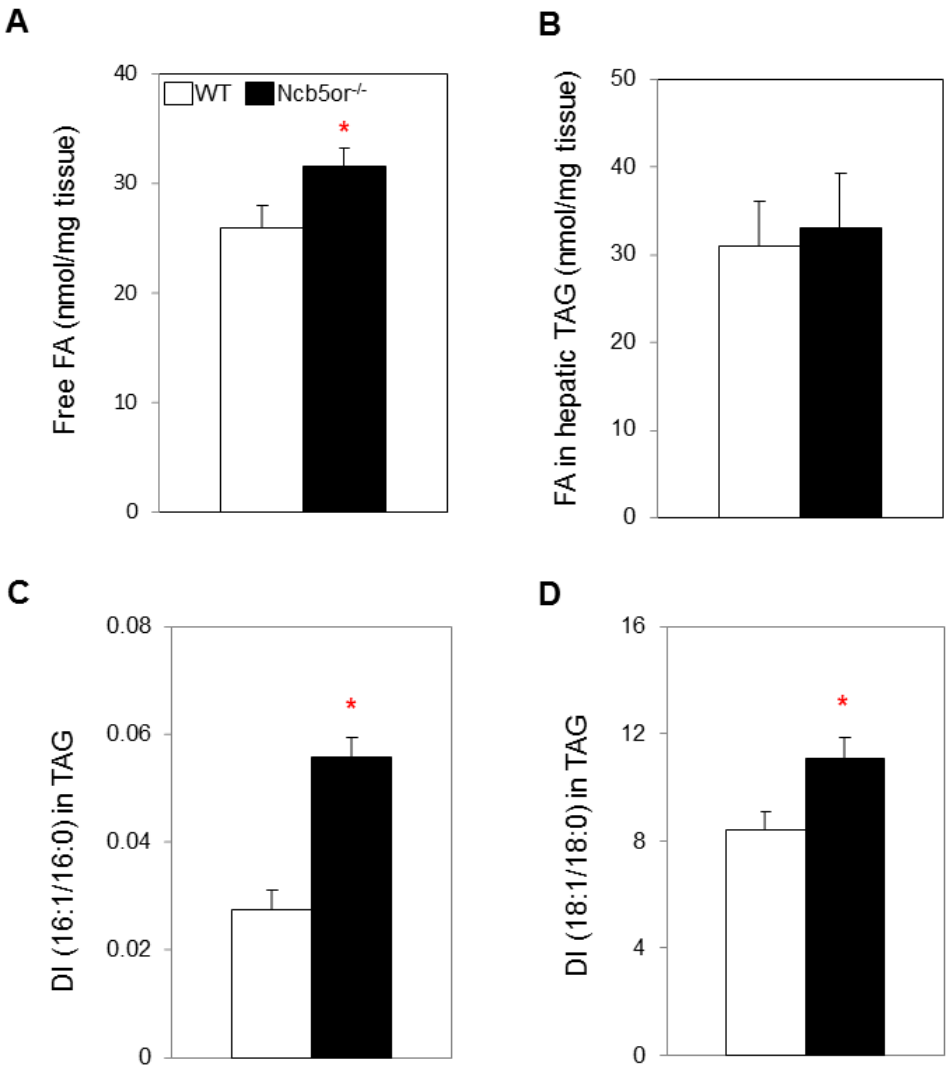

Figure 2.7 Effects of 10-day high-fat feeding on hepatic lipid content of Ncb5or$^{-/-}$ and WT mice. After 10 days on a high-fat diet, the amount of hepatic lipids as FFA (A) and TAG (B) from 4.5-week-old WT (n=9) and Ncb5or$^{-/-}$ (n=6) mice was determined by colorimetric assay and GC-MS, respectively. Desaturation indices of hepatic TAG are plotted for 16:1/16:0 (C) and 18:1/18:0 (D). Results are expressed as mean ± S.E. *, p<0.05. White-bar: WT; Black-bar: Ncb5or$^{-/-}$. I helped with lipid analysis and Dr. WenFang Wang contributed to the rest of this Figure.

Table 2.3 Transcript levels of genes involved in lipid metabolism in 4.5-week-old Ncb5or$^{-/-}$ and WT mouse livers after 10-day high-fat feeding. All values are mean ± S.E. (n=6) and relative to 18S (×10^6). $^a p<0.05$, $^b p<0.01$, $^c p<0.005$.

	WT	Ncb5or$^{-/-}$	Fold ↑ in Ncb5or$^{-/-}$
SCD1	103±12	947±158^c	9.2
SCD2	1.23±0.11	1.75±0.25	1.4
FADS2	26.4±4.3	144±27^c	5.5
GPAT1	19.6±1.8	45.2±7.0^c	2.3
GPAT4	5.69±1.04	16.3±2.2^c	2.9
LIPIN	2.2±0.5	19.8±4.7^c	9.0
DGAT2	52.5±4.4	121±17^c	2.3
Cyb5A	353±9	432±18^c	1.2
FAS	3.19±0.41	21.4±5.4^c	6.7
PGC1α	3.56±0.64	10.4±1.3^c	2.9
PPARα	11.2±1.2	28.4±2.8^c	2.5
PPARβ/δ	0.29±0.05	0.97±0.14^c	3.3
ACSL1	31.2±3.1	41.9±1.7^a	1.3
ACSL3	0.83±0.13	2.03±0.29^c	2.4
ACSL4	4.35±0.51	6.45±0.71^a	1.5
ACSL5	5.72±0.42	15.2±1.7^c	2.7
CD36	6.11±0.52	14.2±2.3^c	2.3
LPL	10.2±0.6	45.6±6.7^c	4.5

2.4.5 Decreased SCD specific activity in Ncb5or$^{-/-}$ liver microsomes

Based on studies described above, we conclude that Ncb5or plays an important role in fatty acid Δ^9 desaturation pathway. However, the exact mechanism through which Ncb5or regulates this pathway still remains unclear. Based on the structural similarity betweenNcb5or and the Cyb5A/Cyb5R3 pair, it is plausible that Ncb5or may function as an alternative electron donor for SCD in Δ^9 desaturation.

We next determined whether the lack of Ncb5or would affect SCD activity. The classic *in vitro* reconstitution assay would include substrates (SFA), purified or enriched enzymes (SCD and its electron donor, i.e., Ncb5or, or Cyb5A and b5R), and NADH. The reaction would be performed to measure MUFA production. It is challenging to purify SCDs, which are integral membrane proteins [137]. Therefore, we directly measured the SCD activity in isolated microsomes from WT and Ncb5or$^{-/-}$ mice.

Specifically, [^{14}C] stearoyl-CoA was used as substrate and mixed with hepatic microsomes from WT or Ncb5or$^{-/-}$ mice. We measured the conversion of [^{14}C] stearoyl-CoA to [^{14}C] oleoyl-CoA in the presence of NADH to calculate the SCD activity, which was then normalized by the SCD protein (or transcript) level to obtain the SCD specific activity.

We observed a near 2-fold increase of SCD activity for Ncb5or$^{-/-}$ microsomes than WT under both chow and HF diet (Figure 2.8 A and C). Ncb5or deficiency resulted in elevated SCD1 transcript levels under chow (1.9-fold, Table 2.1) and HF diet (9.2-fold, Table 2.3), resulting in 20% lower specific activity under chow (Figure 2.8 B) and more than 5 fold lower specific activity under HF diet (Figure 2.8 D) compared to WT.

We confirmed the correlation between transcript and protein levels by performing immunoblot analyses to measure SCD1 protein level in liver of HF-fed mice (Figure 2.8 E). Around 8-fold higher SCD1 protein level compared to loading control (β-actin) was consistent with 9-fold higher transcript levels in Ncb5or$^{-/-}$ liver than WT.

Our above findings strongly suggest that the "working efficiency" of SCD is impaired due to Ncb5or deficiency and that this impairment is dramatically worsened by increased metabolic load (HF diet). It is worth noting that the SCD specific activity remained the same in Cyb5A$^{-/-}$ and WT microsomes (data not shown). This evidence supports our hypothesis that Ncb5or plays an important role in Δ^9 desaturation pathway by facilitating SCD function. Further investigation is needed to determine whether Ncb5or functions as an electron donor for SCD or by other mechanisms, such as providing iron, which is a cofactor of SCD (see Discussion).

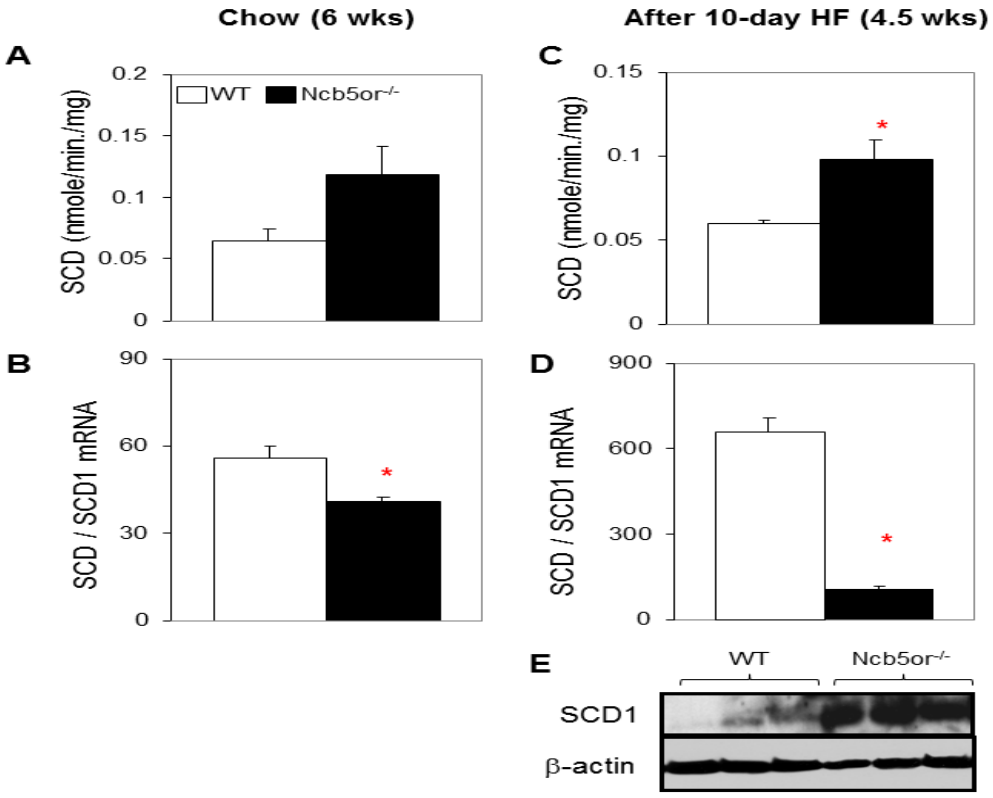

Figure 2.8 Stearoyl-CoA desaturase (SCD) activity and levels of SCD1 transcripts and SCD immunoreactive protein in hepatic microsomes from Ncb5or$^{-/-}$ and WT mice. SCD activities were measured for WT and Ncb5or$^{-/-}$ liver microsomes of 6-week-old chow-fed (A) and 4.5-week-old mice after 10-day high-fat diet feeding (C). Absolute activities (nmole/min./mg) were divided by SCD1 mRNA (calculated as those in Table 2.1 and 2.3) to generate "SCD / SCD1 mRNA" as plotted in (B) and (D), respectively. Results were obtained from 3 (n=3) chow-fed or 6 (n=6) high-fat animal-pairs and expressed as mean ± S.E. (E) Immunoblot analysis showed > 8-fold more SCD1proteins (against β-actin loading control) in liver lysate (n=3 each) of high-fat diet fed Ncb5or$^{-/-}$ than WT mice. White-bar: WT; Black-bar: Ncb5or$^{-/-}$. *, p<0.05. Dr. Hao Zhu performed SCD activity assay.

2.4.6 Further impairment of fatty acid Δ^9 desaturation in mouse livers lacking both Ncb5or and Cyb5A.

Cyb5A and its cognate reductase Cyb5R3 are known electron donors for SCDs *in vitro* [13; 14; 15], although *in vivo* evidence is relatively weak. Our own studies suggest that Ncb5or plays a role in SCD function, potentially as an electron donor.

To dissect the roles of Ncb5or and Cyb5A *in vivo*, we generated a mouse model that lacks both Ncb5or and Cyb5A (double KO, or DKO) in hepatocytes by crossing global Ncb5or$^{-/-}$ mice with hepatic Cyb5A$^{-/-}$ mice (HBN) (Figure 2.9). We found DKO had significantly lower body weight than WT at age 5 weeks, similar to that of Ncb5or$^{-/-}$ mice, whereas HBN mice had the same body weight as WT (Figure 2.9 A).

We next extracted hepatic lipids from these mice and determined fatty acid composition of TAG. We detected that hepatic TAG content decreased in both Ncb5or$^{-/-}$ and DKO mice, but not in HBN mice (Figure 2.9 B). Compared to that of WT, DI (C18) was lower in liver of Ncb5or$^{-/-}$ (by 1.2 fold) and DKO (by 1.3 fold) mice (Figure 2.9 D). Interestingly, DI (C16) appeared to be significantly affected in HBN mice (1.3-fold lower than WT, p=0.07), and DKO had the lowest DI (C16) value (1.5-fold lower than WT, p=0.05) (Figure 2.9 C). Overall, DKO mice had the most impaired Δ^9 desaturation in the liver, likely due to the overlap of Ncb5or and Cyb5A deficiency. However, this impairment in DKO mice is relatively mild in comparison to the greater than 3-fold decrease of both DI (C16) and DI (C18) in liver of SCD1$^{-/-}$ mice [138], suggesting the lack of total knock down of SCD and the potential existence of other electron donors for SCDs.

HBN mice exhibited no major lipid phenotype, as previously reported [132], despite a non-significant trend of lower DI (C16) values (Figure 2.9 C). Remarkably, livers in Ncb5or$^{-/-}$ mice had lower DI (C18), but not DI (C16). These findings indicated that Cyb5A and Ncb5or might have different preference for substrates *in vivo*, namely, Cyb5A for C16:0 and Ncb5or for C18:0. Because C16:0 is the major product of *de novo* fatty acid synthesis, Cyb5A may contribute to desaturation of *de novo* synthesized SFA, whereas Ncb5or may play a more important role in the desaturation of exogenous SFA.

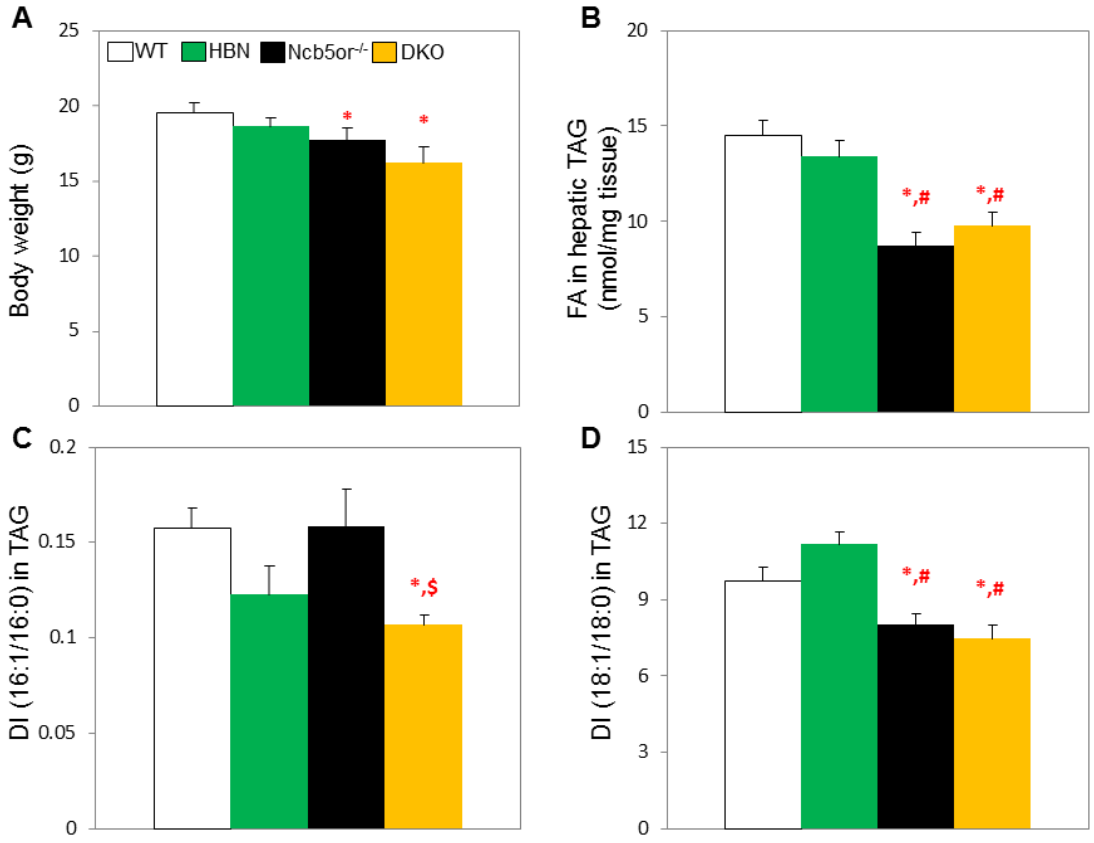

Figure 2.9 Body weight and hepatic lipid profile of WT, HBN, Ncb5or$^{-/-}$ and DKO mice. Body weight (A) was measured from WT (n=10), HBN (n=7), Ncb5or$^{-/-}$ (n=8) and DKO mice (n=7) at 5 weeks. Total TAG content (B), DI, C16 (C) and DI, C18 (D) were measured from livers of these 5-week-old mice by GC-MS. Results are expressed as mean ± S.E. *, $p<0.05$ compared to WT group; #, $p<0.05$ compared to HBN group; $, $p<0.05$ compared to Ncb5or$^{-/-}$.

White-bar: WT; Green-bar: HBN; Black-bar: Ncb5or$^{-/-}$; Yellow-bar: DKO.

2.5 Discussion

2.5.1 Ncb5or and fatty acid metabolism

Our current study focused on fatty acid metabolism in livers and hepatocytes of prediabetic Ncb5or$^{-/-}$ mice. These mice displayed reduced hepatic TAG content and impaired Δ^9 desaturation as early as the weaning age. These observations are consistent with our previous findings in older non-diabetic Ncb5or$^{-/-}$ mice that are transplanted with WT islets [36]. Together, they suggest that Ncb5or is involved in fatty acid metabolism *in vivo*.

To determine the mechanism, we treated primary hepatocytes from prediabetic Ncb5or$^{-/-}$ and WT mice with SFA and MUFA. We confirm that Ncb5or deficiency results in impaired Δ^9 desaturation that affects intracellular FFA and TAG pools. Direct measurement of SCD activity in liver microsomes confirmed that Ncb5or deficiency decreases specific SCD activity.

Our working hypothesis is that Ncb5or directly donates electrons to SCD1, although we cannot rule out the possibility that Ncb5or might be involved in ferric iron reduction to facilitate iron uptake and that iron deficiency in Ncb5or$^{-/-}$ mouse livers (Chapter 4) indirectly affects activity of an iron-dependent SCD enzyme. To further examine the role of Ncb5or in SCD reaction, *in vitro* reconstitution of SCD will be attempted with recombinant Ncb5or and pure SCD proteins that are generated from a cell-free translation system [139].

Ncb5or deficiency also leads to over-accumulation of intracellular FFA. Cytotoxicity of these FFA, especially SFA, will be examined in the next chapter.

2.5.2 Animal vs. primary cell culture model

Our studies employed both animal (*in vivo*) and primary hepatocytes (*ex vivo*) models. Although the same overall conclusion is reached, there are minor differences between the two systems.

Compared to WT, prediabetic Ncb5or$^{-/-}$ mice had lower hepatic TAG content, despite intact TAG synthesis in hepatocytes. A high fat diet rich in SFA and MUFA induces hepatic TAG synthesis in Ncb5or$^{-/-}$ mice to restore the TAG content, which is consistent with that in Ncb5or$^{-/-}$ hepatocytes under co-incubation with SFA and MUFA. However, no altered expression of lipid synthesis enzymes was observed in hepatocytes, in contrast to highly induced expression of these genes in liver of HF fed mice.

Intracellular FFA levels remained higher in liver of Ncb5or$^{-/-}$ mice on HF than WT, but similar in Ncb5or$^{-/-}$ hepatocytes under co-incubation of SFA and MUFA. The following four factors may be responsible for this difference. 1) Nature of lipid species in which the fatty acid equivalents are provided. In the animal model, dietary fatty acids are esterified in TAG form and the amount of FFA is low. In contrast, cells are treated with BSA complexed fatty acids. 2) Treatment duration. Mice were fed high fat diet for 10 days, but hepatocytes were incubated for only 8 hours to observe the acute response. It is possible that co-incubation with SFA and MUFA is beneficial only in the initial phase but causes other problems such as elevated FFA levels at later times. 3) Amount of fatty acids. We treated hepatocytes with 0.25 mM C16:0 and 0.25 mM C18:1. These doses are higher than physiological concentration of fatty acids in circulation. 4) Potential contribution from other tissues in animals. Adipose tissues and skeletal muscles play

important roles in regulating hepatic fatty acid metabolism [48]. All these factors should be considered when we compare studies in animals and those in primary cell cultures.

2.5.3 Ncb5or and Cyb5A

Cyb5A has been long considered a major electron donor for SCD [13; 14; 15]. Our findings of Ncb5or suggest that other electron donors, such as Ncb5or, may play an important role. Our preliminary initiated studies on the functional relationship between Ncb5or and Cyb5A *in vivo*. By using congenic mouse lines lacking Ncb5or, Cyb5A, or both, we discovered that Ncb5or affects more body weight, hepatic TAG content and desaturation of C18 fatty acids than Cyb5A, which appears more responsible for converting C16:0 to C16:1. Among all three lines, mice lacking both Ncb5or and Cyb5A display the biggest defects in fatty acid metabolism, but it is much less severe compared to SCD1 null mice.

One plausible explanation is that both Ncb5or and Cyb5A function as electron donors for SCDs. The phenotype of DKO mice suggests that SCD may use some other electron donors besides Ncb5or and Cyb5A. One such candidate is outer mitochondrial cytochrome b5 (Cyb5B). Microsomes are the major subcellular locus for lipid synthesis, including fatty acid desaturase, therefore, Cyb5B in mitochondria is likely not a natural source of electrons for SCD in WT cells but provides an alternative source when both Ncb5or and Cyb5A are deficient.

Our current study relies on three congenic mutant lines, all of which are in the C57BL/6 genetic background. There are some limitations, however, of these mice. Ncb5or $^{-/-}$ mouse is a global knockout model, whereas HBN mice only have hepatic

deficiency of Cyb5A. Although liver is the focus of our current studies, other tissues in Ncb5or$^{-/-}$ mice might affect hepatic lipid metabolism. Therefore, further experimentation using hepatocytes-specific knockout mouse model is important to dissect the role of Ncb5or and Cyb5A in hepatic fatty acid metabolism. Future experiments may include treating hepatocytes of these mice with isotope-labeled substrates, such as exogenous SFA or acetate (precursor for *de novo* fatty acid synthesis), to determine whether they are preferred substrate for Ncb5or and Cyb5A in fatty acid metabolism.

2.5.4 Conclusion

In this chapter, we systematically studied the role of Ncb5or in fatty acid metabolism and validated the role of Ncb5or in Δ^9 fatty acid desaturation pathway as a potential electron donor with in animal and cell models. We characterized the loss of TAG content as the major defect in Ncb5or$^{-/-}$ hepatocytes and were able to rescue it by 10-dayhigh fat feeding. We also revealed the abnormal response to SFA in Ncb5or$^{-/-}$ hepatocytes. Our preliminary data provided clues about the different roles of Ncb5or and Cyb5A in fatty acid desaturation. All these findings allow us to have a better understanding of lipid metabolism in animals. This knowledge is essential for our future endeavor of developing Ncb5or and its pathway as a potential therapeutic target.

Chapter 3

Ncb5or and oxidative stress

3.1 Abstract

Our recent studies show that Ncb5or is involved in Δ^9 fatty acid desaturation and that Ncb5or deficiency leads to accumulation of SFA in intracellular free fatty acid and triacylglycerol (TAG) pools. Here we investigate the underlying mechanism of cytotoxicity of SFA in Ncb5or$^{-/-}$ hepatocytes. We found that accumulation of SFA in Ncb5or$^{-/-}$ hepatocytes induced mitochondrial biogenesis and fatty acid catabolism through β-oxidation. These responses resulted in oxidative stress, but not ER stress, and cell death, which can be alleviated by co-incubation with palmitate and oleate via channeling free SFA into TAG. We also observed higher mitochondrial content and oxidative stress in Ncb5or$^{-/-}$ liver, as well as elevated whole-body oxygen consumption in prediabetic Ncb5or$^{-/-}$ mice compared to WT. In summary, our study revealed an important role of Ncb5or in protecting cells against SFA-induced oxidative stress.

3.2 Introduction

Over-accumulation of intracellular fatty acids impairs cell function and causes cell death, a process often called "lipotoxicity" [79]. Free SFAs, such as palmitate, are the most toxic fatty acid species. Previous studies show that Ncb5or$^{-/-}$ hepatocytes are more sensitive to cytotoxic effects of SFAs than WT [35; 36]. We have recently shown that Ncb5or$^{-/-}$ hepatocytes over-accumulate free SFAs, which is worsened under SFA treatment but attenuated by co-incubation with SFA and MUFA.

Oxidative stress [83; 84] and ER stress [35; 86; 87] are two major mechanisms that have been implicated in SFA-induced cytotoxicity. In this chapter, we investigated

the functional relationship between SFA accumulation and cell death in Ncb5or$^{-/-}$ hepatocytes and examined the role of oxidative and ER stress in SFA-induced lipotoxicity.

The major source of oxidative stress is reactive oxygen species (ROS), which include superoxide (O_2^-), hydrogen peroxide (H_2O_2) and hydroxyl radical ($HO^{\cdot}$).Glutathione is the most abundant antioxidant inside animal cells, and reduced glutathione (GSH) can convert H_2O_2 to H_2O. Oxidative stress also induces the expression of stress response genes, such as GCLC, HMOX1, and MT1, as described in Chapter 1.

Our recent studies suggested that ER stress is involved in SFA induced cytotoxicity in β-cells [34] and hepatocytes of prediabetic Ncb5or$^{-/-}$ mice [35]. In this study, we also investigated the expression of ER stress response genes as those mentioned in Chapter 1. In this chapter, we employed Ncb5or$^{-/-}$ hepatocytes, liver and whole animals to examine the role of increased fatty acid catabolism, oxidative and ER stress in SFA-induced cytotoxicity.

3.3 Methods

3.3.1 Mouse models

Ncb5or$^{-/-}$ mice in C57BL/6 strain were generated as described in section 2.3.1. All experiments employed pre-diabetic male mice. The glucose levels were measured for these mice using OneTouch Ultra glucometer (LifeScan, Milpitas, CA) to make sure that

the mice were non-diabetic. The experimental protocol was approved by the Institutional Animal Care and Use Committee at the University of Kansas Medical Center. Standard rodent chow (Purina 5015 from LabDiet, St. Paul, MN) was used for mice in C57BL/6.

3.3.2 Hepatocytes isolation and fatty acid treatment.

Same as that described in section 2.3.2

3.3.3 Cell viability assay

Cell viability was determined by intracellular ATP content using CellTiter-Glo (R) Luminescent Cell Viability Assay (Promega) and by live-cell protease activity using MultiTox-Fluro Multiplex Cytotoxicity Assay (Promega). The latter assay uses a fluorogenic and cell-permeant peptide substrate (glycyl-phenylalanyl-amino-fluorocoumarin; GF-AFC), which generates fluorescent signal after being cleaved by protease in live cells. Opaque-walled 96 wells (Corning) were used for assays with 20,000 cells in each well. Triplicates were measured for each condition.

3.3.4 RNA extraction and quantitative PCR

Same as that described in section 2.3.3

3.3.5 Lipid profiling and total content assay

Same as that described in section 2.3.5

3.3.6 Fatty acid oxidation (FAO) assay

The rate of mitochondrial FAO was calculated by measuring the oxidized product of [n9,10-^{3}H] palmitic acid (Perkin Elmer Life Science, Boston, MA) as described [140].

Briefly, 1 x 10^5 hepatocytes were seeded in wells of a 24-well plate, incubated overnight in medium with 10% FBS, and then incubated at 37°C with palmitic acid (BSA-PA complex) (0.125 mM unlabeled plus 0.08 Ci [n9,10-^{3}H]-C16:0) in the presence of carnitine (1 mM) for 2 hours. The amount of substrate taken up by cells within 2 hours represented less than 25% of the total amount in the medium. The H[^{3}H]O product was collected and its [^{3}H] content was determined by liquid scintillation spectrometry (LS6500 Scintillation Counter, Beckman-Coulter, Brea, CA) to calculate the initial reaction rate (mmol/hr/mg protein). The protein contents of cells were measured with a BCA protein analysis kit (Pierce) to normalize the reaction rate.

3.3.7 Extracellular flux analysis

Extracellular flux analysis was performed on a XF24 analyzer (Seahorse Bioscience, Billerica, MA) as previously described [141]. Briefly, 3 x 10^4 hepatocytes were seeded into 24-well plates and cultured overnight in complete medium with 10% FBS (see section 2.3.2). Cells were washed with DMEM without buffer carbonate (0.8 mM $MgSO_4$, 1.8 mM $CaCl_2$, 143 mM NaCl, 5.4 mM KCl, 0.91 mM NaH_2PO_4, 15 mg/ml Phenol Red, 5.5 mM glucose, and 2 mM GlutaMAX from Invitrogen) once and incubated in the same medium at 37°C for 1 hour without CO_2 preincubation. Cells were then loaded into the XF24 analyzer to measure oxygen consumption rate (OCR) in short and repeated intervals as cells alone (baseline) and after injection with buffer or palmitate or oleate (0.125 mM) in the presence of carnitine (1 mM). The mitochondrial integrity was also measured by sequential addition of buffer, oligomycin (inhibitor of mitochondrial ATP synthesis, 10 μM), FCCP (carbonylcyanide-p-trifluoromethoxyphenylhydrazone, mitochondrial uncoupler, 6 μM), and

rotenone / antimycin (inhibitor for complex I / III, 4/8 μM, respectively) in separate plates. OCR values under each condition were normalized to total protein content.

3.3.8 Measurement of glutathione

Reduced and oxidized glutathione in liver tissue or hepatocytes was measured as described [142]. The principle of this assay is that 5,5'-dithiobis-2-nitrobenzoic acid (DTNB) can react with GSH to form 5-thio-2-nitrobenzoate (TNB), which can be detected spectrophotometrically at 412 nm. For GSSG measurement, N-ethylmaleimide (NEM) was used to react with the free thiol in GSH, thus preventing it from reacting with DNTB. GSSG is then reduced back to GSH by glutathione reductase (GR) (Figure 3.1). To avoid interfere with GR reaction, excess NEM were first removed by binding to a C18 SepPak hydrophobic column.

The exact procedure is as follows. Hepatocytes were washed 3 times with ice-old PBS and were then scraped off from the plate in 500 μl ice-cold 3% SSA (3% sulfosalicylic acid with 0.1 mM EDTA) per well to precipitate proteins. Two wells (600,000 cells) of the same treatment were combined as one sample. For liver, frozen tissues (~50 mg) were homogenized in 3% SSA to remove proteins. After vortexing to lyze the cells and precipitating proteins, samples were centrifuged at 16,000g for 5 minutes (4°C) to pellet down proteins.

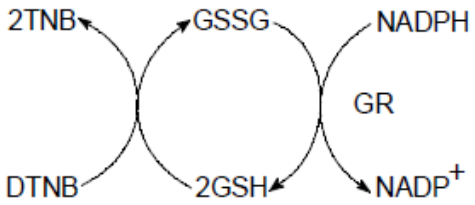

Figure 3.1 Principle of GSSG/GSH assay. DTNB reacts with GSH to form TNB, which can be detected spectrophotometrically at 412 nm.

Each supernatant (total ~ 1 ml) was transferred into two new 1.5-ml tubes, one to be assayed for total glutathione, i.e., GSH + GSSG (500 μl), and the other for GSSG only (500 μl, to be processed as below before the assay). Each protein pellet was dissolved in 10% SDS at room temperature for 1-4 days and measured for protein content with BCA kit (Pierce).The supernatant for GSSG assay was mixed well with 1 ml NEM solution containing 1.25 mg NEM (Sigma) in KPP buffer (100 mM potassium phosphate pH 6.5, 17.5 mM EDTA). Excess NEM and NEM-GSH conjugates were removed by SepPak cartridge (Waters), which was pre-washed with methanol and excess water. The flow-through was collected for assay.

The DNTB reaction system contained two solutions: Solution #1 (1.2 mM DTNB in 600 mM potassium phosphate pH 7.2, 30 mM EDTA, and 0.08% BSA), and Solution #2 (100 mM imidazole pH 7.2, 2 mM EDTA, and 0.04% BSA). All solutions and KPP buffers were warmed to room temperature before the assay. Then 0.5 mg NADPH (Sigma) and 6 μl/ml glutathione reductase (GR) (Sigma) were added into Solution #2. The GSH+GSSG (total) samples were diluted by 100-fold in KPP buffer, but no dilution was needed for GSSG samples. For each sample or standard, 500 μl sample was added into a plastic cuvette, then mixed with 150 μl Solution #1 and 150 μl Solution #2. After 10-minute incubation at room temperature, the absorbance at 412 nm was determined using a UV-Vis spectrophotometer (such as Cary 50, VARIAN). Concentrations of total (GSH+GSSG) and GSSG were calculated using the standard curve. All chemicals were obtained from Sigma unless otherwise indicated.

3.3.9 Measurement of cellular ROS

Cellular hydrogen peroxide and nuclear DNA levels were determined by staining with 2',7'-dichlorofluorescein diacetate (DCFH-DA, Sigma) and Hoechst 33342 (Molecular Probes, Eugene, OR), respectively. DCFH-DA is commonly used to measure the intracellular level of ROS. After diffusing into the cell, DCFH-DA will be deacetylated to nonfluorescent 2',7'-dichlorofluorescin (DCFH), which will then be rapidly oxidized to highly fluorescent 2',7'-dichlorofluorescein (DCF) by ROS. Therefore, the DCF-associated fluorescence can represent intracellular ROS level and be monitored and measured by ocular fluorophotometry.

The exact procedure is described as follows. One well of hepatocytes (300,000) from each group was used. All procedures were performed in dim light or in the dark to avoid degradation of the DCF dye. A stock solution of 2 mM DCFH-DA was made by dissolving the powder in DMSO. The staining medium was made of 2 μM DCFH-DA in Williams' medium E containing penicillin /streptomycin and glutamine, and incubated in a 37°C water bath for one hour immediately before use. Hepatocytes were washed with PBS once before incubation in staining medium (1 ml per well) for 20 minutes at 37°C. Afterwards, medium was removed and cells were washed with PBS once before being incubated in Williams' medium E (1 ml per well) for 20 minutes at 37°C. A florescence microscope (ZEISS, observer A1) was used to observe and record DCF signals with a GFP filter and cell morphology with DIC filter.

For fluorescence reading, cells were washed with PBS once and then incubated in 37°C with 2 μM DCFH-DA and 0.1 μg/ml Hoechst in HBSS (with Ca^{2+} and Mg^{2+} but

without phenol red) for 20 min in the dark. Cells were collected by trypsinization and resuspended in PBS plus 20 mM glucose at a density of 1×10^6 cells/ml. Fluorescence measurements were performed in clear 96-well plates at excitation/emission wavelengths of 480/533 nm for DCF signals or at 355/460 nm for Hoechst signals on a SpectraMax M5 microplate reader (Molecular Devices, Sunnyvale, CA). Cellular ROS level was normalized to nuclear DNA content, which is represented by the DCF:Hoechst ratio.

3.3.10 Ceramide analyses

Upon the completion of fatty acid treatment (0.5 mM C16:0 or C18:1), hepatocytes from each 6-cm plate (900,000 cells) were rinsed with isotonic LiCl before lipid extraction by the method of Bligh and Dyer [143]. Ceramide (CM) species were measured to C8:0-CM internal standard by negative ion ESI (electrospray ionization)/MS as previously described [144] and normalized to sample protein content.

3.3.11 Indirect calorimetry

Indirect calorimetry was conducted in a 4-chamber OxyMax System from Columbus Instruments (Columbus, OH). The O_2 and CO_2 gas fractions were monitored at both the inlet and output ports with a flow rate of 0.4 liter/minute. These measurements were used to compute VO_2 and VCO_2 values (10 minutes per data point) in units of ml/kg/hour. Respiratory exchange rate (RER) was calculated as "VCO_2/VO_2" and used to predict the likely fuel source, i.e., RER = 1.0 (carbohydrates), 0.7 (fat), or 0.85 (proteins or a combination of carbohydrates and fats).

3.3.12 Electron Microscopy

Transmission electron microscopy was performed in the Electron Microscopy core facility at KUMC. Fresh liver pieces (~1 mm^3 in size) were fixed in 2.5% glutaraldehyde in 0.1 M NaCacodylate buffer overnight and post fixed with 2% osmium tetroxide for one hour before being processed and embedded in EPON. Thin sections were placed on copper grids and stained with 1% uranyl acetate. Micrographs were obtained with a JEOL (Tokyo, Japan) 100 CXII transmission electron microscope that was operated at 80 kV. The NIH Image J software was used for counting mitochondrial and cytoplasmic area.

3.3.13 Mitochondrial DNA content measurement

Quantitative PCR was performed to determine the relative copy numbers of mitochondrial DNA (mtDNA) and nuclear DNA (nDNA) in livers from 5-week-old WT and Ncb5or-/- mice. Each reaction (10 µL) contained genomic DNA (100 ng) and forward and reverse primers (0.6 µM each). Hexokinase 2 (intron 9) and 16S rRNA were used as nDNA- and mtDNA-specific targets, respectively, as described by others [145]. A standard dilution series was used to confirm the efficiency of exponential amplification for each primer pair. Mitochondrial to nuclear DNA ratio in each sample was calculated by dividing the value of 16S by that of hexokinase 2.

3.3.14 TNFα level measurement

Duoset Mouse TNFα ELISA kit from R&D systems (Minneapolis, MN) was used to detect the TNFα level in serum according to the manufactory's instruction. Fifty µl of serum was used in each assay.

3.3.15 Data analysis

One-way analysis of variance (ANOVA) was used to detect the significant difference within and between groups. A value of $p<0.05$ was considered statistically significant. Data are presented as the mean ± standard error of the mean (S.E.).

3.4 Results

3.4.1 Increased cell death in Ncb5or$^{-/-}$ hepatocytes under SFA challenge

In our previous study (Chapter 2), we observed higher intracellular levels of free SFAs in Ncb5or$^{-/-}$ hepatocytes than WT under both basal condition and C16:0 treatment (Figure 2.6). Here we examined SFA-induced cytotoxicity in Ncb5or$^{-/-}$ hepatocytes.

Previous studies showed Ncb5or$^{-/-}$ hepatocytes were more sensitive to SFA treatment [35; 36]. In these studies, hepatocytes were potentially starved at the end of treatment, because they were cultured in medium without FBS, which resulted in low level of fatty acids left in medium after a 12-hour treatment. The SFA-induced cytotoxicity in these Ncb5or$^{-/-}$ hepatocytes might be caused by nutrient starving instead of SFA itself. To avoid these complications, we used a nutrient-rich medium containing 10% FBS for preincubation and shortened the duration of fatty acid treatment from 12 to 8 hours. Under these conditions, more than 20% of fatty acids still remained in the medium at the end of treatment.

Under these experimental conditions, we observed that treatment of 0.25 mM palmitate (C16:0) resulted in cell death in 10% of Ncb5or$^{-/-}$ hepatocytes, and the rate

increased to 40% with 0.5 mM C16:0, in contrast to a level below detection and 10% in WT hepatocytes that are treated with 0.25 and 0.5 mM C16:0, respectively (Figure 3.2 A). C18:1 did not affect cell viability in WT or Ncb5or$^{-/-}$ hepatocytes, and co-incubation with C16:0 and C18:1 completely rescued the SFA cytotoxicity in Ncb5or$^{-/-}$ hepatocytes (Figure 3.2 A). The above cell viability was determined by measuring intracellular ATP levels. Since Ncb5or$^{-/-}$ hepatocytes had abnormal metabolism, which may affect the ATP level, we used another assay that measured live-cell protease activity. Similar results were obtained with the latter method (Figure 3.2 B), further confirming increased SFA cytotoxicity in Ncb5or$^{-/-}$ hepatocytes.

To find out whether lipotoxicity is specific to SFA in Ncb5or$^{-/-}$ hepatocytes, we treated Ncb5or$^{-/-}$ and WT hepatocytes with various concentrations of glucose, which is another major source of energy, as well as H_2O_2. We found that Ncb5or$^{-/-}$ and WT hepatocytes had similar cell viability under all concentrations of glucose ranging 11 – 500 mM (Figure 3.3 A). Secondly, we treated Ncb5or$^{-/-}$ and WT hepatocytes with various concentrations of H_2O_2 for 2 hours. We found that Ncb5or$^{-/-}$ hepatocytes displayed higher viability than WT when treated with 0.25 mM (Figure 3.3 B), which likely reflects higher expression levels of antioxidant genes in Ncb5or$^{-/-}$ hepatocytes than WT (discussed below).

Cytotoxicity in Ncb5or$^{-/-}$ hepatocytes appeared to be specifically caused by long-chain SFA, such as C16:0. MUFA not only caused no cytotoxicity but also rescued SFA-induced cytotoxicity (Figure 3.2). This is likely achieved by channeling free SFA to TAG, which were shown in our earlier studies (Figure 2.4 and 2.6).

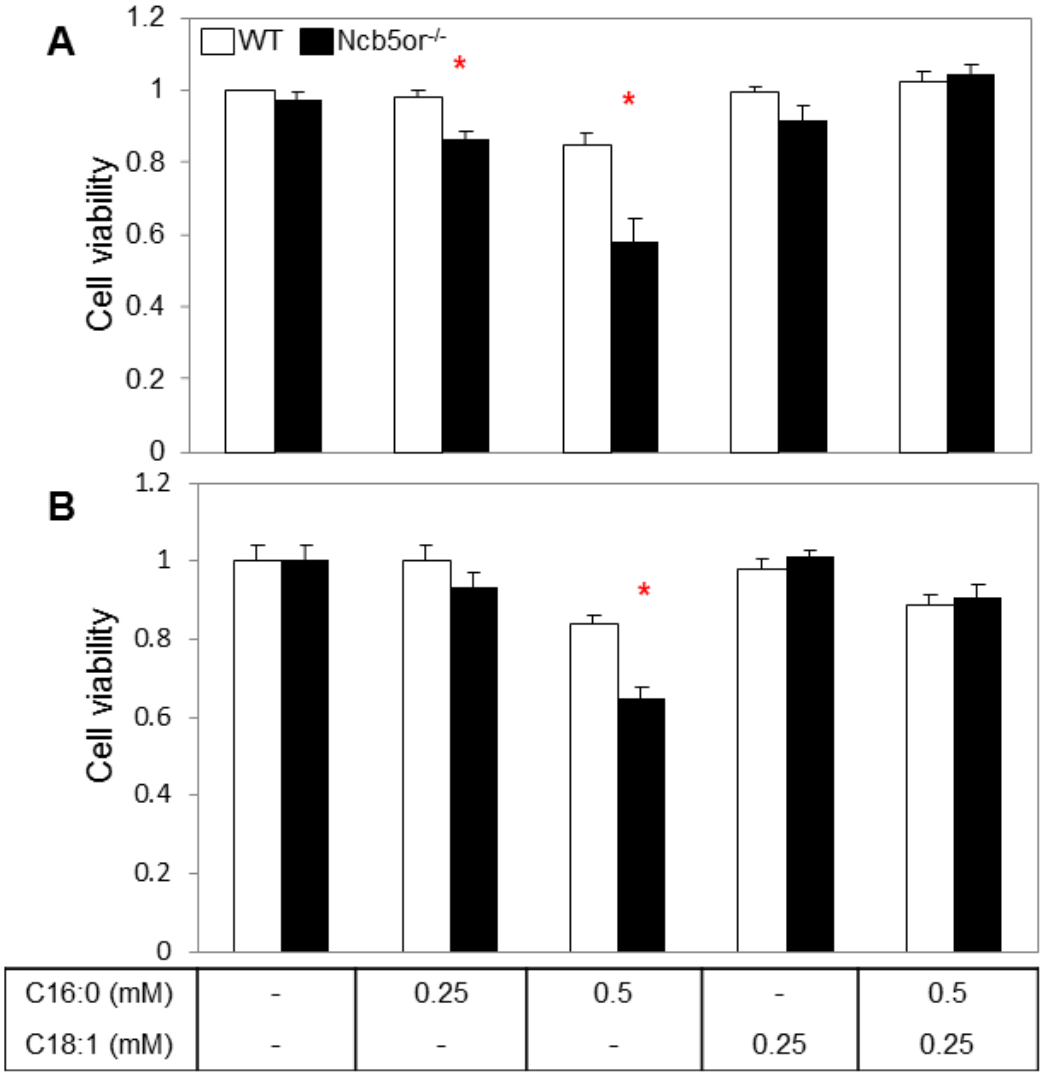

Figure 3.2 Effects of incubation with palmitate and oleate on cell viability in Ncb5or$^{-/-}$ and WT hepatocytes. Hepatocytes were isolated as above and treated with BSA carrier (vehicle control, -) or palmitate (C16:0) or oleate (C18:1) for 8 hours. (A) Cell viability was assessed by measuring cellular ATP content. The results were obtained from 7 animal-pairs (n=7). (B) Cell viability was assessed by measuring live-cell protease activity from 3 animal-pairs (n=3). All results were expressed as mean ± S.E. *, p<0.05. White-bar: WT; Black-bar: Ncb5or$^{-/-}$.

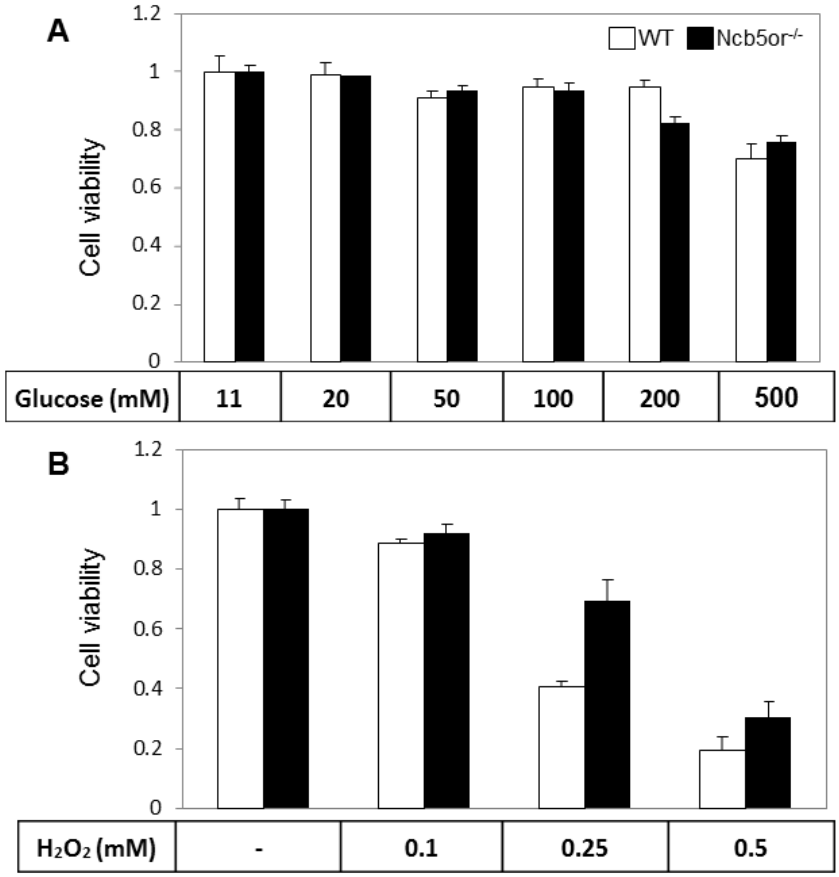

Figure 3.3 Effects of incubation with glucose or H_2O_2 on cell viability in Ncb5or$^{-/-}$ and WT hepatocytes. (A) Hepatocytes were treated with different concentrations of glucose for 8 hours. (B) Hepatocytes were treated with different concentrations of H_2O_2 for 2 hours. All hepatocytes were isolated as above. Cell viability was assessed by measuring cellular ATP content in both cases. All results were obtained from 6-12 wells of cells from 2-4 animal-pairs and expressed as mean ± S.E. *, p<0.05. White-bar: WT; Black-bar: Ncb5or$^{-/-}$. Ncb5or$^{-/-}$ cells displayed a higher viability (p=0.06, n=3) than WT after 0.25 mM H_2O_2 treatment.

3.4.2 Increased oxidative stress in Ncb5or$^{-/-}$ hepatocytes under SFA treatment

We next investigated the mechanism of SFA induced cell death. Previous studies by others suggest that SFAs induce cell death through the following pathways: ceramide signaling [81], phospholipid remodeling [82], oxidative stress [83; 84] and ER stress [35; 86; 87]. Here we examined these pathways one by one.

We measured levels and profiles of intracellular ceramide in Ncb5or$^{-/-}$ and WT hepatocytes after the treatment with 0.5 mM C16:0 or C18:1 or vehicle (BSA) control. Surprisingly, we observed no difference between the two genotypes under all three conditions (Figure 3.4), suggesting that SFA cytotoxicity in Ncb5or$^{-/-}$ hepatocytes is independent of ceramide [81].

Next, we measured the fatty acid composition of phospholipids of these hepatocytes. We found that, under C16:0 incubation, Ncb5or$^{-/-}$ hepatocytes appeared to accumulate less phospholipid (PL) content (p=0.07) and to have lower values of DI (C16) than WT (Figure 3.5). These observations suggested a phospholipid remodeling in Ncb5or$^{-/-}$ hepatocytes, which could lead to the impairment of ER and mitochondrial function (to be tested below).

We evaluated oxidative stress and ER stress response in Ncb5or$^{-/-}$ and WT hepatocytes under SFA treatment. We found that, under basal condition and C16:0 incubation, Ncb5or$^{-/-}$ hepatocytes expressed higher transcript levels of mitochondrial biogenesis gene (PGC1α) and oxidative stress responses genes (HMOX1, GCLC, MT1 and MT2) than WT cells, and the fold of induction increased with increasing concentrations of C16:0. These effects were prevented by co-incubation of C16:0 with C18:1 (Figure 3.6).

To examine whether transcript levels of oxidative stress response genes correlated with intracellular ROS level, we subjected Ncb5or$^{-/-}$ and WT hepatocytes to DCF staining for direct measurement of ROS. We detected stronger signals of DCF by both assessing fluorescence signals (Figure 3.7 A) and confocal microscopy (Figure 3.8) in Ncb5or$^{-/-}$ hepatocytes than WT under the C16:0 treatment.

We next measured intracellular levels of oxidized and reduced glutathione in these cells. We observed higher GSSGH:GSH ratios in SFA-treated Ncb5or$^{-/-}$ hepatocytes than WT cells (Figure 3.7B), whereas no significant difference was found for total glutathione level (Figure 3.7C). Co-incubation with C18:1 decreased GSSG/GSH ratios and intracellular levels of ROS in Ncb5or$^{-/-}$ hepatocytes. To avoid complications from dead cells, we used 0.25 mM C16:0 in these two experiments, under which more than 85% of Ncb5or$^{-/-}$ hepatocytes survived after 8 hours. Because DCF oxidation reflects the level of ROS and because GSSG is generated from GSH through the reduction of ROS, we concluded that SFA induced more ROS in Ncb5or$^{-/-}$ hepatocytes. This observation is concordant to that of SFA induced cell death, which strongly suggested that ROS played an important role in SFA cytotoxicity in Ncb5or$^{-/-}$ hepatocytes. Ncb5or$^{-/-}$ hepatocytes had slightly better tolerance to exogenous ROS compared to WT (Figure 3.3B), suggesting that increased levels of ROS, rather than loss of antioxidant capacity, is likely responsible for cell death.

We also examined the potential involvement of ER stress by measuring transcript levels of ER stress response genes. In contrast to the previous finding [35], no obvious ER stress response was observed in Ncb5or$^{-/-}$ hepatocytes under SFA treatment (Figure 3.9), despite a similar trend of ER stress. Our findings suggest that ER stress is not a major contributor to cell death compared to oxidative stress.

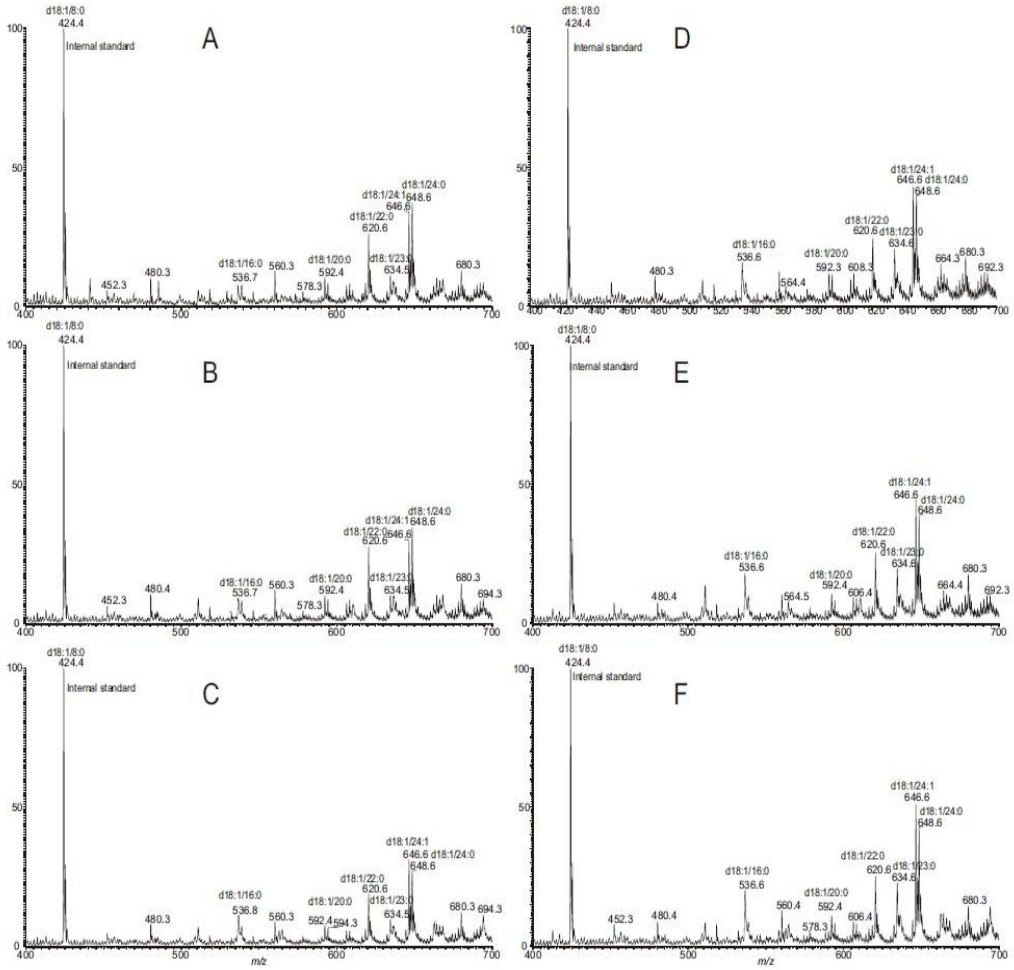

Figure 3.4 Ceramide profile of Ncb5or-/- and WT hepatocytes after fatty acid treatments. Hepatocytes were isolated and treated with palmitate or oleate (0.5 mM each) or BSA carrier alone (control) as above. Total ceramide profiles were measured relative to a C8:0-CM internal standard by negative-ion ESI/MS and normalized to sample protein content. Results were obtained from 3 animal-pairs (n=3) and one representative set is shown with major ceramide species as labeled. (A) WT with BSA carrier; (B) WT with 0.5 mM palmitate; (C) WT with 0.5 mM oleate; (D) Ncb5or$^{-/-}$ with BSA; (E) Ncb5or$^{-/-}$ with 0.5 mM palmitate; (F) Ncb5or$^{-/-}$ with 0.5 mM oleate. Dr. Fong-Fu Hsu in Washington University in St. Louis performed the ceramide analyses.

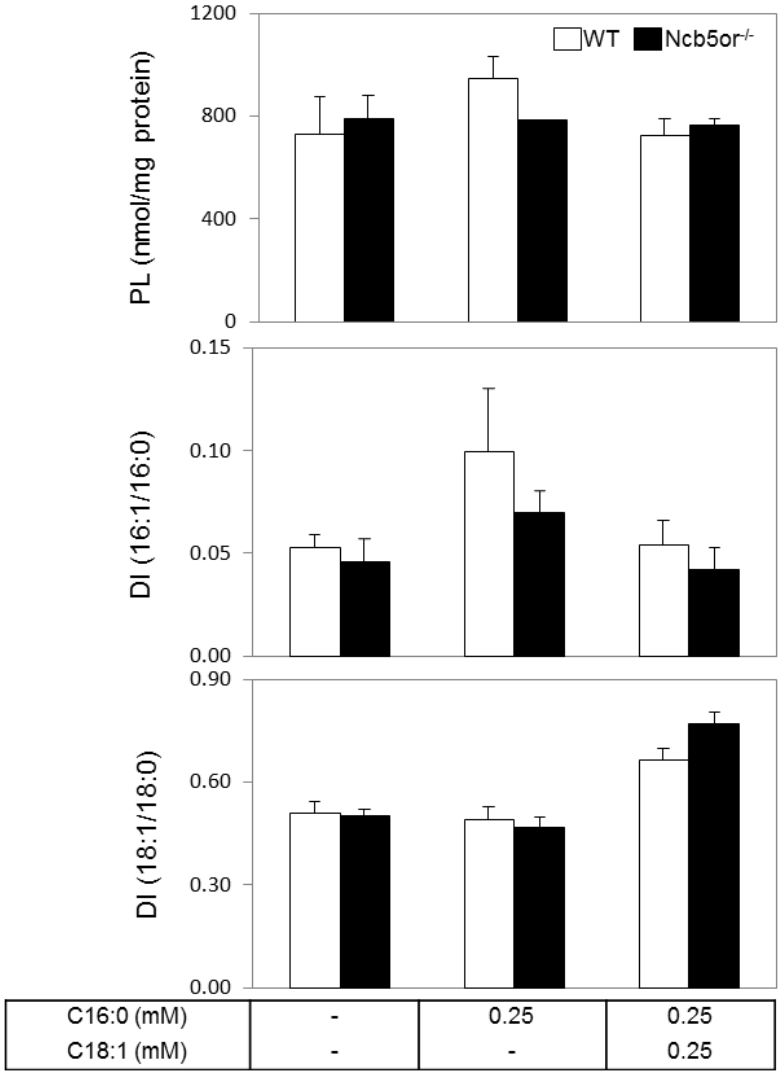

Figure 3.5 Effects of incubation with palmitate and oleate on Ncb5or$^{-/-}$ and WT hepatocyte in PL pools. Hepatocytes were isolated and treated with palmitate or oleate or BSA carrier alone. Intracellular phospholipids were prepared and analyzed for determination of lipid profiles by GC/MS. The total content, desaturation index of C16:1/C16:0 and C18:1/C18:0 were determined. Results were obtained from 3 animal-pairs (n=3) for PL profiling and expressed as mean ± S.E. White-bar: WT; Black-bar: Ncb5or$^{-/-}$.

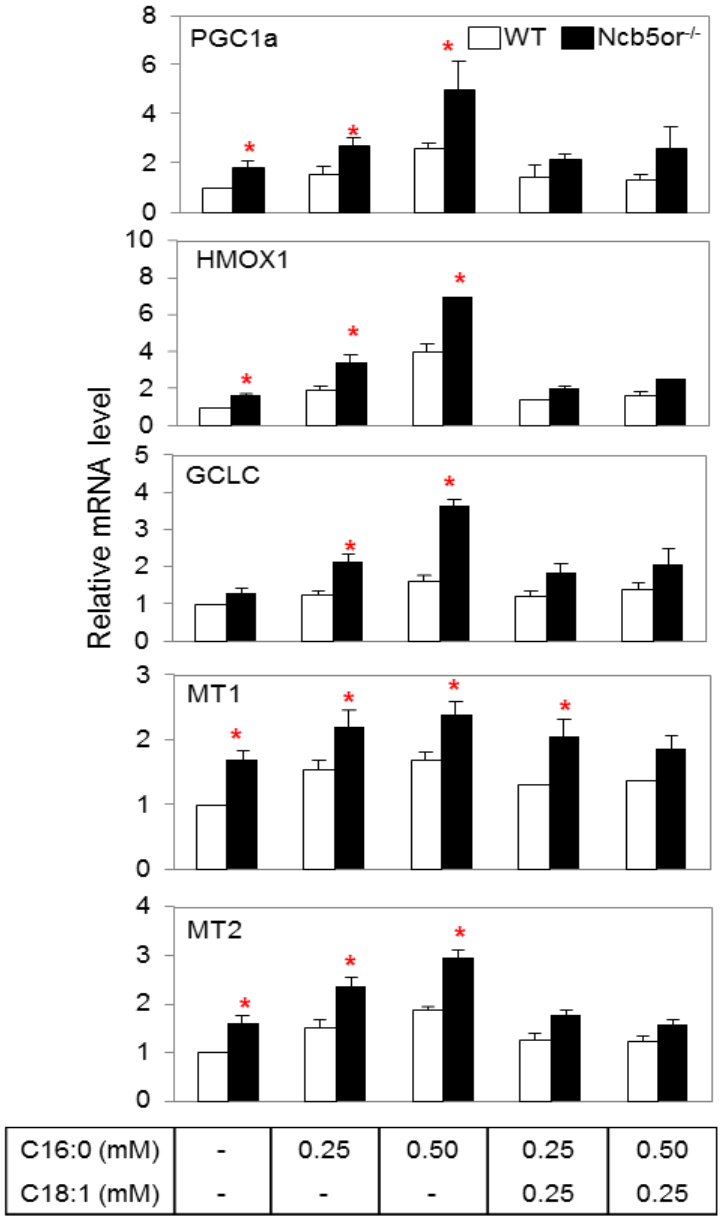

Figure 3.6 Effects of incubation with palmitate and oleate on expression of genes involved in mitochondrial biogenesis and oxidative stress responses in Ncb5or$^{-/-}$ and WT hepatocytes. Hepatocytes were isolated and treated with palmitate or oleate or BSA carrier alone (see above). Total RNAs were collected and used for quantitative RT-PCR. Results were obtained from 4-6 animal-pairs (n=4-6) and expressed as mean ± S.E. *, p<0.05. White-bar: WT; Black-bar: Ncb5or$^{-/-}$.

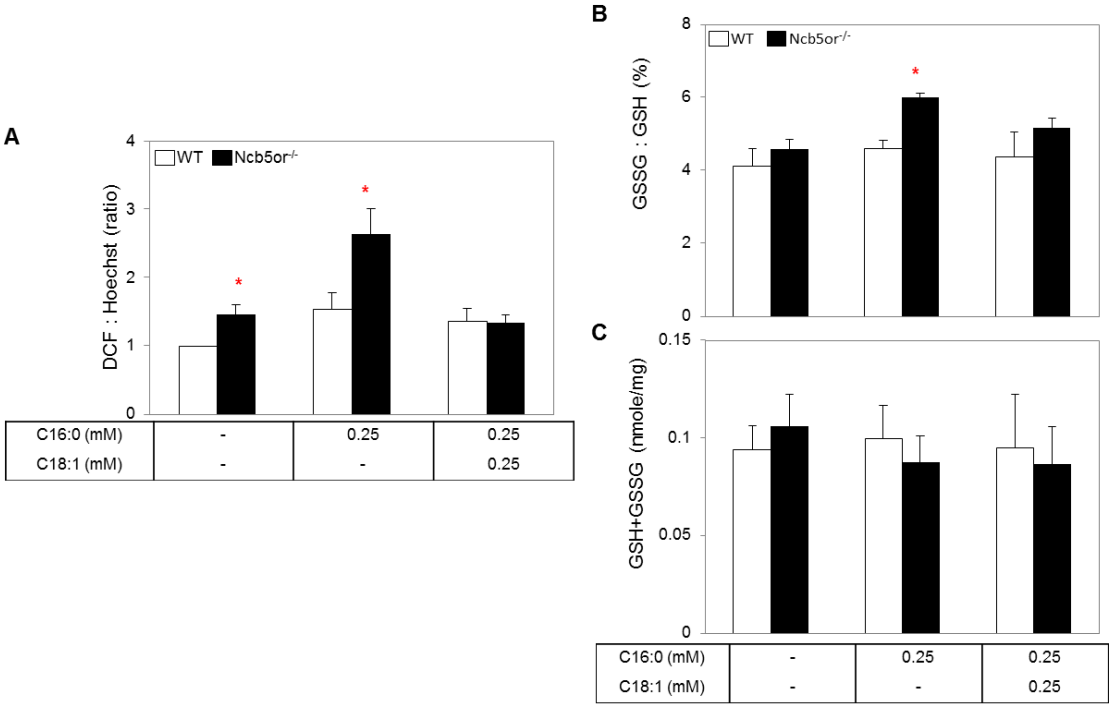

Figure 3.7 Effects of incubation with palmitate and oleate on oxidative stress in Ncb5or$^{-/-}$ and WT hepatocytes. Hepatocytes were isolated as above and treated with BSA carrier (vehicle control, -) or palmitate (C16:0) or oleate (C18:1) for 8 hours. (A) Intracellular H_2O_2 content was assessed with DCFH-DA, and relative intensity of fluorescence signals against nuclear DNA content (Hoechst staining signal) was used in comparison. Intracellular glutathione levels were measured and are displayed as (B) GSSG/GSH ratio and (C) GSH+GSSG (total glutathione content). All results were obtained from 4-6 animal-pairs (n=4-6) and expressed as mean ± S.E. *, p<0.05. White-bar: WT; Black-bar: Ncb5or$^{-/-}$.

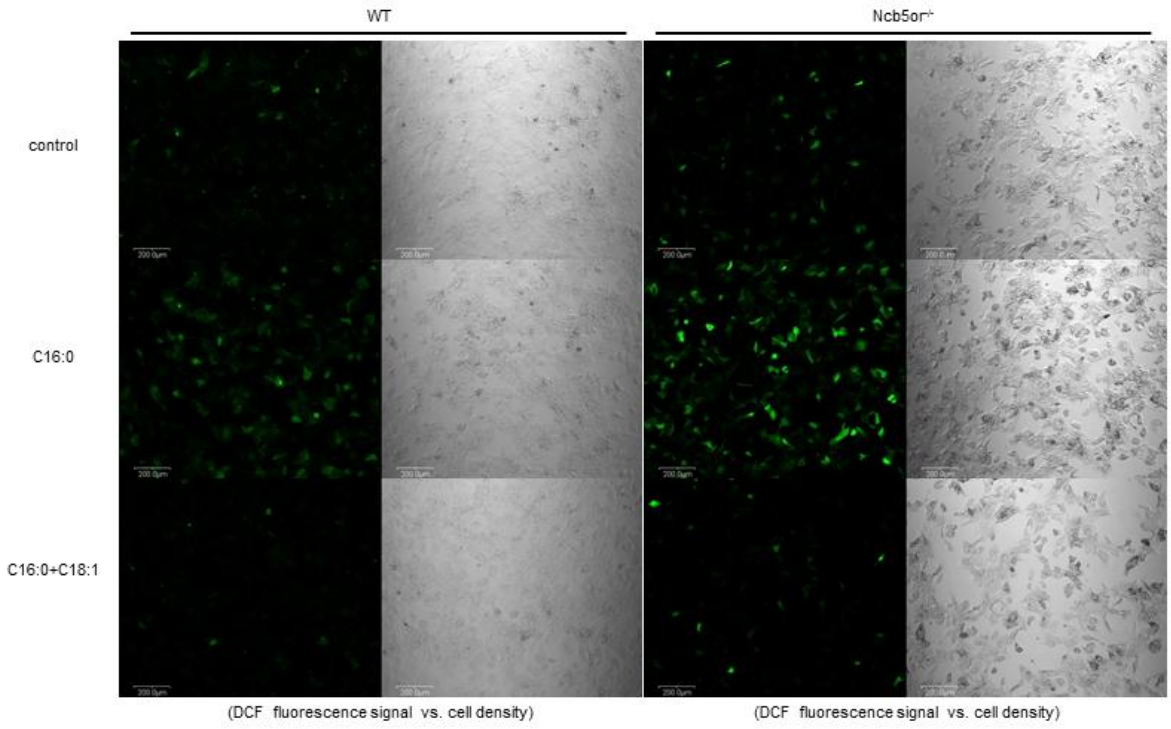

Figure 3.8 Images of DCF-stained hepatocytes after fatty acids treatment. Hepatocytes were isolated and treated with palmitate (C16:0, 0.25 mM) or a combination of palmitate and oleate (C16:0+C18:1, 0.25 mM each) or BSA carrier alone (- control) for 8 hours as above. For confocal microscopy, cells were seeded in 12-well plates and incubated in the dark with 2 μM DCFH-DA at 37°C for 20 minutes in HBSS. Cells were then washed with HBSS once and subjected to Olympus Fluoview 300 confocal microscopy to record fluorescence (488 nm excitation / 530 nm emission) and light microscopy images with the same settings.

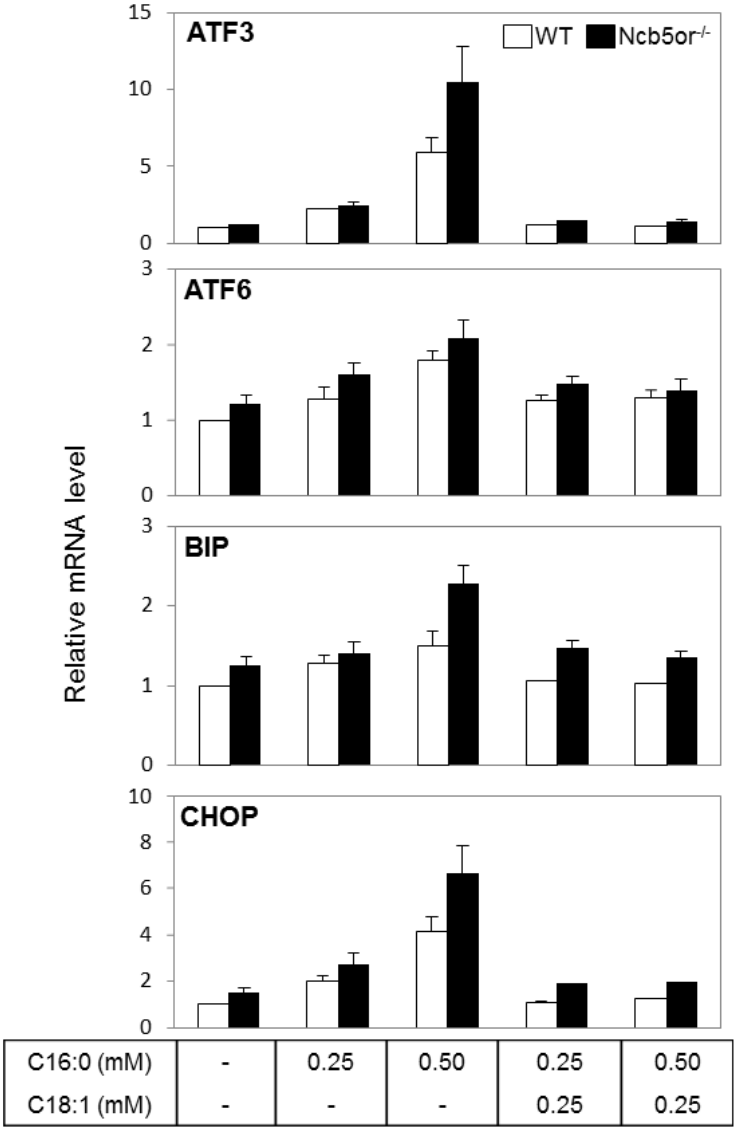

Figure 3.9 Effects of incubation with palmitate and oleate on expression of genes involved in ER oxidative stress responses in Ncb5or$^{-/-}$ and WT hepatocytes. Hepatocytes were isolated and treated with palmitate or oleate or BSA carrier alone (see above). Total RNAs were collected and used for quantitative RT-PCR. Results were obtained from 4-6 animal-pairs (n=4-6) and expressed as mean ± S.E. White-bar: WT; Black-bar: Ncb5or$^{-/-}$.

3.4.3 Higher rates of hepatic fatty acid oxidation and cellular respiration in Ncb5or$^{-/-}$ hepatocytes than WT

Our findings suggest that oxidative stress is the major contributor to cell death in Ncb5or$^{-/-}$ hepatocytes. Also, phospholipid remodeling induced mitochondrial dysfunction, which might also play a role. Here, we further examine the cause of SFA induced oxidative stress in Ncb5or$^{-/-}$ hepatocytes.

There are four major cellular sources for ROS production as described in Chapter 1. Elevated level of NADPH oxidase (NOX) is a possibility, but it is excluded by the fact that no difference in hepatic transcript levels of NOX3 and NOX4 was found between Ncb5or$^{-/-}$ and WT mice (data not shown).

The second potential source is peroxisomes, which can generate H_2O_2 through β-oxidation of long chain fatty acids when mitochondrial β-oxidation is overwhelmed [102]. We measured the transcript levels of ACOX, the peroxisome specific enzyme catalyzing the first oxidation step, in the hepatocytes that were treated with SFA or MUFA. We observed no significant difference between the two genotypes under all treatments, even with 0.5 mM C16:0 (data not shown). We concluded that SFA induced ROS generation is independent of peroxisome.

ER is estimated to contribute as much as 25% of total cellular ROS production [129]. We detected mild ER stress in Ncb5or$^{-/-}$ hepatocytes (Figure 3.9) but not under the same condition that oxidative stress was detected, i.e., 0.25 mM C16:0 treatment (Figures 3.6 and 3.7). These findings suggest that Ncb5or$^{-/-}$ hepatocytes are more sensitive to

oxidative stress than ER stress and that oxidative stress is a more prominent event in these cells.

Here we examined mitochondrial source in depth, because a high flux of ETC can induce electron leakage to generate ROS. We showed earlier (Figure 2.6) that Ncb5or$^{-/-}$ hepatocytes accumulate more palmitate, which is a common substrate for β-oxidation.

We determined the rates of fatty acid oxidation (FAO) in Ncb5or$^{-/-}$ and WT hepatocytes using isotope labeled substrate, i.e. [n9,10-^{3}H] palmitate and measuring its end product through FAO ([^{3}H]HO). After 2 hours of incubation, we observed a 30% increase of FAO rates in Ncb5or$^{-/-}$ hepatocytes than WT (Figure 3.10 A). This increase in FAO mostly occurred in mitochondria, since we observed no difference between the two genotypes in expression of genes involved in peroxisomal FAO (see above).

Higher FAO rates indicate that cells produce at higher levels not only $FADH_2$ and NADH, but also acetyl-CoA, all of which can increase the flux of ETC either directly or indirectly through the TCA cycle. To determine whether this is the case in Ncb5or$^{-/-}$ hepatocytes, we measured total cellular oxygen consumption rate (OCR) of these hepatocytes under basal condition and upon the addition of SFA and MUFA. Excess carnitine was added to facilitate mitochondrial entry in this experiment as well as in FAO assay. The ETC in mitochondria consumes oxygen to produce ATP, thus the baseline OCR represents the rate of ETC. We observed that Ncb5or$^{-/-}$ hepatocytes had higher OCR values than WT under the basal condition and that the addition of either C16:0 or C18:1 increased OCR in both Ncb5or$^{-/-}$ and WT hepatocytes (Figure 3.10 B). It is important to note that C16:0 induced a significantly bigger increase in OCR in Ncb5or$^{-/-}$ hepatocytes

than WT, whereas the difference between the two genotypes was not significant with the addition of C18:1 (Figure 3.10 C). Compared to WT, higher basal OCR values in Ncb5or$^{-/-}$ hepatocytes suggested a more active flux of ETC in these cells. The greater induction of OCR by C16:0, but not C18:1, in Ncb5or$^{-/-}$ hepatocytes reflects their higher capacity to catabolize SFA, which are more abundant in these cells than in WT.

We next investigated whether significantly higher ROS levels in Ncb5or$^{-/-}$ hepatocytes than WT (Figure 3.7) could be due to mitochondrial dysfunction, which has been shown to exaggerate the ROS production. By using an extracellular flux analyzer, we measured mitochondrial function in response to the following compounds that were added in sequence to primary hepatocytes. The first compound was oligomycin that inhibits mitochondrial ATP synthesis and its associated oxygen consumption. The trace of OCR correlates to cellular respiration independent of ATP synthesis, which is caused by H^+ leakage from ETC. The second compound was carbonyl cyanide-p-trifluoromethoxy phenylhydrazone (FCCP). FCCP is a potent uncoupler of mitochondrial proton gradient and makes cells to bypass the ATP synthesis and to dissipate the proton gradient for heat. Upon the addition of FCCP, OCR increases to the maximum level, which represents the maximum respiratory capacity. The third compound was a mixture of rotenone and antimycin, which inhibits complex I and III, respectively. In this case, the flow of electrons in mitochondrial ETC will completely cease and all mitochondrial respiration will stop.

As shown in Figure 3.11, Ncb5or$^{-/-}$ and WT hepatocytes displayed a similar response to all the above compounds. This indicates that there is no difference between the two genotypes in H^+ leakage and in maximum respiratory capacity of mitochondria in

hepatocytes. In other words, the mitochondria in Ncb5or$^{-/-}$ hepatocytes remained intact and functional. Therefore, higher rates of FAO and OCR in Ncb5or$^{-/-}$ hepatocytes could simply reflect the increases in mitochondrial capacity in association with the over-abundance of substrates (SFAs) and higher mitochondrial density (see below) in these cells.

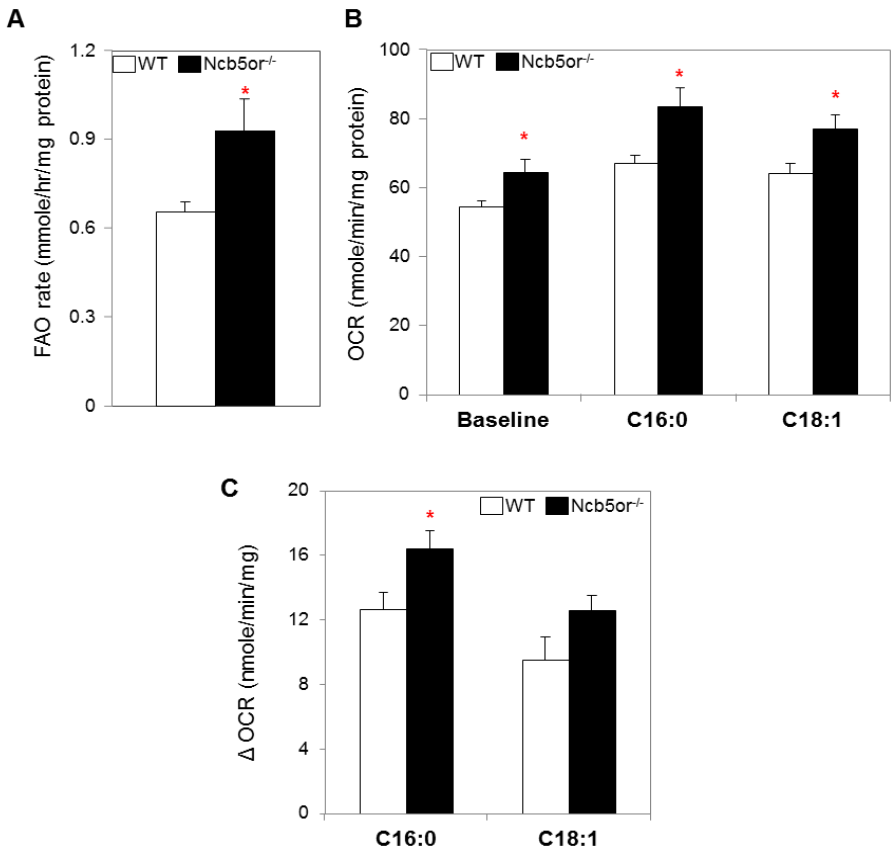

Figure 3.10 Mitochondrial fatty acid oxidation in Ncb5or$^{-/-}$ and WT hepatocytes (A) The rate of mitochondrial fatty acid oxidation (FAO) rate was determined by incubating cells in 37°C for 2 hours with 0.125 mM palmitate (mixed with 0.8 μCi [n9,10-^{3}H]palmitate) in the presence of 1 mM carnitine, and measuring the oxidation product ([^{3}H]HO) in media. (B) The same hepatocytes were subjected to extracellular flux analysis to measure oxygen consumption rate (OCR) before (baseline) and after the addition of 0.125 mM C16:0 or C18:1 in the presence of 1 mM carnitine. These values were used to calculate the increase in OCR (ΔOCR), shown in (C). All results were obtained from 4 animal-pairs (n=4), standardized against total proteins of hepatocytes and expressed as mean ± S.E. The flux analyses were performed in collaboration with Dr. Russell Swerdlow's laboratory.*, p<0.05. White-bar: WT; Black-bar: Ncb5or$^{-/-}$.

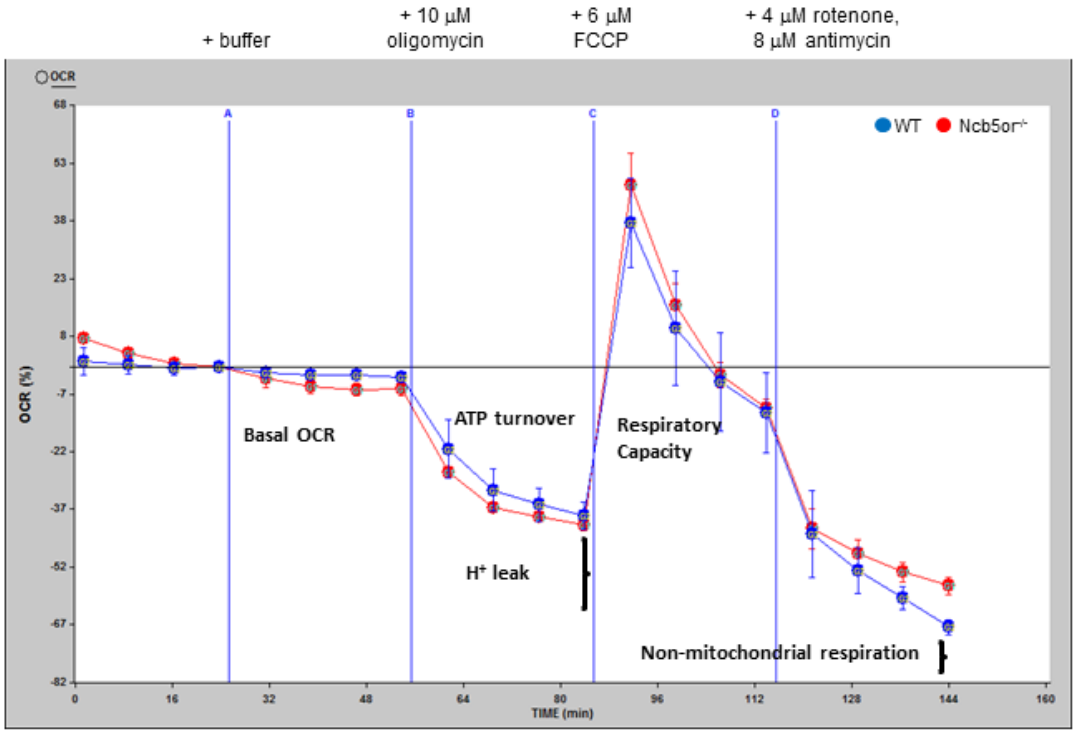

Figure 3.11 Changes in oxygen consumption rate (%OCR) in Ncb5or$^{-/-}$ and WT hepatocytes in response to ETC related compounds. Hepatocytes were isolated and OCR were measured after sequential additions of (A) buffer, (B) oligomycin (inhibitor of mitochondrial ATP synthesis, 10 µM), (C) FCCP (carbonyl cyanide-p-trifluoromethoxy phenylhydrazone, mitochondrial uncoupler, 6 µM), and (D) rotenone/antimycin (complex I/III inhibitor, 4/8 µM, respectively). Three sets of WT and Ncb5or$^{-/-}$ hepatocytes (n=3) were tested and resulted in the same finding. One representative pair is shown here with each data point measured in triplicates. Percentage change in OCR was calculated from comparison to the baseline OCR (prior to treatment). Blue-bar: WT; Red-bar: Ncb5or$^{-/-}$. This experiment was performed in collaboration with Dr. Russell Swerdlow's laboratory.

3.4.4 Increased oxygen consumption and mitochondrial density in prediabetic Ncb5or$^{-/-}$ mice

We measured the whole body oxygen consumption of 5-week-old WT and Ncb5or$^{-/-}$ mice using indirect calorimetry. We found Ncb5or$^{-/-}$ mice consumed significantly more O_2 than WT mice during fasting and fed periods (Figure 3.12 A). However, we did not observe any difference in respiration exchange ratios between WT and Ncb5or$^{-/-}$ mice (Figure 3.12 B), suggesting no difference between the two genotypes in fuel substrates.

We previously observed increased mitochondrial biogenesis and oxidative metabolism in the hepatocytes of prediabetic Ncb5or$^{-/-}$mice. To determine whether these cells have increased mitochondrial density, we used transmission electron microscopy to compare the ultrastructure of hepatocytes of Ncb5or$^{-/-}$ and WT mice. We found that Ncb5or$^{-/-}$ hepatocytes had higher mitochondrial numbers (Figure 3.13 A) and areas (Figure 3.13 B) than WT.

To further confirm this finding, we used a different method to determine the ratio between mitochondrial and nuclear DNA, assuming that each mitochondrion contained the same copy number of DNA. , We observed higher mitochondrial : nuclear DNA ratios in Ncb5or$^{-/-}$mice than WT (Figure 3.13 C).

All these data suggest that Ncb5or$^{-/-}$mice had increased mitochondrial density in the liver at age 5 weeks. Notably, we did not observe any difference in mitochondrial density between the two genotypes at age 2 weeks (Figure 3.14). These results are consistent with PGC1α expression levels at these two ages (Table 2.1).

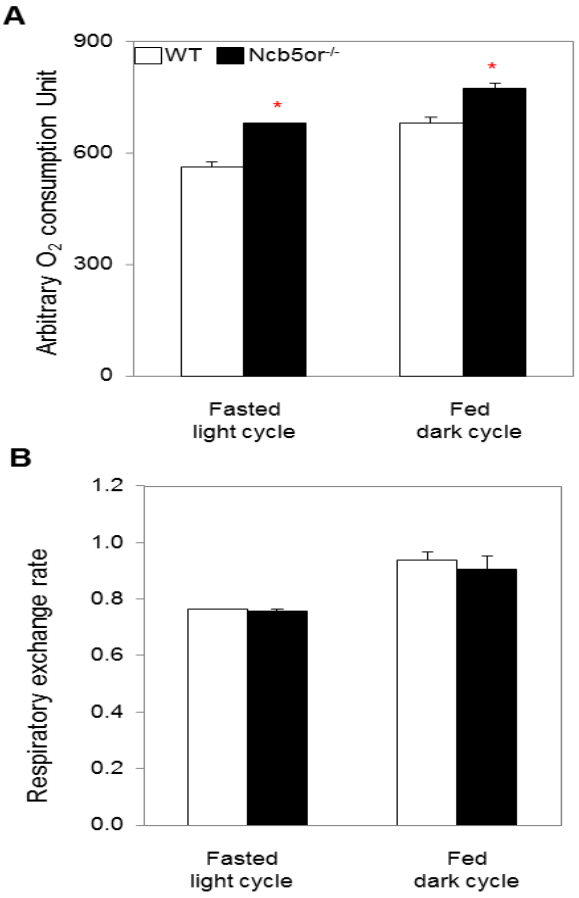

Figure 3.12 Whole body O_2 consumption and respiration exchange ratio of chow-fed Ncb5or$^{-/-}$ and WT mice. (A) O_2 consumption of 5-week-old Ncb5or$^{-/-}$ and WT mice was measured by indirect calorimetry and plotted as a function of time. Area-under-the-curve was calculated for each mouse during light (fasting) or dark (fed) cycle. (B) Respiration exchange ratio of CO_2 production vs. O_2 consumption (RER) of each mouse was calculated for each time point and averaged for the entire light (fasting) or dark (fed) cycle. Results in (A) and (B) were obtained from 3 pairs (n=3) and plotted as mean ± S.E. Results are expressed as mean ± S.E. *, $p<0.05$. White-bar: WT; Black-bar: Ncb5or$^{-/-}$.

Dr. WenFang Wang fully contributed to this figure.

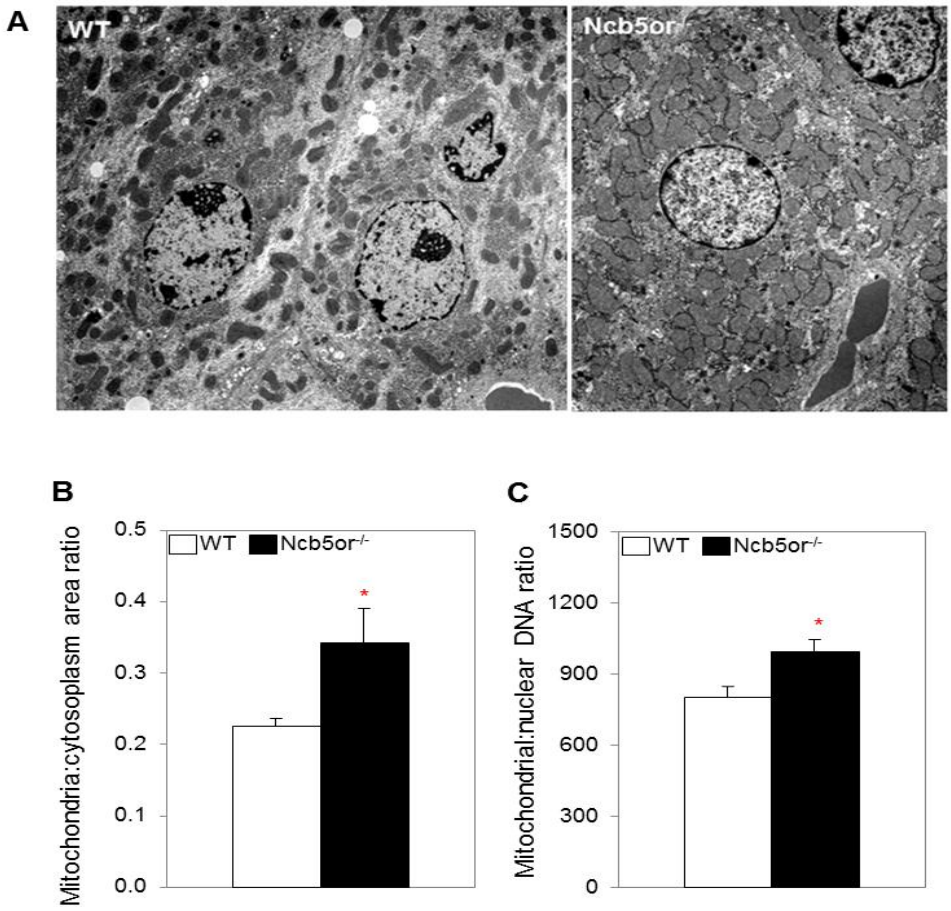

Figure 3.13 Hepatic mitochondrial content of chow-fed 5 week old Ncb5or$^{-/-}$ and WT mice. (A) Representative TEM micrographs of Ncb5or$^{-/-}$ and WT hepatocytes at five weeks of age (B) Area of mitochondrial and cytosolic space was measured by the NIH ImageJ software and used to calculate the "mitochondria:cytoplasmic area". A total of three pairs (n=3, >10 cells per animal) were analyzed and results are expressed as mean ± S.E. (C) Ratios of "mitochondria:nuclear DNA" (16s rRNA:hexokinase 2) were determined by qPCR. A total of seven pairs (n=7) were analyzed and results are expressed as mean ± S.E. *, p<0.05. White-bar: WT; Black-bar: Ncb5or$^{-/-}$.

Dr. WenFang Wang performed OxyMax measurement and analyses, as well as most of TEM studies and image collection.

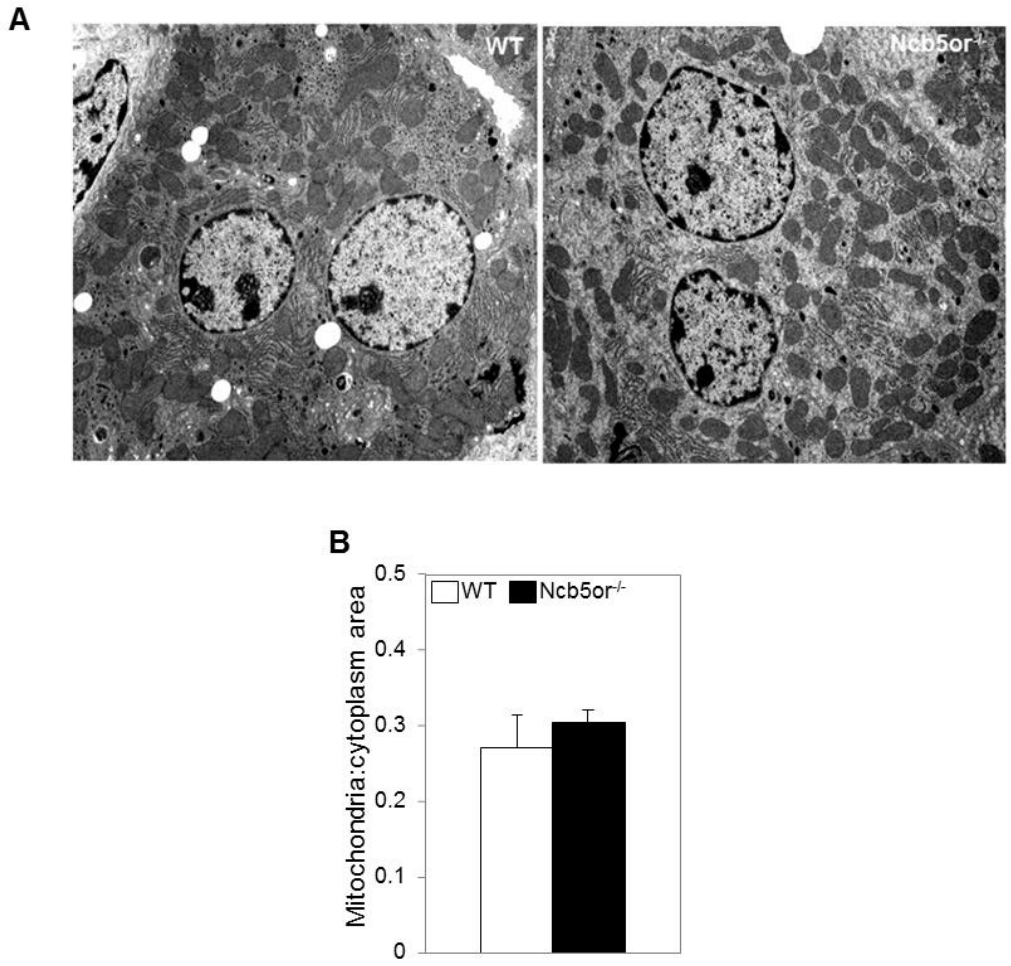

Figure 3.14 Hepatic mitochondrial content of chow-fed 2 week old Ncb5or$^{-/-}$ and WT mice. (A) Representative TEM micrographs of WT and Ncb5or$^{-/-}$ hepatocytes at age two weeks. (B) Area of mitochondrial and cytosolic space was measured by the NIH ImageJ software and used to calculate the "mitochondria:cytoplasmic area". A total of three pairs (n=3, >10 cells per animal) were analyzed and results are expressed as mean ± S.E. All results are expressed as mean ± S.E. *, $p<0.05$.

White-bar: WT; Black-bar: Ncb5or$^{-/-}$. Dr. WenFang Wang fully contributed to this figure.

3.4.5 Oxidative stress in liver of prediabetic Ncb5or$^{-/-}$ mice

Ncb5or$^{-/-}$ hepatocytes displayed higher rates of oxygen consumption, greater mitochondrial density, and higher levels of ROS and stress response than WT. Here we examined whether liver of Ncb5or$^{-/-}$ mice had similar defects.

We measured the transcript levels of oxidative stress response genes (MT1, MT2, HMOX1 and GSTT3) in the liver of newborn Ncb5or$^{-/-}$ and WT mice and at age 2, 3, and 5 weeks (Table 3.1). We found that all of the oxidative stress response genes were up-regulated in liver of Ncb5or$^{-/-}$ mice by 5 weeks but not earlier. The timing of this response correlates to that of altered fatty acid metabolism in Ncb5or$^{-/-}$ mice.

Consistent with the above finding, a higher ratio of oxidized to reduced glutathione was observed in liver of Ncb5or$^{-/-}$ mice than WT (Figure 3.15). There was no difference between the two genotypes, however, in the total glutathione level. Higher transcript levels of oxidative stress response genes were also observed in liver of Ncb5or$^{-/-}$ mice than WT after high-fat feeding (Table 3.2). Although HF diet restored hepatic TAG levels in Ncb5or$^{-/-}$ mice, it did not attenuate the elevated levels of intracellular free fatty acid levels (Figure 2.7 A) and oxidative stress response in the livers. This result is different from that in hepatocytes. Contributing factors to the difference between cell and animal models have been discussed previously (Section 2.5.2).

3.4.6 Lack of inflammation in liver of prediabetic Ncb5or$^{-/-}$ mice

We next investigated whether increased oxidative stress could lead to pathophysiologic damage to liver of Ncb5or$^{-/-}$ mice. Compared to WT, Ncb5or$^{-/-}$ mice

displayed no elevation of hepatic marker enzymes in serum (data not shown), indicating no severe liver damage.

We examined the following four markers of inflammation in the liver of these mice. Tumor necrosis factor-alpha (TNFα) is a cytokine involved in systemic acute phase inflammation [146] and is found to be stimulated by SFA-induced hepatic cytotoxicity [147]. Serum amyloid A (SAA) is also secreted during the acute phase of inflammation. SAA1 and 2 are major isoforms in livers and are regulated by proinflammatory cytokines such as TNFα and can be induced up to 1000-fold in livers under acute inflammatory condition [148].

A significant but mild up-regulation of all these markers (7-fold for TNFα and 2-fold for SAAs) was observed in Ncb5or$^{-/-}$ livers relative to WT at age 5 weeks (Table 3.1) and after HF feeding (Table 3.2). This minor induction in the expression of markers, however, did not lead to inflammatory response. We measured TNFα protein levels in sera of Ncb5or$^{-/-}$ and WT mice at age 5 weeks but found no difference between the two genotypes (data not shown). In addition, histologic analyses revealed no sign of inflammation in the liver of Ncb5or$^{-/-}$ mice (Figure 3.16). These tissues displayed no apoptosis by TUNEL staining (data not shown). Therefore, we concluded that no inflammation in Ncb5or$^{-/-}$ mice up to age 5 weeks.

Table 3.1 Transcript levels of genes involved in oxidative stress and inflammatory responses in newborn, 2-, 3-, 5-week-old Ncb5or$^{-/-}$ and WT mouse livers. All values are mean ± S.E. (n=6) and relative to 18S ($\times 10^6$). [a]$p<0.05$, [b]$p<0.01$, [c]$p<0.005$. The transcript levels in bold indicate the significant difference. N.D. : Not determined

	Newborn		2-week		3-week		5-week		
	WT	Ncb5or$^{-/-}$	WT	Ncb5or$^{-/-}$	WT	Ncb5or$^{-/-}$	WT	Ncb5or$^{-/-}$	Fold ↑ Ncb5or$^{-/-}$
MT1	**1061±85**	**1576±136[a]**	**94.5±16.1**	**286±93[a]**	273±62	394±102	**9.52±2.74**	**93.8±17.6[c]**	9.9
MT2	249±37	362±47	15.5±3.1	50.6±19.9	56.6±13.7	90.6±12.8	**1.02±0.38**	**14.7±3.6[c]**	14
HMOX1	26.8±4.7	23.3±1.7	**4.86±0.86**	**12.6±2.5[a]**	11.6±0.6	14.7±1.4	**2.48±0.44**	**5.00±0.30[c]**	2
GSTT3	2.61±0.27	2.70±0.22	**2.55±0.30**	**4.12±0.53[a]**	7.12±1.01	6.37±1.41	**3.49±0.84**	**7.42±2.2[a]**	2.1
TNF-α	1.0±0.3	0.68±0.09	**0.20±0.04**	**0.64±0.18[a]**	N.D.	N.D.	**0.19±0.06**	**1.3±0.7[a]**	7.0
Saa1	0.70±0.15	0.52±0.12	0.60±0.08	3.3±1.4	N.D.	N.D.	**3.7±0.3**	**8.9±1.8[b]**	2.4
Saa2	0.035±0.008	0.025±0.008	**0.10±0.02**	**1.1±0.5[a]**	N.D.	N.D.	**1.3±0.3**	**1.9±0.3[b]**	1.5

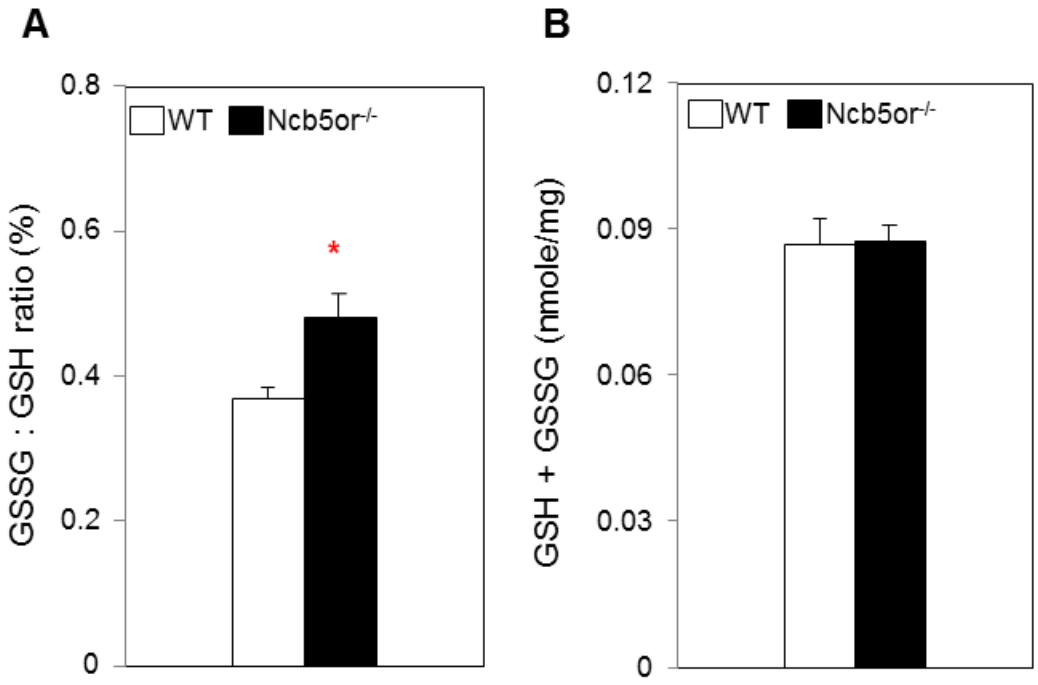

Figure 3.15 Oxidative stress markers in chow-fed Ncb5or$^{-/-}$ and WT mouse liver tissue. Intracellular GSSG and GSH levels of six pairs of liver samples were measured (n=6) and shown as GSSG/GSH ratio in (A) and GSH+GSSG (total glutathione content) in (B). All results were obtained from 5-week-old mice and expressed as mean ± S.E.

*, $p<0.05$ White-bar: WT; Black-bar: Ncb5or$^{-/-}$.

Table 3.2 Transcript levels of genes involved in oxidative stress and inflammatory responses in high-fat diet treated 5-week-old Ncb5or$^{-/-}$ and WT mouse livers. All values are mean ± S.E. (n=6) and relative to 18S (×10^6). [a]$p<0.05$, [b]$p<0.01$, [c]$p<0.005$.

	WT	Ncb5or$^{-/-}$	Fold ↑ in Ncb5or$^{-/-}$
MT1	37.8±9.1	354±70[c]	**9.4**
MT2	7.40±2.04	89.1±14.7[c]	**12**
HMOX1	3.12±0.39	10.6±1.4[c]	**3.4**
GSTT3	1.96±0.38	9.50±2.23[c]	**4.9**
TNF-α	0.40±0.05	0.61±0.11	**1.5**
Saa1	3.63±0.72	8.40±2.67	**2.3**
Saa2	0.77±0.12	2.82±1.13[a]	**3.7**

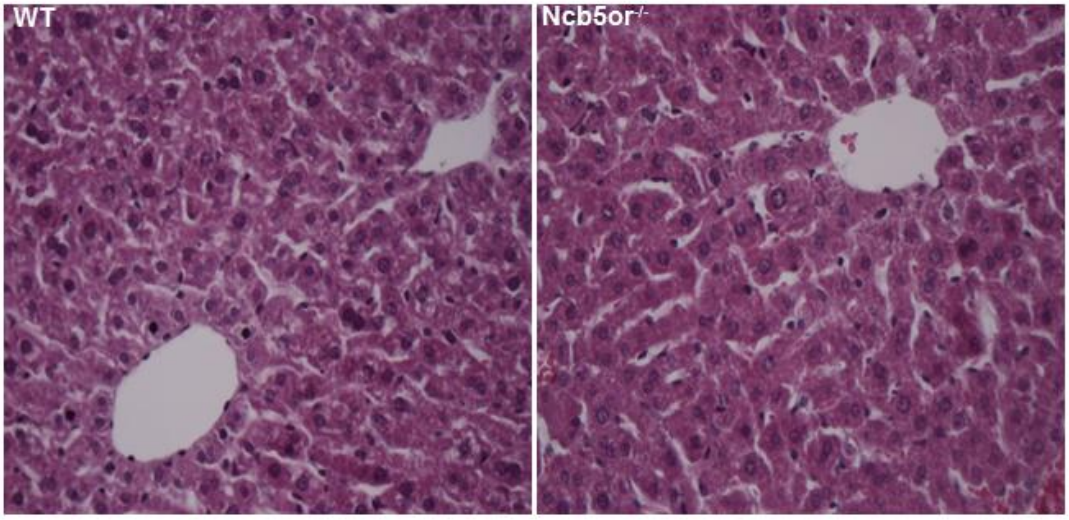

Figure 3.16 Hematoxylin and eosin (H & E) staining of representative liver sections of Ncb5or$^{-/-}$ and WT mice under rodent chow. No macrophage or neutrophil infiltration was observed. Dr. WenFang Wang fully contributed to this figure.

3.5 Discussion

3.5.1 Altered fatty acid metabolism in Ncb5or$^{-/-}$ hepatocytes

Our previous findings suggest that Ncb5or is an important enzyme involved in cellular metabolism of exogenous saturated fatty acid s. This pathway protects cells from SFA-induced cytotoxicity through converting SFA into MUFA and channeling MUFA and SFA into TAG pool. Our goal in the current study is to better understand how Ncb5or deficiency alters metabolism of SFAs and physiology of hepatocytes.

Exogenous SFA have three metabolic fates after entering cells: 1) They stay inside the cell as intracellular nonesterified (free) fatty acids; 2) They are activated to their CoA esters for oxidation to provide energy; or 3) They are activated for phospholipids and TAG synthesis. Ncb5or$^{-/-}$ hepatocytes accumulate more intracellular FFA in parallel to a more active catabolism under basal conditions.

3.5.2 ER stress and oxidative stress

Ncb5or deficiency results in over-accumulation of intracellular free SFA, which has been shown to induce ER stress in many other studies [35; 86; 87]. Our data has shown that, when cells are pre-incubated in a nutrient rich medium, Ncb5or$^{-/-}$ hepatocytes display less severe SFA-induced ER stress than that previously reported. However, our study reveals that Ncb5or deficiency predominantly results in increased fatty acid catabolism and a more active flux in mitochondrial ETC, which correlates to increased ROS production.

It is worth noting that ER stress plays an equally important, if not a more prominent, role in β-cell dysfunction and loss in Ncb5or$^{-/-}$ mice. In our most recent study, we observed severe ER distension and significantly higher expression levels of ER stress response genes in Ncb5or$^{-/-}$ β-cells than WT [34]. A better penetrance of ER stress in β-cells may be due to a lower tolerance to ER stress imposed by their higher load for insulin synthesis and processing in β-cells compared to hepatocytes. Over-accumulation of intracellular free fatty acids and increased ROS production are observed in β-cells and hepatocytes of prediabetic Ncb5or$^{-/-}$ mice, suggesting that altered fatty acid metabolism and increased ROS production are common cellular defects as a result of Ncb5or deficiency.

3.5.3 Mechanism of cell death

Ncb5or$^{-/-}$ hepatocytes are more susceptible to SFA-induced cytotoxicity. Our current study has ruled out ceramide, phospholipid remodeling, and ER stress as the primary cause of cell death in Ncb5or$^{-/-}$ hepatocytes. However, it is still unclear how increased oxidative stress causes cell death. More experiments, such as treating Ncb5or$^{-/-}$ hepatocytes with antioxidant reagents with SFA, may help to address this point.

Ncb5or$^{-/-}$ hepatocytes have been previously shown to have increased TUNEL staining and Annexin V binding signals under SFA treatment [35; 36] . We also detected higher caspase 3/7 activity in these cells than WT (data not shown). These findings suggest that apoptosis is at least partially responsible for cell death in Ncb5or$^{-/-}$ hepatocytes. Measurement of lactate dehydrogenase in culture medium will be helpful to determine whether necrosis is also involved in Ncb5or$^{-/-}$ hepatocytes.

In our current study, we were able to rescue SFA-induced cytotoxicity in Ncb5or$^{-/-}$ hepatocytes by co-incubation with MUFA, which channels free SFA into TAG pool. A similar regiment with a high-fat diet rich in both SFA and MUFA, however, still causes SFA-accumulation and oxidative stress in Ncb5or$^{-/-}$ mice. It is worthwhile to use a MUFA-rich diet for similar rescue experiments.

3.5.4 Conclusion

In this chapter, we have characterized abnormal fatty acid metabolism, especially fatty acid catabolism and mitochondrial hyperactivity in Ncb5or$^{-/-}$ hepatocytes and investigated the mechanism of SFA-induced cytotoxicity. We have also confirmed that Ncb5or$^{-/-}$ mice have increased catabolism. We concluded that altered fatty acid metabolism in Ncb5or$^{-/-}$ hepatocytes includes free SFA accumulation, enhanced fatty acid oxidation, compromised phospholipid synthesis and increased sensitivity to MUFA channeling. The aberration results in oxidative stress and eventually caused cell death, possibly by apoptosis. MUFAs rescue cell death and oxidative stress, apparently by decreasing the level of intracellular free SFA. Our study reveals an important role of Ncb5or in preventing oxidative stress and SFA cytotoxicity. It has also expanded our knowledge of lipotoxicity.

Chapter 4

Discussions and conclusions

4.1 Summary of current findings

Obesity and metabolic syndrome affect more than 20% of the population in the Unites States [47] and have become a major health issue in the past 20 years. Obesity increases the risk of coronary heart disease, type 2 diabetes, cancers, hypertension, stroke and fatty liver [149]. A better understanding of cellular fatty acid metabolism is critically important to our combat against this global health issue.

We have shown that Ncb5or plays an important role in cellular fatty acid metabolism [36]. Ncb5or deficiency results in overt diabetes around 7 weeks of age. Our studies in Chapter 2 examine the role of Ncb5or in fatty acid metabolism by employing hepatocytes and liver of pre-diabetic mice to avoid complications from diabetes. Our data suggest that Ncb5or facilitates SCD to convert SFA to MUFA, which is an essential part of TAG synthesis. We reveal a significant role of Ncb5or, in addition to Cyb5A, in fatty acid desaturation. Together, these findings establish the role of Ncb5or in fatty acid metabolism.

In Chapter 3, we explore the role of Ncb5or in protecting cells from oxidative stress. Oxidative stress has been implicated as a cause in a variety of diseases including atherosclerosis, Parkinson's disease, heart failure, myocardial infarction, Alzheimer's disease, cancer, fatty liver and diabetes. Our data suggest that Ncb5or exerts its effect by converting SFA to MUFA, which favors TAG synthesis and decreases levels of intracellular FFA and oxidative stress. Notably, Ncb5or deficiency does not impair cellular antioxidant system or MUFA's ability of channeling SFA to intracellular TAG pool, because MUFA can alleviate SFA-induced cytotoxicity in Ncb5or-nul cells.

4.2 Future directions

Future studies are needed to answer some remaining questions and to test hypotheses as follows.

In Chapter 2, we showed that Ncb5or facilitates the function of SCD. However, it still remains unclear how Ncb5or fulfills this role. One hypothesis is that Ncb5or directly donates electrons to SCD. Further enzymatic activity assays using purified SCD protein will provide further evidence.

Also in Chapter 2, we provided preliminary data on the functional relationship between Ncb5or and Cyb5A in Δ^9 fatty acid desaturation. We will further dissect these pathways by applying isotope (^{13}C) labeled exogenous SFA and acetate, which is the substrate of *de no* synthesis for SFA, to primary hepatocytes lacking either or both genes and tracing the metabolic fates of these isotope-labeled substrates, as previously described in studies using hepatoma cell lines [150].

Our recent preliminary data suggest that Ncb5or may be involved in cellular iron metabolism, potentially as a ferric reductase or its redox partner in cellular iron absorption. Iron deficiency and altered iron metabolism was observed in liver and duodenum of prediabetic Ncb5or null mice. This defect may indirectly affect the activity of SCD, which requires iron for its catalytic activity. We present background information and preliminary data in the next section.

In Chapter 3, we showed that Ncb5or$^{-/-}$ hepatocytes displayed higher levels of intracellular ROS and more cell death under SFA challenge, which is related to higher levels of intracellular free SFA in these cells than WT. Whether and how oxidative stress

causes cell death in Ncb5or$^{-/-}$ hepatocytes is yet to be determined. Treatment of these cells with antioxidants, such as N-Acetyl Cysteine (NAC), may help to answer this question. Further efforts to detect apoptosis and necrosis of Ncb5or$^{-/-}$ hepatocytes will be helpful to determine cell death pathway for these cells.

To better understand the physiological function of Ncb5or, it is important to identify the redox or physical partner of Ncb5or. Structural characterization of Ncb5or is desirable to further unravel the biochemical properties of Ncb5or.

4.3 Potential role of Ncb5or in iron metabolism

4.3.1 Iron metabolism

Iron plays an essential role in a wide spectrum of redox reactions of metabolic pathways in all living organisms. This function is due to iron's readiness to accept and donate electrons by changing between ferric (Fe^{3+}) and ferrous (Fe^{2+}) redox states.

Heme and iron-sulfur (FeS) clusters are two major forms of iron in proteins. Iron-containing proteins are involved in essential biological processes, including oxygen binding, heme synthesis, energy generation, detoxification, nuclei acids metabolism, cell growth, and cell defending [151-153]. Iron homeostasis is critical for cellular physiology, because iron deficiency can impair cellular function, retard cell growth, and induce cell death [154; 155], whereas iron overload can induce oxidative stress and toxicity [156].

Dietary non-heme iron uptake occurs in duodenal enterocytes (Figure 4.1). Ferric iron (Fe^{3+}) is reduced to the ferrous form (Fe^{2+}), presumably by duodenal cytochrome b

(DcytB, or Cybrd1), before being transported into cytoplasm *via* divalent metal transporter (DMT1) [157]. Cybrd1 null mice display mild abnormality in iron metabolism, suggesting the existence of other ferric reductases [158]. These irons are then released from enterocytes into plasma through ferroportin (FPN), the basolateral iron exporter [159; 160]. Prior to binding to transferrin (TF) for circulation, Fe^{2+} needs to be oxidized to Fe^{3+} by hephaestin, because TF has higher affinity for Fe^{3+} than for Fe^{2+} [161].

Macrophages are the major places for iron recycle (Figure 4.1). The heme in aged and damaged erythrocytes are first exported from phagocytic vesicles by natural resistance-associated macrophages protein 1 (NRAMP1), a homologous to DMT1 [162], and iron is released by heme oxygenase (HMOX1) in cytosol, which are then exported into circulation similarly as in duodenum. For most tissues, TF-bound iron is the major source of iron, and transferrin receptor (TFR1) plays a key role in cellular iron uptake. Following endocytosis of TF-iron molecules, Fe^{3+} is released from TF and reduced to Fe^{2+} by STEAP (Six-transmembrane epithelial antigen of prostate) family for transport into cytosol *via* DMT1 [157; 163]. Meanwhile, apo-TF and TFR1 are recycled to cell surface for later use. Moreover, cells can also uptake iron *via* a TFR-independent pathway, in which ZRT/IRT-like protein 14 (ZIP14) and DMT1 are thought to play an important role [164].

Iron homeostasis is maintained at both systemic and cellular levels in animals. At the systemic level, hepcidin (a peptide produced in liver) plays a key role in regulating the balance between iron demands (majorly from erythrocytes) and iron storage (mainly in hepatocytes, enterocytes and macrophages) by binding to FPN to trigger its internalization, ubiquitination, and degradation [165; 166]. This inhibits the release of

iron from cells and decreases levels of iron in circulation. Hepcidin expression is regulated by signals of iron abundance [167], bone morphogenesis, such as BMP6 [168; 169], inflammation [170; 171], ER stress [172; 173], erythropoiesis [174], and hypoxia [175].

At the cellular level, iron homeostasis is maintained by coordination of iron uptake, export, storage and utilization. Iron regulatory proteins 1 and 2 (IRP1 and IRP2) are two key regulators that bind to iron response elements (IREs) in target transcripts to either degrade or stabilize them [153]. Under iron deficient conditions, cellular iron uptake (TFR1 and DMT1) is induced, whereas iron storage (ferritin), export (FPN1) and utilization (heme synthesis) is repressed. The opposite processes take place when cells are overloaded with iron [153].

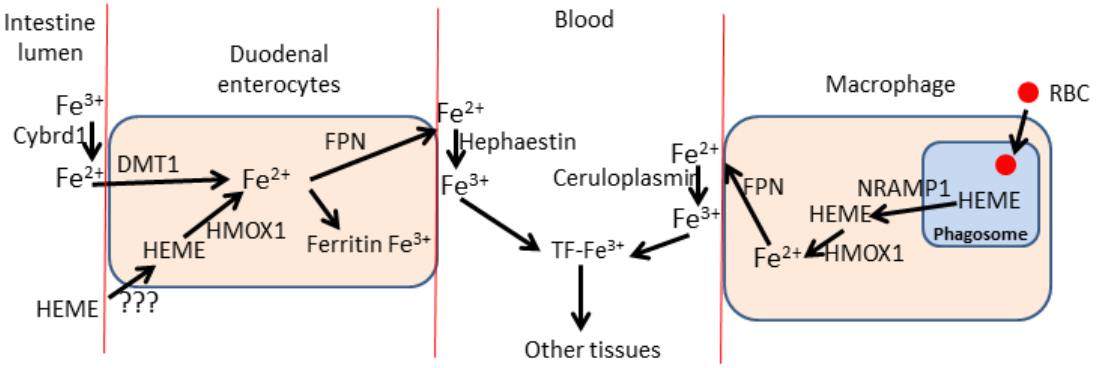

Figure 4.1 Schematic diagram of iron metabolism. For uptake and absorption, dietary Fe^{3+} is first reduced to Fe^{2+} on the apical membrane of duodenal enterocytes, potentially by Cybrd1. Iron is then transported into the cytoplasm via DMT1. Dietary heme is absorbed by an unknown mechanism, and iron is released from heme mainly by HMOX1. The major site for iron recycle is macrophages. The heme in aged and damaged red blood cells (RBC) is first exported from phagocytic vesicles by NRAMP1 and iron is released by HMOX1 in cytosol. Cytosolic Fe^{2+} is exported to circulation via ferroportin, oxidized to Fe^{3+} by hephaestin (enterocytes) or ceruloplasmin (macrophage), and then bound by transferrin for transportation to other tissues.

4.3.2 Iron deficiency in prediabetic Ncb5or$^{-/-}$ mice

To understand the biological function of Ncb5or, we performed microarray analyses of livers from Ncb5or$^{-/-}$ and wild-type (WT) mice at age 5 weeks. We found significantly higher level of TFR1, HMOX1, MT1 and MT2 and > 20−fold lower level of hepcidin in Ncb5or$^{-/-}$ livers compared to WT (data not shown). Altered expression of these genes has been observed in iron deficient rats [176]. Therefore, Ncb5or may play a role in iron metabolism, potentially reducing ferric irons *in vivo*, similar to its reductase property *in vitro* [6]. As shown below, Ncb5or deficiency leads to iron deficiency in liver, which could indirectly decrease the specific activity of stearoyl-CoA desaturase (Chapter 2), an iron-binding redox enzyme.

We performed a survey of non-heme iron content among tissues of prediabetic Ncb5or$^{-/-}$ mice at age 5 weeks. By following a bathophenanthroline-based spectrophotometric protocol [177], we observed lower iron content in liver, spleen, and duodenum in Ncb5or$^{-/-}$ mice compared to WT, but similar iron content in brain, kidney, testis, ileum, and the whole pancreas between the two genotypes, under both fed and fasting states (Figure 4.2). For unknown reasons, the iron content in heart is significantly lower in Ncb5or$^{-/-}$ than WT only in mice fasted overnight. Liver and spleen are two key organs for iron storage and recycle, respectively. Iron deficiency in these tissues progresses as Ncb5or$^{-/-}$ mice age (data not shown). Iron content in isolated islets will be measured through atomic absorption, which has a higher sensitivity (as low as 5 ppm) than the above method. Results of our pilot runs indicate a general trend of lower iron content in islets of prediabetic Ncb5or$^{-/-}$ mice than WT (data not shown).

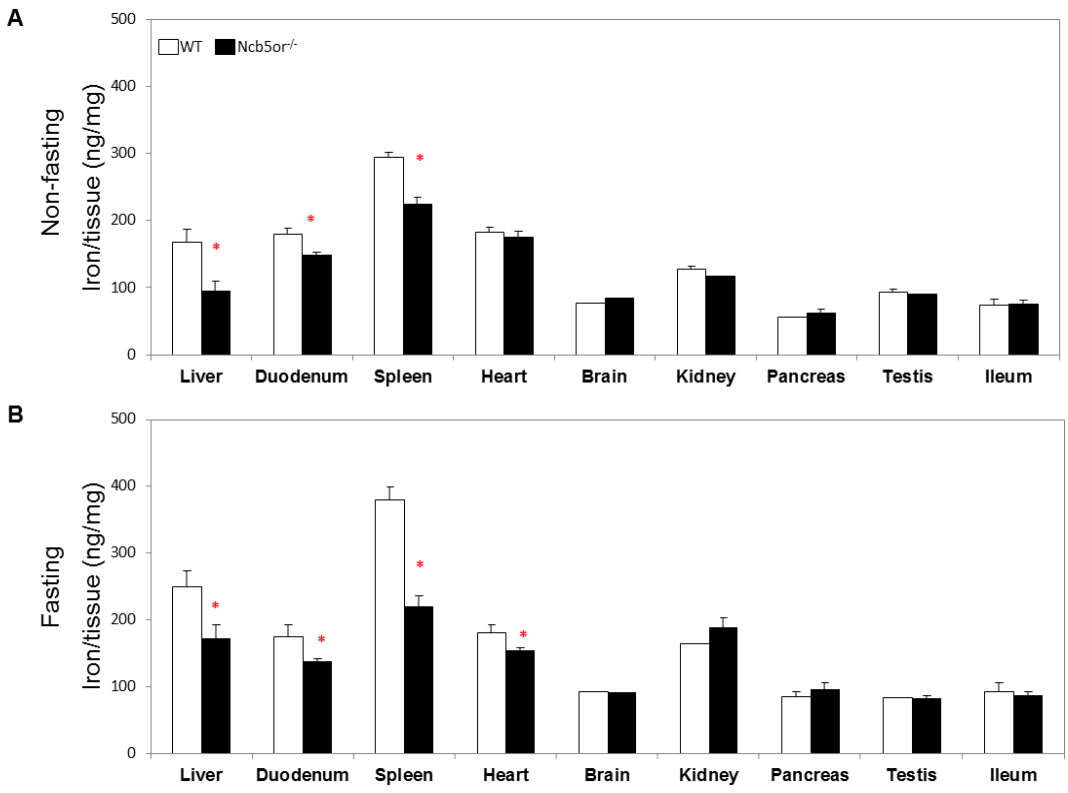

Figure 4.2 Non-heme iron contents in tissues of prediabetic Ncb5or$^{-/-}$ and WT mice under non-fasting and fasting states. Non-heme iron contents were measured in different tissues collected from 5-week-old Ncb5or$^{-/-}$ and WT mice (C57BL/6 strain) at non-fasting state (A) or after fasted overnight (B). All values are expressed as mean ± S.E. (n>7)

*, p<0.05 Blue-bar: WT; Red-bar: Ncb5or$^{-/-}$.

Ncb5or$^{-/-}$ mice at age 5 weeks display lower iron saturation of TF in circulation than WT and mild anemia (data not shown), suggesting a general iron deficiency. To better understand Ncb5or's potential role in iron absorption (duodenum) and storage (liver), as well as in diabetes that may be related to iron deficiency (islets), we performed qRT-PCR to analyze expression of key genes involved in iron metabolism.

As shown in Table 4.1, Ncb5or$^{-/-}$ duodenum displayed elevated levels of transcripts of TFR1 and DMT1 for iron uptake than WT under the fasting state, in which duodenums acquire iron mainly from circulation (TF-bound iron). Increased iron uptake in Ncb5or$^{-/-}$ mice was likely to compensate for their lower serum iron content (data not shown). This is supported by the lack of induction of TFR1 and DMT1 expression under non-fasting state, in which dietary iron is the main source for iron uptake in duodenum. No difference between the two genotypes was observed for HMOX1 and hephaestin transcript levels, indicating intact heme uptake and iron oxidation in Ncb5or$^{-/-}$ duodenum.

Notably, a 4 fold higher level of Cybrd1transcript was observed in Ncb5or$^{-/-}$ duodenum under non-fasting state. Cybrd1 has been proposed to play an important role in reducing dietary Fe^{3+} to Fe^{2+} prior to iron uptake via DMT1. The fact that Ncb5or deficiency induced Cybrd1 leads us to hypothesize that Ncb5or might played a similar role as Cybrd1 *in vivo* and that the induction of Cybrd1 compensates Ncb5or deficiency. This hypothesis will be further tested by: 1) Performing confocal immunofluorescence microscopy to determine whether Ncb5or may be associated with apical membranes of enterocytes, the same as Cybrd1; 2) Comparing iron deficiency in Ncb5or$^{-/-}$ mice with Cybrd1 null and Ncb5or/Cybrd1 double null mice; 3) Measuring ferric reductase activity and iron absorption in duodenum of Ncb5or-null mice.

Table 4.1 Levels of transcripts of genes involved in duodenal iron metabolism in prediabetic Ncb5or$^{-/-}$ and WT mice under both non-fasting and fasting states. Duodenum were collected from 5-week-old Ncb5or$^{-/-}$ and WT mice (C57BL/6 strain) under non-fasting or fasting state. All values are mean ± S.E. (n=6) and relative to 18S ($\times 10^6$). The transcript levels in bold indicate the significant difference.

Duodenum								
	Non-fasting			**fold**	**Fasting**			**fold**
	Wild-type	Ncb5or$^{-/-}$	*p*-value	**KO/WT**	Wild-type	Ncb5or$^{-/-}$	*p*-value	**KO/WT**
TFR1	31.6±5.6	33.3±3.2	N.S.	**1.06**	**20.0±2.3**	**34.4±5.4**	**0.0239**	**1.72**
DMT1	13.6±4.8	18.9±6.4	N.S.	**1.38**	**4.3±0.6**	**15.7±8.1**	**0.0367**	**3.65**
FPN1	61.6±22.0	112±30	N.S.	**1.82**	36.9±25.5	49.5±29.1	0.4873	**1.34**
HMOX1	6.0±0.4	5.0±0.5	N.S.	**0.82**	3.8±0.3	7.8±2.6	0.2673	**2.01**
Cybrd1	**11.7±4.0**	**45.8±15.7**	**0.0235**	**3.91**	2.2±0.7	2.3±0.6	N.S.	**1.05**
Steap1	6.5±2.4	5.5±2.3	N.S.	**0.84**	1.4±0.2	1.5±0.2	N.S.	**1.09**
Steap2	23.8±4.5	23.3±4.3	N.S.	**0.98**	11.8±0.9	12.3±0.5	N.S.	**1.04**
Steap4	4.9±1.4	4.1±1.5	N.S.	**0.84**	1.8±0.2	2.2±0.3	N.S.	**1.21**
ZIP14	16.9±3.0	13.3±1.6	N.S.	**0.79**	23.0±2.9	27.5±3.8	N.S.	**1.20**

To better understand iron mechanism in liver of Ncb5or$^{-/-}$ mice, we measured levels of transcripts of iron metabolism genes at different ages (Table 4.2). Compared to WT, Ncb5or$^{-/-}$ livers had similar gene expression pattern after birth, except slightly higher expression of IRP1, ferritin light chain (FTL), and Steap4. After these mice reached age 2 weeks, they started to show more significant alteration of iron metabolism in liver. Most (or all) of STEAP isoforms and DMT1 were up-regulated in Ncb5or$^{-/-}$ livers at age 2 and 5 weeks. The levels of TFR1 and ZIP14 transcripts were also higher in these livers at age 5 weeks than WT. TF bound irons are the main iron source in hepatocytes. After TF binds TFR, Fe^{3+} is released and reduced to Fe^{2+} by STEAPs and transported into cytosol by DMT. Up-regulation of genes in this pathway in Ncb5or$^{-/-}$ livers indicates a potential compensation for impaired iron uptake in these cells.

Ncb5or might play a role in reducing ferric iron by itself or together with STEAPs. Unlike other STEAPs, STEAP1 has no flavin-binding reductase domain [178], therefore can function only in the presence of a reductase such as Ncb5or. The strong induction (more than 15 fold) of STEAP1 at age of 5 weeks, compared to moderate induction (less than 2 fold) of other STEAPs, appears to suggest that Ncb5or may be a potential working partner with STEAP1. Interestingly, STEAP1 was down-regulated at age 2 weeks while other STEAP isoforms were up-regulated. This could be a transient stage for the regulation of STEAP1, and may suggest that STEAP1 works differently than other STEAPs. ZIP14 played roles in both TFR dependent and independent pathways for iron uptake. Induction of this gene was consistent with a compensation mechanism of iron deficiency in Ncb5or$^{-/-}$ livers.

Transcript levels of mitofn (mitoferrin)1 and 2 were similar between the two genotypes, indicating that Ncb5or$^{-/-}$ hepatocytes have intact mitochondrial iron transport.

Hepcidin is the major regulator for systematic iron homeostasis. We observed a noticeable age-dependent regulation of hepcidin in Ncb5or$^{-/-}$ mouse model. Hepcidin was expressed at a level that was > 9-fold higher in Ncb5or$^{-/-}$ livers than WT at age 2 weeks (Table 4.2) and 3 weeks (data not shown). Elevated hepcidin expression increased the degradation of FPN and resulted in decreased iron export. This could explain why 3-week-old Ncb5or$^{-/-}$ mice had similar hepatic iron content (data not shown) despite impaired iron uptake. However, at age 5 weeks, Ncb5or$^{-/-}$ livers had 10-fold lower hepcidin level compared to WT. Although this difference was not significant due to individual variance, the opposite trend between this and earlier age (2 and 3 weeks) is intriguing and deserves more investigation.

Since hepatocytes served as major iron storage sites, their major role under fasting state was to export iron to other tissues. The two genotypes displayed similar expression pattern (data not shown) under this state, indicating no major defect of iron export in Ncb5or$^{-/-}$ livers. Less than 2 fold induction of ZIP14 was the only exception. The role of ZIP14 requires more investigation due to its inconsistent regulation in Ncb5or$^{-/-}$ mouse livers.

Table 4.2 Levels of transcripts of genes involved in hepatic iron metabolism in newborn, 2 and 5-week-old Ncb5or$^{-/-}$ and WT mice under non-fasting state. Livers were collected from newborn, two and five weeks old Ncb5or$^{-/-}$ and WT mice (C57BL/6 strain). All values are mean ± S.E. (n=6) and relative to 18S ($\times 10^6$). The transcript levels in bold indicate the significant difference.

	new born			fold	2-week			fold	5-week			fold
	Wild-type	Ncb5or$^{-/-}$	*p*-value	KO/WT	Wild-type	Ncb5or$^{-/-}$	*p*-value	KO/WT	Wild-type	Ncb5or$^{-/-}$	*p*-value	KO/WT
Hamp1	500±128	372±92	0.4871	**0.74**	**1.3±0.4**	**12.0±5.1**	**0.0160**	**9.04**	351±58	38.0±28.0	0.1294	**0.11**
TFR1	19.9±4.7	21.1±2.5	0.9833	**1.06**	17.2±2.3	19.9±5.3	0.9394	**1.16**	**0.55±0.1**	**3.6±1.2**	**0.0026**	**6.52**
DMT1	0.73±0.13	0.60±0.09	0.4553	**0.82**	**0.43±0.07**	**0.98±0.21**	**0.0391**	**2.27**	**0.24±0.04**	**0.47±0.08**	**0.0263**	**1.93**
IRP1	**3.1±0.3**	**5.0±0.5**	**0.0087**	**1.60**	6.3±1.0	5.8±0.7	0.8488	**0.92**	6.3±0.7	7.8±0.7	0.1970	**1.24**
IRP2	2.6±0.4	3.4±0.2	0.2563	**1.28**	2.6±0.4	3.2±0.5	0.3854	**1.21**	2.2±0.2	2.4±0.2	0.4070	**1.12**
FPN1	4.6±0.7	6.4±0.9	0.2229	**1.38**	8.1±0.5	10.6±2.0	0.3323	**1.30**	5.2±0.7	6.6±0.5	0.1926	**1.28**
FTH	120.4±15.1	156.7±14.1	0.1646	**1.30**	49.7±3.9	55.8±5.2	0.4213	**1.12**	50.2±8.2	72.6±4.4	0.0794	**1.44**
FTL	**148.0±19.6**	**268.2±55.8**	**0.0376**	**1.81**	201±38	248±24	0.2671	**1.23**	566±95	640±50	0.5560	**1.13**
ZIP14	1.9±0.3	2.8±0.8	0.2499	**1.45**	5.0±0.9	6.3±0.8	0.3279	**1.24**	**3.7±0.7**	**8.2±2.0**	**0.0443**	**2.23**
Steap1	0.33±0.12	0.41±0.04	0.1972	**1.25**	**0.90±0.21**	**0.52±0.08**	**0.0360**	**0.58**	**0.14±0.07**	**2.19±0.99**	**0.0025**	**15.54**
Steap2	3.6±0.5	2.8±0.2	0.2599	**0.78**	**3.7±0.3**	**5.6±0.5**	**0.0055**	**1.50**	**3.1±0.3**	**5.8±0.7**	**0.0031**	**1.85**
Steap3	0.85±0.20	2.0±0.6	0.0599	**2.40**	**0.37±0.07**	**0.71±0.17**	**0.0217**	**1.94**	0.54±0.12	0.66±0.15	0.6162	**1.21**
Steap4	**1.6±0.2**	**2.5±0.2**	**0.0128**	**1.54**	**12.2±1.9**	**32.5±12.2**	**0.0170**	**2.67**	**13.8±1.1**	**25.9±4.1**	**0.0079**	**1.88**
Mitofn1									2.1±0.1	2.3±0.4	0.7023	**1.09**
Mitofn2									2.4±0.2	2.3±0.1	0.6382	**0.95**

Iron has been found to play an important role in diabetes. Iron overload is strongly associated with type 2 diabetes [179]. Excessive tissue iron could lead to oxidative stress through Fenton reaction and induce insulin resistance [180]. Iron overload could decrease glucose utilization and increase glucose production [181]. What is more, iron deficiency could protect high-fat induced muscle insulin resistance [182]. These studies provide valuable knowledge about the relationship between iron metabolism and diabetes. Our model is unique, however, because diabetes in Ncb5or$^{-/-}$ mice is associated with iron deficiency instead of iron overload.

We also determined levels of transcripts of genes involved in islet iron metabolism by qRT-PCR. We observed altered iron metabolism in Ncb5or$^{-/-}$ islets at age 5 weeks at the transcript level (Table 4.3). It is foreseeable that iron deficiency in Ncb5or$^{-/-}$ islets causes improper function of key enzymes, and resulted in altered fatty acid metabolism and β-cell death. The exact mechanism and relationship between iron deficiency and diabetes, however, is far from clear and requires more in-depth studies.

Based on the above preliminary data, we hypothesize that Ncb5or is important for dietary iron absorption in duodenum and for cellular iron uptake in hepatocytes. Ncb5or functions either as a ferric reductase or an electron donor of ferric reductase, such as Cybrd1, to facilitate iron update. Our future study will test this hypothesis and explore the mechanism of iron deficiency in Ncb5or-null cells, especially its functional relationship to altered fatty acid metabolism. If our hypothesis is proven to be correct, the new knowledge will help us to understand how iron homeostasis contributes to cellular fatty acid metabolism.

Table 4.3 Levels of transcripts of genes involved in islet iron metabolism Ncb5or$^{-/-}$ and WT mice at age 3 and 5 weeks. Islets were collected Ncb5or$^{-/-}$ and WT mice (C57BL/6 strain). All values are mean ± S.E. (n=6) and relative to 18S ($\times 10^6$). The transcript levels in bold indicate the significant difference.

Dr. Wenfang Wang contributed to this table.

	3-week			**fold**	**5-week**			**fold**
	Wild-type	Ncb5or$^{-/-}$	*p*-value	**KO/WT**	Wild-type	Ncb5or$^{-/-}$	*p*-value	**KO/WT**
TFR1	16.1±3.7	16.9±3.7	0.8985	**1.05**	**1.7±0.3**	**7.0±1.5**	**0.0010**	**4.15**
IRP1	8.4±2.2	6.7±0.7	0.4949	**0.79**	**1.1±0.2**	**4.4±0.4**	**0.0003**	**4.11**
IRP2	16.0±4.4	11.8±3.4	0.5429	**0.74**	**2.4±0.6**	**9.9±2.0**	**0.0034**	**4.13**
DMT1	5.2±1.1	4.2±0.1	0.3609	**0.80**	**0.37±0.07**	**1.4±0.5**	**0.0141**	**3.83**
FPN1	11.8±0.9	8.8±2.2	0.3645	**0.74**	**1.0±0.23**	**4.2±1.0**	**0.0056**	**4.11**
Cybrd1	**1.0±0.2**	**6.8±2.4**	**0.0109**	**6.67**	0.21±0.09	0.60±0.30	0.2684	**2.84**
FTH	357±59	498±49	0.1657	**1.39**	43.9±10.4	64.6±18.8	0.3982	**1.47**
FTL	3499±753	4696±742	0.3609	**1.34**	311±59	378±92	0.5879	**1.22**
ZIP14	**6.7±0.6**	**3.8±0.4**	**0.0162**	**0.56**	**0.98±0.06**	**2.3±0.5**	**0.0126**	**2.32**
Steap1	464±66	806±2	0.1133	**1.74**	55.1±10.5	54.9±0.5	0.9066	**1.00**
Steap2	**274±56**	**473±51**	**0.0380**	**1.73**	28.1±6.9	40.9±5.4	0.1221	**1.46**
Steap3	3.8±1.0	1.7±0.3	0.0792	**0.44**	**0.46±0.21**	**1.9±0.7**	**0.0157**	**4.05**
Steap4	313±51	386±29	0.2199	**1.23**	32.7±7.0	38.5±10.9	0.7732	**1.18**
Mitofn1	3.5±0.7	4.1±0.16	0.3055	**1.19**	**0.62±0.2**	**1.8±0.5**	**0.0234**	**2.94**
Mitofn2	8.3±1.8	7.0±1.7	0.6147	**0.84**	**1.2±0.3**	**6.6±1.1**	**0.0003**	**5.41**

References

[1] H. Zhu, H. Qiu, H.W. Yoon, S. Huang, and H.F. Bunn, Identification of a cytochrome b-type NAD(P)H oxidoreductase ubiquitously expressed in human cells. Proc Natl Acad Sci U S A 96 (1999) 14742-7.

[2] J.A. Garcia-Ranea, G. Mirey, J. Camonis, and A. Valencia, p23 and HSP20/alpha-crystallin proteins define a conserved sequence domain present in other eukaryotic protein families. FEBS Lett 529 (2002) 162-7.

[3] C.A. Davis, I.K. Dhawan, M.K. Johnson, and M.J. Barber, Heterologous expression of an endogenous rat cytochrome b(5)/cytochrome b(5) reductase fusion protein: identification of histidines 62 and 85 as the heme axial ligands. Arch Biochem Biophys 400 (2002) 63-75.

[4] P.A. Karplus, M.J. Daniels, and J.R. Herriott, Atomic structure of ferredoxin-NADP+ reductase: prototype for a structurally novel flavoenzyme family. Science 251 (1991) 60-6.

[5] B. Deng, S. Parthasarathy, W. Wang, B.R. Gibney, K.P. Battaile, S. Lovell, D.R. Benson, and H. Zhu, Study of the individual cytochrome b5 and cytochrome b5 reductase domains of Ncb5or reveals a unique heme pocket and a possible role of the CS domain. J Biol Chem 285 30181-91.

[6] H. Zhu, K. Larade, T.A. Jackson, J. Xie, A. Ladoux, H. Acker, U. Berchner-Pfannschmidt, J. Fandrey, A.R. Cross, G.S. Lukat-Rodgers, K.R. Rodgers, and H.F. Bunn, NCB5OR is a novel soluble NAD(P)H reductase localized in the endoplasmic reticulum. J Biol Chem 279 (2004) 30316-25.

[7] Z.Q. Wang, Y.H. Wang, W.H. Wang, L.L. Xue, X.Z. Wu, Y. Xie, and Z.X. Huang, The effect of mutation at valine-45 on the stability and redox potentials of trypsin-cleaved cytochrome b5. Biophys Chem 83 (2000) 3-17.

[8] P.D. Barker, J.C. Ferrer, M. Mylrajan, T.M. Loehr, R. Feng, Y. Konishi, W.D. Funk, R.T. MacGillivray, and A.G. Mauk, Transmutation of a heme protein. Proc Natl Acad Sci U S A 90 (1993) 6542-6.

[9] B.J. Curry, S.D. Roman, C.A. Wallace, R. Scott, E. Miriami, and R.J. Aitken, Identification and characterization of a novel splice variant of mouse and rat cytochrome b5/cytochrome b5 reductase. Genomics 83 (2004) 425-38.

[10] K. Larade, and H.F. Bunn, Promoter characterization and transcriptional regulation of Ncb5or, a novel reductase necessary for pancreatic beta-cell maintenance. Biochim Biophys Acta 1759 (2006) 257-62.

[11] K. Larade, Z.G. Jiang, A. Dejam, H. Zhu, and H.F. Bunn, The reductase NCB5OR is responsive to the redox status in beta-cells and is not involved in the ER stress response. Biochem J 404 (2007) 467-76.

[12] F. Lederer, R. Ghrir, B. Guiard, S. Cortial, and A. Ito, Two homologous cytochromes b5 in a single cell. Eur J Biochem 132 (1983) 95-102.

[13] N. Borgese, D. Aggujaro, P. Carrera, G. Pietrini, and M. Bassetti, A role for N-myristoylation in protein targeting: NADH-cytochrome b5 reductase requires myristic acid for association with outer mitochondrial but not ER membranes. J Cell Biol 135 (1996) 1501-13.

[14] R. Jeffcoat, P.R. Brawn, R. Safford, and A.T. James, Properties of rat liver microsomal stearoyl-coenzyme A desaturase. Biochem J 161 (1977) 431-7.

[15] P. Strittmatter, L. Spatz, D. Corcoran, M.J. Rogers, B. Setlow, and R. Redline, Purification and properties of rat liver microsomal stearyl coenzyme A desaturase. Proc Natl Acad Sci U S A 71 (1974) 4565-9.

[16] E.R. Jaffe, Methaemoglobinaemia. Clin Haematol 10 (1981) 99-122.

[17] E.R. Jaffe, Methemoglobin pathophysiology. Prog Clin Biol Res 51 (1981) 133-51.

[18] M.K. Akhtar, S.L. Kelly, and M.A. Kaderbhai, Cytochrome b(5) modulation of 17{alpha} hydroxylase and 17-20 lyase (CYP17) activities in steroidogenesis. J Endocrinol 187 (2005) 267-74.

[19] G.R. Borthiry, W.E. Antholine, B. Kalyanaraman, J.M. Myers, and C.R. Myers, Reduction of hexavalent chromium by human cytochrome b5: generation of hydroxyl radical and superoxide. Free Radic Biol Med 42 (2007) 738-55; discussion 735-7.

[20] J.R. Kurian, N.A. Chin, B.J. Longlais, K.L. Hayes, and L.A. Trepanier, Reductive detoxification of arylhydroxylamine carcinogens by human NADH cytochrome b5 reductase and cytochrome b5. Chem Res Toxicol 19 (2006) 1366-73.

[21] J.B. Schenkman, and I. Jansson, The many roles of cytochrome b5. Pharmacol Ther 97 (2003) 139-52.

[22] H. Yamazaki, M. Nakamura, T. Komatsu, K. Ohyama, N. Hatanaka, S. Asahi, N. Shimada, F.P. Guengerich, T. Shimada, M. Nakajima, and T. Yokoi, Roles of NADPH-P450 reductase and apo- and holo-cytochrome b5 on xenobiotic oxidations catalyzed by 12 recombinant human cytochrome P450s expressed in membranes of Escherichia coli. Protein Expr Purif 24 (2002) 329-37.

[23] R.D. Finn, L.A. McLaughlin, S. Ronseaux, I. Rosewell, J.B. Houston, C.J. Henderson, and C.R. Wolf, Defining the in vivo role for cytochrome b5 in cytochrome P450 function through the conditional hepatic deletion of microsomal cytochrome b5. J Biol Chem 283 (2008) 31385–31393.

[24] L.A. McLaughlin, S. Ronseaux, R.D. Finn, C.J. Henderson, and C. Roland Wolf, Deletion of microsomal cytochrome b5 profoundly affects hepatic and extrahepatic drug metabolism. Mol Pharmacol 78 269-78.

[25] R.D. Finn, L.A. McLaughlin, C. Hughes, C. Song, C.J. Henderson, and C. Roland Wolf, Cytochrome b (5) null mouse: a new model for studying inherited skin disorders and the role of unsaturated fatty acids in normal homeostasis. Transgenic Res 20 (2011) 491-502.

[26] T. Ogishima, J.Y. Kinoshita, F. Mitani, M. Suematsu, and A. Ito, Identification of outer mitochondrial membrane cytochrome b5 as a modulator for androgen synthesis in Leydig cells. J Biol Chem 278 (2003) 21204-11.

[27] N. Borgese, and R. Longhi, Both the outer mitochondrial membrane and the microsomal forms of cytochrome b5 reductase contain covalently bound myristic acid. Quantitative analysis on the polyvinylidene difluoride-immobilized proteins. Biochem J 266 (1990) 341-7.

[28] M.J. Percy, and T.R. Lappin, Recessive congenital methaemoglobinaemia: cytochrome b(5) reductase deficiency. Br J Haematol 141 (2008) 298-308.

[29] J. Xie, H. Zhu, K. Larade, A. Ladoux, A. Seguritan, M. Chu, S. Ito, R.T. Bronson, E.H. Leiter, C.Y. Zhang, E.D. Rosen, and H.F. Bunn, Absence of a reductase,

NCB5OR, causes insulin-deficient diabetes. Proc Natl Acad Sci U S A 101 (2004) 10750-5.

[30] N. Takasu, I. Komiya, T. Asawa, Y. Nagasawa, and T. Yamada, Streptozocin- and alloxan-induced H2O2 generation and DNA fragmentation in pancreatic islets. H2O2 as mediator for DNA fragmentation. Diabetes 40 (1991) 1141-5.

[31] F.M. Matschinsky, Banting Lecture 1995. A lesson in metabolic regulation inspired by the glucokinase glucose sensor paradigm. Diabetes 45 (1996) 223-41.

[32] S.S. Fajans, G.I. Bell, and K.S. Polonsky, Molecular mechanisms and clinical pathophysiology of maturity-onset diabetes of the young. N Engl J Med 345 (2001) 971-80.

[33] G. Andersen, L. Wegner, C.S. Rose, J. Xie, H. Zhu, K. Larade, A. Johansen, J. Ek, J. Lauenborg, T. Drivsholm, K. Borch-Johnsen, P. Damm, T. Hansen, H.F. Bunn, and O. Pedersen, Variation in NCB5OR: studies of relationships to type 2 diabetes, maturity-onset diabetes of the young, and gestational diabetes mellitus. Diabetes 53 (2004) 2992-7.

[34] W.F. Wang, Y. Guo, M. Xu, H. Huang, L. Novikova, K. Larade, Z. Jiang, T.C. Thayer, j.r. Frontera, D. Aires, H. Ding, J. Turk, C.T. Mathews, H.F. Bunn, L. Stehno-Bittel, and H. Zhu, Development of Diabetes in Lean Ncb5or-Null Mice is Associated with Manifestations of Endoplasmic Reticulum and Oxidative Stress in Beta Cells. . Biochimica et Biophysica Acta in press (2011).

[35] Y. Zhang, K. Larade, Z.G. Jiang, S. Ito, W. Wang, H. Zhu, and H.F. Bunn, The flavoheme reductase Ncb5or protects cells against endoplasmic reticulum stress-induced lipotoxicity. J Lipid Res 51 53-62.

[36] K. Larade, Z. Jiang, Y. Zhang, W. Wang, S. Bonner-Weir, H. Zhu, and H.F. Bunn, Loss of Ncb5or results in impaired fatty acid desaturation, lipoatrophy, and diabetes. J Biol Chem 283 (2008) 29285-91.

[37] H. Sampath, M. Miyazaki, A. Dobrzyn, and J.M. Ntambi, Stearoyl-CoA desaturase-1 mediates the pro-lipogenic effects of dietary saturated fat. J Biol Chem 282 (2007) 2483-93.

[38] M. Miyazaki, A. Dobrzyn, P.M. Elias, and J.M. Ntambi, Stearoyl-CoA desaturase-2 gene expression is required for lipid synthesis during early skin and liver development. Proc Natl Acad Sci U S A 102 (2005) 12501-6.

[39] M. Miyazaki, S.M. Bruggink, and J.M. Ntambi, Identification of mouse palmitoyl-coenzyme A Delta9-desaturase. J Lipid Res 47 (2006) 700-4.

[40] W.C. Man, M. Miyazaki, K. Chu, and J. Ntambi, Colocalization of SCD1 and DGAT2: implying preference for endogenous monounsaturated fatty acids in triglyceride synthesis. J Lipid Res 47 (2006) 1928-39.

[41] J.M. Ntambi, M. Miyazaki, J.P. Stoehr, H. Lan, C.M. Kendziorski, B.S. Yandell, Y. Song, P. Cohen, J.M. Friedman, and A.D. Attie, Loss of stearoyl-CoA desaturase-1 function protects mice against adiposity. Proc Natl Acad Sci U S A 99 (2002) 11482-6.

[42] M. Miyazaki, M.T. Flowers, H. Sampath, K. Chu, C. Otzelberger, X. Liu, and J.M. Ntambi, Hepatic stearoyl-CoA desaturase-1 deficiency protects mice from carbohydrate-induced adiposity and hepatic steatosis. Cell Metab 6 (2007) 484-96.

[43] Z.Z. Li, M. Berk, T.M. McIntyre, and A.E. Feldstein, Hepatic lipid partitioning and liver damage in nonalcoholic fatty liver disease: role of stearoyl-CoA desaturase. J Biol Chem 284 (2009) 5637-44.

[44] R.A. Mathias, S. Sergeant, I. Ruczinski, D.G. Torgerson, C.E. Hugenschmidt, M. Kubala, D. Vaidya, B. Suktitipat, J.T. Ziegler, P. Ivester, D. Case, L.R. Yanek, B.I. Freedman, M.E. Rudock, K.C. Barnes, C.D. Langefeld, L.C. Becker, D.W. Bowden, D.M. Becker, and F.H. Chilton, The impact of FADS genetic variants on omega6 polyunsaturated fatty acid metabolism in African Americans. BMC Genet 12 50.

[45] H.P. Cho, M.T. Nakamura, and S.D. Clarke, Cloning, expression, and nutritional regulation of the mammalian Delta-6 desaturase. J Biol Chem 274 (1999) 471-7.

[46] A.E. Leonard, B. Kelder, E.G. Bobik, L.T. Chuang, J.M. Parker-Barnes, J.M. Thurmond, P.E. Kroeger, J.J. Kopchick, Y.S. Huang, and P. Mukerji, cDNA cloning and characterization of human Delta5-desaturase involved in the biosynthesis of arachidonic acid. Biochem J 347 Pt 3 (2000) 719-24.

[47] E.S. Ford, W.H. Giles, and W.H. Dietz, Prevalence of the metabolic syndrome among US adults: findings from the third National Health and Nutrition Examination Survey. JAMA 287 (2002) 356-9.

[48] D.M. Muoio, and C.B. Newgard, Obesity-related derangements in metabolic regulation. Annu Rev Biochem 75 (2006) 367-401.

[49] D.L. Nelson, and M.M. Cox, Lehninger Principles of Biochemistry, 2004.

[50] C.A. Nagle, L. Vergnes, H. Dejong, S. Wang, T.M. Lewin, K. Reue, and R.A. Coleman, Identification of a novel sn-glycerol-3-phosphate acyltransferase

isoform, GPAT4, as the enzyme deficient in Agpat6-/- mice. J Lipid Res 49 (2008) 823-31.

[51] J. Phan, and K. Reue, Lipin, a lipodystrophy and obesity gene. Cell Metab 1 (2005) 73-83.

[52] S. Cases, S.J. Stone, P. Zhou, E. Yen, B. Tow, K.D. Lardizabal, T. Voelker, and R.V. Farese, Jr., Cloning of DGAT2, a second mammalian diacylglycerol acyltransferase, and related family members. J Biol Chem 276 (2001) 38870-6.

[53] Y. Lee, H. Hirose, M. Ohneda, J.H. Johnson, J.D. McGarry, and R.H. Unger, Beta-cell lipotoxicity in the pathogenesis of non-insulin-dependent diabetes mellitus of obese rats: impairment in adipocyte-beta-cell relationships. Proc Natl Acad Sci U S A 91 (1994) 10878-82.

[54] L.L. Listenberger, X. Han, S.E. Lewis, S. Cases, R.V. Farese, Jr., D.S. Ory, and J.E. Schaffer, Triglyceride accumulation protects against fatty acid-induced lipotoxicity. Proc Natl Acad Sci U S A 100 (2003) 3077-82.

[55] D.G. Hardie, The AMP-activated protein kinase pathway--new players upstream and downstream. J Cell Sci 117 (2004) 5479-87.

[56] D. Carling, The AMP-activated protein kinase cascade--a unifying system for energy control. Trends Biochem Sci 29 (2004) 18-24.

[57] B.B. Kahn, T. Alquier, D. Carling, and D.G. Hardie, AMP-activated protein kinase: ancient energy gauge provides clues to modern understanding of metabolism. Cell Metab 1 (2005) 15-25.

[58] W.W. Winder, H.A. Wilson, D.G. Hardie, B.B. Rasmussen, C.A. Hutber, G.B. Call, R.D. Clayton, L.M. Conley, S. Yoon, and B. Zhou, Phosphorylation of rat muscle

acetyl-CoA carboxylase by AMP-activated protein kinase and protein kinase A. J Appl Physiol 82 (1997) 219-25.

[59] Z. Wu, P. Puigserver, U. Andersson, C. Zhang, G. Adelmant, V. Mootha, A. Troy, S. Cinti, B. Lowell, R.C. Scarpulla, and B.M. Spiegelman, Mechanisms controlling mitochondrial biogenesis and respiration through the thermogenic coactivator PGC-1. Cell 98 (1999) 115-24.

[60] R.P. Fisher, T. Lisowsky, M.A. Parisi, and D.A. Clayton, DNA wrapping and bending by a mitochondrial high mobility group-like transcriptional activator protein. J Biol Chem 267 (1992) 3358-67.

[61] N.G. Larsson, J. Wang, H. Wilhelmsson, A. Oldfors, P. Rustin, M. Lewandoski, G.S. Barsh, and D.A. Clayton, Mitochondrial transcription factor A is necessary for mtDNA maintenance and embryogenesis in mice. Nat Genet 18 (1998) 231-6.

[62] R.C. Scarpulla, Nuclear activators and coactivators in mammalian mitochondrial biogenesis. Biochim Biophys Acta 1576 (2002) 1-14.

[63] C.A. Virbasius, J.V. Virbasius, and R.C. Scarpulla, NRF-1, an activator involved in nuclear-mitochondrial interactions, utilizes a new DNA-binding domain conserved in a family of developmental regulators. Genes Dev 7 (1993) 2431-45.

[64] M. Biswas, and J.Y. Chan, Role of Nrf1 in antioxidant response element-mediated gene expression and beyond. Toxicol Appl Pharmacol 244 16-20.

[65] L. Michalik, J. Auwerx, J.P. Berger, V.K. Chatterjee, C.K. Glass, F.J. Gonzalez, P.A. Grimaldi, T. Kadowaki, M.A. Lazar, S. O'Rahilly, C.N. Palmer, J. Plutzky, J.K. Reddy, B.M. Spiegelman, B. Staels, and W. Wahli, International Union of

Pharmacology. LXI. Peroxisome proliferator-activated receptors. Pharmacol Rev 58 (2006) 726-41.

[66] R.M. Evans, G.D. Barish, and Y.X. Wang, PPARs and the complex journey to obesity. Nat Med 10 (2004) 355-61.

[67] M. Gottlicher, E. Widmark, Q. Li, and J.A. Gustafsson, Fatty acids activate a chimera of the clofibric acid-activated receptor and the glucocorticoid receptor. Proc Natl Acad Sci U S A 89 (1992) 4653-7.

[68] T.C. Leone, C.J. Weinheimer, and D.P. Kelly, A critical role for the peroxisome proliferator-activated receptor alpha (PPARalpha) in the cellular fasting response: the PPARalpha-null mouse as a model of fatty acid oxidation disorders. Proc Natl Acad Sci U S A 96 (1999) 7473-8.

[69] L.M. Sanderson, P.J. de Groot, G.J. Hooiveld, A. Koppen, E. Kalkhoven, M. Muller, and S. Kersten, Effect of synthetic dietary triglycerides: a novel research paradigm for nutrigenomics. PLoS One 3 (2008) e1681.

[70] E.D. Rosen, P. Sarraf, A.E. Troy, G. Bradwin, K. Moore, D.S. Milstone, B.M. Spiegelman, and R.M. Mortensen, PPAR gamma is required for the differentiation of adipose tissue in vivo and in vitro. Mol Cell 4 (1999) 611-7.

[71] H.E. Xu, M.H. Lambert, V.G. Montana, D.J. Parks, S.G. Blanchard, P.J. Brown, D.D. Sternbach, J.M. Lehmann, G.B. Wisely, T.M. Willson, S.A. Kliewer, and M.V. Milburn, Molecular recognition of fatty acids by peroxisome proliferator-activated receptors. Mol Cell 3 (1999) 397-403.

[72] L.M. Sanderson, T. Degenhardt, A. Koppen, E. Kalkhoven, B. Desvergne, M. Muller, and S. Kersten, Peroxisome proliferator-activated receptor beta/delta

(PPARbeta/delta) but not PPARalpha serves as a plasma free fatty acid sensor in liver. Mol Cell Biol 29 (2009) 6257-67.

[73] A. Cao, H. Li, Y. Zhou, M. Wu, and J. Liu, Long chain acyl-CoA synthetase-3 is a molecular target for peroxisome proliferator-activated receptor delta in HepG2 hepatoma cells. J Biol Chem 285 16664-74.

[74] S. Kyrylenko, and A. Baniahmad, Sirtuin family: a link to metabolic signaling and senescence. Curr Med Chem 17 2921-32.

[75] J.T. Rodgers, C. Lerin, W. Haas, S.P. Gygi, B.M. Spiegelman, and P. Puigserver, Nutrient control of glucose homeostasis through a complex of PGC-1alpha and SIRT1. Nature 434 (2005) 113-8.

[76] C. Canto, Z. Gerhart-Hines, J.N. Feige, M. Lagouge, L. Noriega, J.C. Milne, P.J. Elliott, P. Puigserver, and J. Auwerx, AMPK regulates energy expenditure by modulating NAD+ metabolism and SIRT1 activity. Nature 458 (2009) 1056-60.

[77] J. St-Pierre, S. Drori, M. Uldry, J.M. Silvaggi, J. Rhee, S. Jager, C. Handschin, K. Zheng, J. Lin, W. Yang, D.K. Simon, R. Bachoo, and B.M. Spiegelman, Suppression of reactive oxygen species and neurodegeneration by the PGC-1 transcriptional coactivators. Cell 127 (2006) 397-408.

[78] P. Puigserver, J. Rhee, J. Lin, Z. Wu, J.C. Yoon, C.Y. Zhang, S. Krauss, V.K. Mootha, B.B. Lowell, and B.M. Spiegelman, Cytokine stimulation of energy expenditure through p38 MAP kinase activation of PPARgamma coactivator-1. Mol Cell 8 (2001) 971-82.

[79] R.T. Brookheart, C.I. Michel, and J.E. Schaffer, As a matter of fat. Cell Metab 10 (2009) 9-12.

[80] H. Malhi, S.F. Bronk, N.W. Werneburg, and G.J. Gores, Free fatty acids induce JNK-dependent hepatocyte lipoapoptosis. J Biol Chem 281 (2006) 12093-101.

[81] L.L. Listenberger, D.S. Ory, and J.E. Schaffer, Palmitate-induced apoptosis can occur through a ceramide-independent pathway. J Biol Chem 276 (2001) 14890-5.

[82] D.B. Ostrander, G.C. Sparagna, A.A. Amoscato, J.B. McMillin, and W. Dowhan, Decreased cardiolipin synthesis corresponds with cytochrome c release in palmitate-induced cardiomyocyte apoptosis. J Biol Chem 276 (2001) 38061-7.

[83] J.M. Cacicedo, S. Benjachareowong, E. Chou, N.B. Ruderman, and Y. Ido, Palmitate-induced apoptosis in cultured bovine retinal pericytes: roles of NAD(P)H oxidase, oxidant stress, and ceramide. Diabetes 54 (2005) 1838-45.

[84] S. Nakamura, T. Takamura, N. Matsuzawa-Nagata, H. Takayama, H. Misu, H. Noda, S. Nabemoto, S. Kurita, T. Ota, H. Ando, K. Miyamoto, and S. Kaneko, Palmitate induces insulin resistance in H4IIEC3 hepatocytes through reactive oxygen species produced by mitochondria. J Biol Chem 284 (2009) 14809-18.

[85] T. Inoguchi, P. Li, F. Umeda, H.Y. Yu, M. Kakimoto, M. Imamura, T. Aoki, T. Etoh, T. Hashimoto, M. Naruse, H. Sano, H. Utsumi, and H. Nawata, High glucose level and free fatty acid stimulate reactive oxygen species production through protein kinase C--dependent activation of NAD(P)H oxidase in cultured vascular cells. Diabetes 49 (2000) 1939-45.

[86] N.M. Borradaile, K.K. Buhman, L.L. Listenberger, C.J. Magee, E.T. Morimoto, D.S. Ory, and J.E. Schaffer, A critical role for eukaryotic elongation factor 1A-1 in lipotoxic cell death. Mol Biol Cell 17 (2006) 770-8.

[87] N.M. Borradaile, X. Han, J.D. Harp, S.E. Gale, D.S. Ory, and J.E. Schaffer, Disruption of endoplasmic reticulum structure and integrity in lipotoxic cell death. J Lipid Res 47 (2006) 2726-37.

[88] S. Corda, C. Laplace, E. Vicaut, and J. Duranteau, Rapid reactive oxygen species production by mitochondria in endothelial cells exposed to tumor necrosis factor-alpha is mediated by ceramide. Am J Respir Cell Mol Biol 24 (2001) 762-8.

[89] P. Schonfeld, and L. Wojtczak, Fatty acids as modulators of the cellular production of reactive oxygen species. Free Radic Biol Med 45 (2008) 231-41.

[90] W. Droge, Free radicals in the physiological control of cell function. Physiol Rev 82 (2002) 47-95.

[91] P. Chiarugi, G. Pani, E. Giannoni, L. Taddei, R. Colavitti, G. Raugei, M. Symons, S. Borrello, T. Galeotti, and G. Ramponi, Reactive oxygen species as essential mediators of cell adhesion: the oxidative inhibition of a FAK tyrosine phosphatase is required for cell adhesion. J Cell Biol 161 (2003) 933-44.

[92] M.B. Grisham, Reactive oxygen species in immune responses. Free Radic Biol Med 36 (2004) 1479-80.

[93] J.L. Evans, I.D. Goldfine, B.A. Maddux, and G.M. Grodsky, Oxidative stress and stress-activated signaling pathways: a unifying hypothesis of type 2 diabetes. Endocr Rev 23 (2002) 599-622.

[94] T. Satoh, Y. Enokido, H. Aoshima, Y. Uchiyama, and H. Hatanaka, Changes in mitochondrial membrane potential during oxidative stress-induced apoptosis in PC12 cells. J Neurosci Res 50 (1997) 413-20.

[95] K. Bedard, and K.H. Krause, The NOX family of ROS-generating NADPH oxidases: physiology and pathophysiology. Physiol Rev 87 (2007) 245-313.

[96] D. Javesghani, S.A. Magder, E. Barreiro, M.T. Quinn, and S.N. Hussain, Molecular characterization of a superoxide-generating NAD(P)H oxidase in the ventilatory muscles. Am J Respir Crit Care Med 165 (2002) 412-8.

[97] C. Heymes, J.K. Bendall, P. Ratajczak, A.C. Cave, J.L. Samuel, G. Hasenfuss, and A.M. Shah, Increased myocardial NADPH oxidase activity in human heart failure. J Am Coll Cardiol 41 (2003) 2164-71.

[98] D. Gao, S. Nong, X. Huang, Y. Lu, H. Zhao, Y. Lin, Y. Man, S. Wang, J. Yang, and J. Li, The effects of palmitate on hepatic insulin resistance are mediated by NADPH Oxidase 3-derived reactive oxygen species through JNK and p38MAPK pathways. J Biol Chem 285 29965-73.

[99] K. Mahadev, H. Motoshima, X. Wu, J.M. Ruddy, R.S. Arnold, G. Cheng, J.D. Lambeth, and B.J. Goldstein, The NAD(P)H oxidase homolog Nox4 modulates insulin-stimulated generation of H2O2 and plays an integral role in insulin signal transduction. Mol Cell Biol 24 (2004) 1844-54.

[100] N. Bashan, J. Kovsan, I. Kachko, H. Ovadia, and A. Rudich, Positive and negative regulation of insulin signaling by reactive oxygen and nitrogen species. Physiol Rev 89 (2009) 27-71.

[101] B.P. Tu, and J.S. Weissman, Oxidative protein folding in eukaryotes: mechanisms and consequences. J Cell Biol 164 (2004) 341-346.

[102] M. Elsner, W. Gehrmann, and S. Lenzen, Peroxisome-generated hydrogen peroxide as important mediator of lipotoxicity in insulin-producing cells. Diabetes 60 200-8.

[103] T. Yamamoto, T. Suzuki, A. Kobayashi, J. Wakabayashi, J. Maher, H. Motohashi, and M. Yamamoto, Physiological significance of reactive cysteine residues of Keap1 in determining Nrf2 activity. Mol Cell Biol 28 (2008) 2758-70.

[104] S.C. Lu, Regulation of glutathione synthesis. Mol Aspects Med 30 (2009) 42-59.

[105] S.C. Lu, Regulation of hepatic glutathione synthesis: current concepts and controversies. FASEB J 13 (1999) 1169-83.

[106] J. Cai, Z.Z. Huang, and S.C. Lu, Differential regulation of gamma-glutamylcysteine synthetase heavy and light subunit gene expression. Biochem J 326 (Pt 1) (1997) 167-72.

[107] D.E. Baranano, M. Rao, C.D. Ferris, and S.H. Snyder, Biliverdin reductase: a major physiologic cytoprotectant. Proc Natl Acad Sci U S A 99 (2002) 16093-8.

[108] R. Ozono, New biotechnological methods to reduce oxidative stress in the cardiovascular system: focusing on the Bach1/heme oxygenase-1 pathway. Curr Pharm Biotechnol 7 (2006) 87-93.

[109] A. Yachie, Y. Niida, T. Wada, N. Igarashi, H. Kaneda, T. Toma, K. Ohta, Y. Kasahara, and S. Koizumi, Oxidative stress causes enhanced endothelial cell injury in human heme oxygenase-1 deficiency. J Clin Invest 103 (1999) 129-35.

[110] M.V. Kumari, M. Hiramatsu, and M. Ebadi, Free radical scavenging actions of metallothionein isoforms I and II. Free Radic Res 29 (1998) 93-101.

[111] S. Ghaemmaghami, W.K. Huh, K. Bower, R.W. Howson, A. Belle, N. Dephoure, E.K. O'Shea, and J.S. Weissman, Global analysis of protein expression in yeast. Nature 425 (2003) 737-41.

[112] D. Scheuner, and R.J. Kaufman, The unfolded protein response: a pathway that links insulin demand with beta-cell failure and diabetes. Endocr Rev 29 (2008) 317-33.

[113] H. Yoshida, T. Matsui, A. Yamamoto, T. Okada, and K. Mori, XBP1 mRNA is induced by ATF6 and spliced by IRE1 in response to ER stress to produce a highly active transcription factor. Cell 107 (2001) 881-91.

[114] J. Hollien, and J.S. Weissman, Decay of endoplasmic reticulum-localized mRNAs during the unfolded protein response. Science 313 (2006) 104-7.

[115] J. Wu, D.T. Rutkowski, M. Dubois, J. Swathirajan, T. Saunders, J. Wang, B. Song, G.D. Yau, and R.J. Kaufman, ATF6alpha optimizes long-term endoplasmic reticulum function to protect cells from chronic stress. Dev Cell 13 (2007) 351-64.

[116] J.W. Hershey, Protein phosphorylation controls translation rates. J Biol Chem 264 (1989) 20823-6.

[117] S.R. Kimball, Eukaryotic initiation factor eIF2. Int J Biochem Cell Biol 31 (1999) 25-9.

[118] Y. Ma, J.W. Brewer, J.A. Diehl, and L.M. Hendershot, Two distinct stress signaling pathways converge upon the CHOP promoter during the mammalian unfolded protein response. J Mol Biol 318 (2002) 1351-65.

[119] H.P. Harding, Y. Zhang, A. Bertolotti, H. Zeng, and D. Ron, Perk is essential for translational regulation and cell survival during the unfolded protein response. Mol Cell 5 (2000) 897-904.

[120] S.J. Marciniak, C.Y. Yun, S. Oyadomari, I. Novoa, Y. Zhang, R. Jungreis, K. Nagata, H.P. Harding, and D. Ron, CHOP induces death by promoting protein synthesis and oxidation in the stressed endoplasmic reticulum. Genes Dev 18 (2004) 3066-77.

[121] S. Oyadomari, K. Takeda, M. Takiguchi, T. Gotoh, M. Matsumoto, I. Wada, S. Akira, E. Araki, and M. Mori, Nitric oxide-induced apoptosis in pancreatic beta cells is mediated by the endoplasmic reticulum stress pathway. Proc Natl Acad Sci U S A 98 (2001) 10845-50.

[122] S. Oyadomari, A. Koizumi, K. Takeda, T. Gotoh, S. Akira, E. Araki, and M. Mori, Targeted disruption of the Chop gene delays endoplasmic reticulum stress-mediated diabetes. J Clin Invest 109 (2002) 525-32.

[123] S.B. Cullinan, D. Zhang, M. Hannink, E. Arvisais, R.J. Kaufman, and J.A. Diehl, Nrf2 is a direct PERK substrate and effector of PERK-dependent cell survival. Mol Cell Biol 23 (2003) 7198-209.

[124] R.V. Rao, H.M. Ellerby, and D.E. Bredesen, Coupling endoplasmic reticulum stress to the cell death program. Cell Death Differ 11 (2004) 372-80.

[125] C. Hetz, P. Bernasconi, J. Fisher, A.H. Lee, M.C. Bassik, B. Antonsson, G.S. Brandt, N.N. Iwakoshi, A. Schinzel, L.H. Glimcher, and S.J. Korsmeyer, Proapoptotic BAX and BAK modulate the unfolded protein response by a direct interaction with IRE1alpha. Science 312 (2006) 572-6.

[126] P. Hu, Z. Han, A.D. Couvillon, R.J. Kaufman, and J.H. Exton, Autocrine tumor necrosis factor alpha links endoplasmic reticulum stress to the membrane death receptor pathway through IRE1alpha-mediated NF-kappaB activation and down-regulation of TRAF2 expression. Mol Cell Biol 26 (2006) 3071-84.

[127] H. Yamazaki, N. Hiramatsu, K. Hayakawa, Y. Tagawa, M. Okamura, R. Ogata, T. Huang, S. Nakajima, J. Yao, A.W. Paton, J.C. Paton, and M. Kitamura, Activation of the Akt-NF-kappaB pathway by subtilase cytotoxin through the ATF6 branch of the unfolded protein response. J Immunol 183 (2009) 1480-7.

[128] J.D. Malhotra, and R.J. Kaufman, Endoplasmic reticulum stress and oxidative stress: a vicious cycle or a double-edged sword? Antioxid Redox Signal 9 (2007) 2277-93.

[129] B.P. Tu, and J.S. Weissman, Oxidative protein folding in eukaryotes: mechanisms and consequences. J Cell Biol 164 (2004) 341-6.

[130] J. Jacobson, and M.R. Duchen, Mitochondrial oxidative stress and cell death in astrocytes--requirement for stored Ca2+ and sustained opening of the permeability transition pore. J Cell Sci 115 (2002) 1175-88.

[131] M.J. Berridge, The endoplasmic reticulum: a multifunctional signaling organelle. Cell Calcium 32 (2002) 235-49.

[132] R.D. Finn, L.A. McLaughlin, S. Ronseaux, I. Rosewell, J.B. Houston, C.J. Henderson, and C.R. Wolf, Defining the in Vivo Role for cytochrome b5 in cytochrome P450 function through the conditional hepatic deletion of microsomal cytochrome b5. J Biol Chem 283 (2008) 31385-93.

[133] N.E. Wolins, J.R. Skinner, M.J. Schoenfish, A. Tzekov, K.G. Bensch, and P.E. Bickel, Adipocyte protein S3-12 coats nascent lipid droplets. J Biol Chem 278 (2003) 37713-21.

[134] M. Miyazaki, H.J. Kim, W.C. Man, and J.M. Ntambi, Oleoyl-CoA is the major de novo product of stearoyl-CoA desaturase 1 gene isoform and substrate for the biosynthesis of the Harderian gland 1-alkyl-2,3-diacylglycerol. J Biol Chem 276 (2001) 39455-61.

[135] H.P. Guan, Y. Li, M.V. Jensen, C.B. Newgard, C.M. Steppan, and M.A. Lazar, A futile metabolic cycle activated in adipocytes by antidiabetic agents. Nat Med 8 (2002) 1122-8.

[136] M. Xu, W. Wang, J.R. Frontera, M.C. Neely, J. Lu, D. Aires, F.F. Hsu, J. Turk, R.H. Swerdlow, S.E. Carlson, and H. Zhu, Ncb5or deficiency increases fatty acid catabolism and oxidative stress. J Biol Chem 286 11141-54.

[137] J. Shanklin, E. Whittle, and B.G. Fox, Eight histidine residues are catalytically essential in a membrane-associated iron enzyme, stearoyl-CoA desaturase, and are conserved in alkane hydroxylase and xylene monooxygenase. Biochemistry 33 (1994) 12787-94.

[138] M. Miyazaki, Y.C. Kim, and J.M. Ntambi, A lipogenic diet in mice with a disruption of the stearoyl-CoA desaturase 1 gene reveals a stringent requirement of endogenous monounsaturated fatty acids for triglyceride synthesis. J Lipid Res 42 (2001) 1018-24.

[139] M.A. Goren, and B.G. Fox, Wheat germ cell-free translation, purification, and assembly of a functional human stearoyl-CoA desaturase complex. Protein Expr Purif 62 (2008) 171-8.

[140] F. Djouadi, J.P. Bonnefont, A. Munnich, and J. Bastin, Characterization of fatty acid oxidation in human muscle mitochondria and myoblasts. Mol Genet Metab 78 (2003) 112-8.

[141] L. Zhang, C. Yu, F.E. Vasquez, N. Galeva, I. Onyango, R.H. Swerdlow, and R.T. Dobrowsky, Hyperglycemia alters the schwann cell mitochondrial proteome and decreases coupled respiration in the absence of superoxide production. J Proteome Res 9 (2010) 458-71.

[142] H. Jaeschke, and J.R. Mitchell, Use of isolated perfused organs in hypoxia and ischemia/reperfusion oxidant stress. Methods Enzymol 186 (1990) 752-9.

[143] E.G. Bligh, and W.J. Dyer, A rapid method of total lipid extraction and purification. Can J Biochem Physiol 37 (1959) 911-7.

[144] F.F. Hsu, and J. Turk, Characterization of ceramides by low energy collisional-activated dissociation tandem mass spectrometry with negative-ion electrospray ionization. J Am Soc Mass Spectrom 13 (2002) 558-70.

[145] M. Lagouge, C. Argmann, Z. Gerhart-Hines, H. Meziane, C. Lerin, F. Daussin, N. Messadeq, J. Milne, P. Lambert, P. Elliott, B. Geny, M. Laakso, P. Puigserver, and J. Auwerx, Resveratrol improves mitochondrial function and protects against metabolic disease by activating SIRT1 and PGC-1alpha. Cell 127 (2006) 1109-22.

[146] B. Beutler, I.W. Milsark, and A.C. Cerami, Passive immunization against cachectin/tumor necrosis factor protects mice from lethal effect of endotoxin. Science 229 (1985) 869-71.

[147] A.E. Feldstein, N.W. Werneburg, A. Canbay, M.E. Guicciardi, S.F. Bronk, R. Rydzewski, L.J. Burgart, and G.J. Gores, Free fatty acids promote hepatic lipotoxicity by stimulating TNF-alpha expression via a lysosomal pathway. Hepatology 40 (2004) 185-94.

[148] N. Zhang, M.H. Ahsan, A.F. Purchio, and D.B. West, Serum amyloid A-luciferase transgenic mice: response to sepsis, acute arthritis, and contact hypersensitivity and the effects of proteasome inhibition. J Immunol 174 (2005) 8125-34.

[149] P. Kulozik, A. Jones, F. Mattijssen, A.J. Rose, A. Reimann, D. Strzoda, S. Kleinsorg, C. Raupp, J. Kleinschmidt, K. Muller-Decker, W. Wahli, C. Sticht, N. Gretz, C. von Loeffelholz, M. Stockmann, A. Pfeiffer, S. Stohr, G.M. Dallinga-Thie, P.P. Nawroth, M. Berriel Diaz, and S. Herzig, Hepatic Deficiency in Transcriptional Cofactor TBL1 Promotes Liver Steatosis and Hypertriglyceridemia. Cell Metab 13 389-400.

[150] D.A. Wong, S. Bassilian, S. Lim, and W.N. Paul Lee, Coordination of peroxisomal beta-oxidation and fatty acid elongation in HepG2 cells. J Biol Chem 279 (2004) 41302-9.

[151] G. Cairo, F. Bernuzzi, and S. Recalcati, A precious metal: Iron, an essential nutrient for all cells. Genes Nutr 1 (2006) 25-39.

[152] A.S. Zhang, and C.A. Enns, Iron homeostasis: recently identified proteins provide insight into novel control mechanisms. J Biol Chem 284 (2009) 711-5.

[153] S. Recalcati, G. Minotti, and G. Cairo, Iron regulatory proteins: from molecular mechanisms to drug development. Antioxid Redox Signal 13 1593-616.

[154] Y. Yu, Z. Kovacevic, and D.R. Richardson, Tuning cell cycle regulation with an iron key. Cell Cycle 6 (2007) 1982-94.

[155] F. Zhang, W. Wang, Y. Tsuji, S.V. Torti, and F.M. Torti, Post-transcriptional modulation of iron homeostasis during p53-dependent growth arrest. J Biol Chem 283 (2008) 33911-8.

[156] K.M. Utzschneider, and K.V. Kowdley, Hereditary hemochromatosis and diabetes mellitus: implications for clinical practice. Nat Rev Endocrinol 6 26-33.

[157] H. Gunshin, B. Mackenzie, U.V. Berger, Y. Gunshin, M.F. Romero, W.F. Boron, S. Nussberger, J.L. Gollan, and M.A. Hediger, Cloning and characterization of a mammalian proton-coupled metal-ion transporter. Nature 388 (1997) 482-8.

[158] A.T. McKie, The role of Dcytb in iron metabolism: an update. Biochem Soc Trans 36 (2008) 1239-41.

[159] A. Donovan, A. Brownlie, Y. Zhou, J. Shepard, S.J. Pratt, J. Moynihan, B.H. Paw, A. Drejer, B. Barut, A. Zapata, T.C. Law, C. Brugnara, S.E. Lux, G.S. Pinkus, J.L. Pinkus, P.D. Kingsley, J. Palis, M.D. Fleming, N.C. Andrews, and L.I. Zon, Positional cloning of zebrafish ferroportin1 identifies a conserved vertebrate iron exporter. Nature 403 (2000) 776-81.

[160] A.T. McKie, P. Marciani, A. Rolfs, K. Brennan, K. Wehr, D. Barrow, S. Miret, A. Bomford, T.J. Peters, F. Farzaneh, M.A. Hediger, M.W. Hentze, and R.J. Simpson, A novel duodenal iron-regulated transporter, IREG1, implicated in the basolateral transfer of iron to the circulation. Mol Cell 5 (2000) 299-309.

[161] M. Wessling-Resnick, Iron imports. III. Transfer of iron from the mucosa into circulation. Am J Physiol Gastrointest Liver Physiol 290 (2006) G1-6.

[162] S. Soe-Lin, S.S. Apte, B. Andriopoulos, Jr., M.C. Andrews, M. Schranzhofer, T. Kahawita, D. Garcia-Santos, and P. Ponka, Nramp1 promotes efficient macrophage recycling of iron following erythrophagocytosis in vivo. Proc Natl Acad Sci U S A 106 (2009) 5960-5.

[163] M.D. Fleming, M.A. Romano, M.A. Su, L.M. Garrick, M.D. Garrick, and N.C. Andrews, Nramp2 is mutated in the anemic Belgrade (b) rat: evidence of a role for Nramp2 in endosomal iron transport. Proc Natl Acad Sci U S A 95 (1998) 1148-53.

[164] J.P. Liuzzi, F. Aydemir, H. Nam, M.D. Knutson, and R.J. Cousins, Zip14 (Slc39a14) mediates non-transferrin-bound iron uptake into cells. Proc Natl Acad Sci U S A 103 (2006) 13612-7.

[165] E. Nemeth, and T. Ganz, Regulation of iron metabolism by hepcidin. Annu Rev Nutr 26 (2006) 323-42.

[166] E. Nemeth, M.S. Tuttle, J. Powelson, M.B. Vaughn, A. Donovan, D.M. Ward, T. Ganz, and J. Kaplan, Hepcidin regulates cellular iron efflux by binding to ferroportin and inducing its internalization. Science 306 (2004) 2090-3.

[167] T. Goswami, and N.C. Andrews, Hereditary hemochromatosis protein, HFE, interaction with transferrin receptor 2 suggests a molecular mechanism for mammalian iron sensing. J Biol Chem 281 (2006) 28494-8.

[168] B. Andriopoulos, Jr., E. Corradini, Y. Xia, S.A. Faasse, S. Chen, L. Grgurevic, M.D. Knutson, A. Pietrangelo, S. Vukicevic, H.Y. Lin, and J.L. Babitt, BMP6 is a

key endogenous regulator of hepcidin expression and iron metabolism. Nat Genet 41 (2009) 482-7.

[169] D. Meynard, L. Kautz, V. Darnaud, F. Canonne-Hergaux, H. Coppin, and M.P. Roth, Lack of the bone morphogenetic protein BMP6 induces massive iron overload. Nat Genet 41 (2009) 478-81.

[170] A. Pietrangelo, U. Dierssen, L. Valli, C. Garuti, A. Rump, E. Corradini, M. Ernst, C. Klein, and C. Trautwein, STAT3 is required for IL-6-gp130-dependent activation of hepcidin in vivo. Gastroenterology 132 (2007) 294-300.

[171] H. Huang, M. Constante, A. Layoun, and M.M. Santos, Contribution of STAT3 and SMAD4 pathways to the regulation of hepcidin by opposing stimuli. Blood 113 (2009) 3593-9.

[172] S.J. Oliveira, J.P. Pinto, G. Picarote, V.M. Costa, F. Carvalho, M. Rangel, M. de Sousa, and S.F. de Almeida, ER stress-inducible factor CHOP affects the expression of hepcidin by modulating C/EBPalpha activity. PLoS One 4 (2009) e6618.

[173] C. Vecchi, G. Montosi, K. Zhang, I. Lamberti, S.A. Duncan, R.J. Kaufman, and A. Pietrangelo, ER stress controls iron metabolism through induction of hepcidin. Science 325 (2009) 877-80.

[174] M. Pak, M.A. Lopez, V. Gabayan, T. Ganz, and S. Rivera, Suppression of hepcidin during anemia requires erythropoietic activity. Blood 108 (2006) 3730-5.

[175] C. Peyssonnaux, A.S. Zinkernagel, R.A. Schuepbach, E. Rankin, S. Vaulont, V.H. Haase, V. Nizet, and R.S. Johnson, Regulation of iron homeostasis by the hypoxia-inducible transcription factors (HIFs). J Clin Invest 117 (2007) 1926-32.

[176] A. Robertson, J.N. Morrison, A.M. Wood, and I. Bremner, Effects of iron deficiency on metallothionein-I concentrations in blood and tissues of rats. J Nutr 119 (1989) 439-45.

[177] J.D. Torrance, and T.H. Bothwell, A simple technique for measuring storage iron concentrations in formalinised liver samples. S Afr J Med Sci 33 (1968) 9-11.

[178] R.S. Ohgami, D.R. Campagna, A. McDonald, and M.D. Fleming, The Steap proteins are metalloreductases. Blood 108 (2006) 1388-94.

[179] J.M. Fernandez-Real, A. Lopez-Bermejo, and W. Ricart, Cross-talk between iron metabolism and diabetes. Diabetes 51 (2002) 2348-54.

[180] A. Whaley-Connell, P.A. McCullough, and J.R. Sowers, The role of oxidative stress in the metabolic syndrome. Rev Cardiovasc Med 12 21-9.

[181] J. Huang, D. Jones, B. Luo, M. Sanderson, J. Soto, E.D. Abel, R.C. Cooksey, and D.A. McClain, Iron overload and diabetes risk: a shift from glucose to Fatty Acid oxidation and increased hepatic glucose production in a mouse model of hereditary hemochromatosis. Diabetes 60 80-7.

[182] P. Aisen, C. Enns, and M. Wessling-Resnick, Chemistry and biology of eukaryotic iron metabolism. Int J Biochem Cell Biol 33 (2001) 940-59.